Computational Studies of Three Chemical Systems

A Dissertation

Presented to

The Faculty of the Graduate School

University of Missouri-Columbia

In Partial Fulfillment

Of the Requirements for the Degree

Doctor of Philosophy

---

by

Haunani Thomas

Prof. Carol A. Deakyne, Dissertation Supervisor

December 2011

The undersigned, appointed by the dean of the Graduate School, have examined the dissertation entitled

COMPUTATIONAL STUDIES OF THREE CHEMICAL SYSTEMS

Presented by Haunani Thomas,

a candidate for the degree of doctor of philosophy of Chemistry,

and hereby certify that, in their opinion, it is worthy of acceptance.

Professor Carol Deakyne (Chair)

Professor John Adams (Member)

Professor Michael Greenlief (Member)

Professor Giovanni Vignale (Outside Member)

ACKNOWLEDGEMENTS

I am forever indebted to my dissertation supervisor, Professor Carol Deakyne, for her guidance and support. She has been an excellent and patient mentor through the graduate school process, always mindful of the practical necessities of my progress, introducing me to the field of Chemistry, and allowing me to advance professionally through attendance and presentations at ACS meetings. I am fully aware that, in this respect, not all graduate students are as fortunate as I have been. I am also grateful to Professor John Adams for all his support and teaching throughout my graduate career. I am appreciative of my entire committee, Professor Deakyne, Professor Adams, Professor Michael Greenlief, and Professor Giovanni Vignale, for their sound advice, patience, and flexibility.

I would also like to thank my experimental collaborators and their groups, Professor Joel Liebman of the University of Maryland, Baltimore County, Professor Michael Van Stip Donk of Wichita State University, and Professor Jerry Atwood of the University of Missouri – Columbia. I am thankful to my fellow graduate students, Jerry Brightwell, and the Department of Chemistry at the University of Missouri – Columbia for all their help throughout the years.

TABLE OF CONTENTS

LIST OF TABLES

LIST OF FIGURES

ABSTRACT

The subject of this dissertation is the use of electronic structure calculations to examine and supplement the experimental observations of three different chemical systems. The first topic is the study of pyrogallol[4]arene with R-groups R=H and R=phenyl (ph). This macrocycle self-assembles into dimeric and hexameric nanocapsules. The purpose of this study is to use DFT methods to gain knowledge of this process. While several conformations of pyrogallol[4]arene are thermodynamically stable, experimental evidence suggests that aryl-substituted pyrogallol[4]arene exists in the Chair conformation. During the formation of the nanocapsules, the Chair isomer must convert to the Cone isomer. The relative energies of different structures and their solvent interactions are examined to better understand the process by which self-assembly of the nanocapsule occurs.

Ligated vanadium oxides have generated interest from many fields due to their unique catalytic properties. These systems can be induced to either donate or accept electron density through control of the ligand field and charge on the metal center. In the second study, electrospray ionization mass spectrometry, DFT and conventional ab initio calculations are used to study the addition and ligand-exchange reactions of vanadium oxide cations. Specifically investigated is the addition of H_2O and O_2 to vanadyl complexes of the form $[VOX(NCCH_3)]^+$ where X = F^-, Cl^-, Br^-, I^-, and OH^-. Changing the identity of X allows the observation of how the electron density on the metal center influences the addition of H_2O or O_2. The results of different DFT methods suggest the need for higher-level single-point calculations.

The final chapters discuss the high-level quantum chemical calculations performed to study the structure and energetics of isomers of CH_2BF on both the singlet and triplet PES. MP2 optimizations were used to identify minima and transition states. A series of CCSD(T) single-point calculations were used to extrapolate to the complete basis set limit. A wide variety of structures with a large range of energies were found. All of these species on both PES's are compared as well as the transition states that connect the most stable isomers. For the singlet system, comparison was made to the previously studied protonated counterparts of the species, $[B, C, F, H_3]^+$.

1 A Computational Study of Phenyl-Substituted Pyrogallol[4]arene Macrocycles

The macrocycle C-alkylpyrogallol[4]arene forms self-assembled dimeric and hexameric nanocapsules. Several conformations of pyrogallol[4]arene have been found to be thermodynamically stable with the most stable structures typically being a chair and cone. Experimental evidence suggests that aryl-substituted pyrogallol[4]arene exists in the chair conformation. However, because the cone is the necessary conformer of the subunits of the capsules, the chair must undergo some transition to the cone. The study that is the topic of this chapter uses DFT methods to investigate stereoisomers of the R=H and R=phenyl (ph) systems and solvent interactions to understand the structures and their relative stabilities, the interconversions between stereoisomers, and ultimately the mechanism by which self-assembly of the nanocapsule occurs.

1.1 Introduction

Supramolecular nanocapsules are relatively new yet highly promising species with applications in several areas of chemical research[1]. Understanding and manipulating these enclosed chemical spaces promise many exciting advances in the areas of fuel storage, nanomedicine, magnetism and optics, organic nanotubes,

molecular scaffolding building blocks for supramolecular engineering, and cloistered nanoscale reactions. Experimentalists are able to very rapidly synthesize a wide variety of self-assembled hydrogen-bonded or metal-organic nanostructures from resorcin[4]arenes and pyrogallol[4]arenes[2]. The current work focuses on the use of pyrogallol[4]arene as a monomer for complexation as dimeric and hexameric capsules (see Figure 1.1). Pyrogallol[4]arene hexamers can further self-assemble into spherical and tubular superstructures[3]. The macrocycles are basic building blocks and can be expanded upon. The size of the capsule can be extended by adding groups to the upper rim of the macrocycle[4].

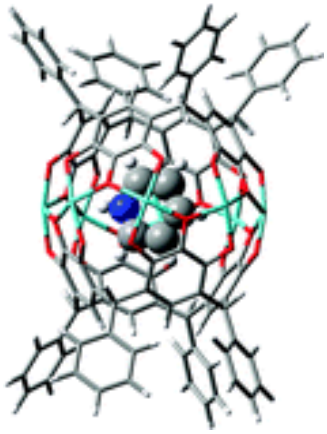

Figure 1.1. Schematic representation of [Zn_8[*C*-phenylpyrogallol[4]arene]$_2$[pyridine]$_8$⊂[pyridine]] Zn: aqua, O: red, N: blue, C: grey, H: white

While there are many factors influencing the self-assembly and the role of the solvent and metal are both under investigation, it as been shown that it is possible to do a one-step synthesis of pyrogallol[4]arene, which then independently self-assembles into hexameric nanocapsules, without solvent[5]. Although solvent is not

necessary for self-assembly to occur, understanding how the solvent interacts with the macrocycles can help direct the formation of different superstructures[6]. The identity of the R-groups also plays an important role in directing the nature of capsule-capsule interactions, specifically in the crystal packing structure. When the R-group is an alky chain, the length of the chain determines the space available between capsules in the solid state[7].

Investigation of the interior of the capsules can be accomplished by encapsulation of guest species such as the fluorophore 4-[3-(9-anthryl)propyl]-N,N-dimethylaniline (ADMA)[8-10]. Spectroscopic studies can give insight into the molecular environment of the inside of the capsule. This is important to the understanding of not only the host-guest interactions but also interactions between species separated by the capsule wall. Communication across pyrogallol[4]arene nanocapsule walls has been shown to impact interior fluid species[11]. It has already been shown that *C*-alkylpyrogallol[4]arene can be disassembled in a controlled manner to enable the uptake of molecular hydrogen that becomes a trapped guest when the capsules reassemble into hexamers[12].

Hydrogen bonding of covalently bound macrocylces has been the main interaction of interest for these capsules, but ionic dimers of pyrogallol[4]arene have also been found to form stable capsules and potentially have the ability to encapsulate multiple guests[13]. It is also possible to halogenate the lower rim of the pyrogallol[4]arene macrocycle and still form self-assemblages, in this case, bi-layer structures or hexameric capsules[14]. Gallium-pyrogallol[4]arene capsules contain aqueous gates in their walls that allow metal ions or ion pairs to enter the capsule and

interact with the aromatic regions of the cavitand[15]. Mixed-metal capsules containing Ga/Zn and Ga/Cu have been formed[16,17]. Adding copper to a solution of macrocycles forms metal-seemed capsules. Adding copper or zinc to gallium-seemed capsules creates a mixed-metal system[18,19]. When nickel and cobalt are used, antiferromagnetic exchange has been observed in the capsule[20]. Gaining control of the magnetic properties of nanostructures can be advantageous in many applications.

The nanocapsules can be used as a molecular-sized container to encapsulate pharmaceuticals. Unlike the conventional capsules used today, the nano-scale versions offer the possibility of more controlled drug release and delivery while at the same time drastically reducing necessary dosages and negative side effects[21]. Potentially, the capsule can be designed with receptors attached to the exterior that enable it to recognize the drug delivery target. This research contributes to the understanding of extracellular communication and molecular recognition. With the walls of the nanocapsule effectively acting as a barrier separating the drug from the receptor, the safer administration of many medicines, such as chemotherapeutics, that are not tolerable or dangerous at the required dosage is possible. Nanocapsules are already being used in topical and ophthalmic applications, in which the nanocapsules decrease the systemic absorption of the drugs and related negative effects[22]. Understanding the properties of the capsule wall is necessary for the design of pharmaceutical applications.

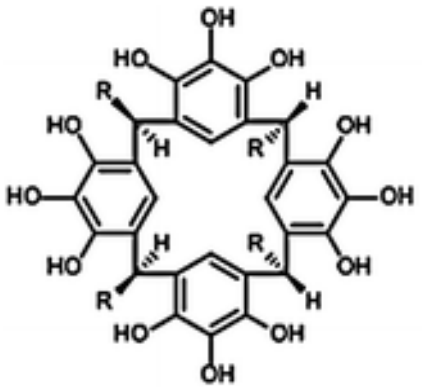

Figure 1.2 *C*-alkylpyrogallol[4]arene structure [R: phenyl]

A primary goal of the work has been to understand and ultimately direct the self-assembly process, the host-guest interactions, and properties of the supramolecular assemblage of capsules, tubes, or layers. In the current study, only a subset of the possible mechanisms for capsule formation is examined. The capsules at the focus of this work are dimers of pyrogallol[4]arene. This macrocycle is made of four pyrogallol subunits that are connected by CHR linker groups (Figure 1.2). It is easily produced by an acid-catalyzed condensation reaction of pyrogallol and aldehyde. Once formed, the ring of hydroxyl groups on the upper rim of *C*-alkylpyrogallol[4]arene can interact with the hydroxyl groups on another macrocycle, thus enabling the structures to assemble into hydrogen-bonded dimers and hexamers. Metal-insertion of eight zinc atoms into these hydrogen bonds creates a metal seem around the capsule. When R is an aryl group, the addition of a pentacoordinate zinc[II] complex, specifically $Zn[NO_3]_2pyridine_3$, produces the first phenyl-substituted zinc dimeric nanocapsules[23], with eight zinc atoms bound to the hydroxyl oxygen atoms. Much research has been done on the R=alkyl systems because the dominant conformer is the cone. Already possessing the requisite half-capsule

geometry, cones need only seem with other cones to form capsules. It was found that when R=aryl the chair is the preferred conformation, rather than the cone. However, dimeric capsules still form, indicating that a conformational change from the chair to the cone must occur at some point either before or during the self-assembly process. The boat is the preferred conformation for calix[4]pyrogallol[24]. Selective formation of the *rccc* axial Cone stereoisomer has been shown to be possible when forming capsules using a quick, one-step synthesis that employs microwave irradiation[25]. The *rccc* term refers to the fact that all the R-groups are in a cis formation relative to a reference R-group. When all the groups are cis to each other, they can all be either axial or equatorial. The use of "*t*" in this notation denotes that an R-group is trans to the reference R-group, "*r*". In the structures with both axial and equatorial R-groups, the reference R-group is always in the axial position.

This study is an investigation of the possible conformations of *C*-phenylpyrogallol[4]arene and pyrogallol[4]arene, their relative stabilities, and solvent interactions to add to the understanding of how the self-assembly process occurs

1.1.1 Experimental Background

The experimental portion of this study has been conducted by Andrew K. Maerz of the Jerry Atwood Group at the University of Missouri-Columbia (please see Ref. [6]). Four pyrogallol molecules come together to form the macrocycle

pyrogallol[4]arene by a simple reaction of equal molarities of pyrogallol and benzaldehyde in a mixture of ethanol and HCl. After refluxing for 24 hours, the solution is filtered with cold methanol producing an 80.6% yield of white crystals. To produce R-substituted pyrogallol[4]arene, the desired group need only be part of the aldehyde used in the synthesis to be easily incorporated into the structure of the macrocycle.

Resorcinol can also be used in a similar reaction to produce macrocycles composed of four subunits. Each resorcinol subunit lacks one hydroxyl group (in the medial position, compared to pyrogallol). The same result has also been seen for calix[4]arenes, which on the upper rim have no hydroxyl groups but only one R-group. Previous work showed the preferred conformation for both of these macrocycles to be the Cone. Both the Cone and Chair are initially formed but as the reaction is allowed to proceed the concentration of Chair product decreases. If allowed to reflux long enough, for 11 hours, only the Cone is present.

Because the Cone is such a commonly preferred product for resorcinol[4]arene and calyx[4]arene, and pyrogallol[4]arene has even more hydroxyl groups to favorably interact to form a stabilizing hydrogen bond network along the upper rim of the macrocycle when in a Cone conformation, the Cone was the expected stereostructure for C-phenylpyrogallol[4]arene. Additionally, when no R-group is present, R=H, the product is the Cone. However, NMR and X-ray crystallography analysis confirmed that, when the R-group is an aryl compound, formation of the Chair occurs, rather than the Cone. Even if the reaction is put under reflux conditions for a week, the Chair does not convert to the Cone. A large variety of alkyl-, nitro-,

hydroxyl-, and methoxyl- substituted phenyl groups were used to test the effect of R-group on stereoisomer formation. In all cases, the Chair was produced and in a few cases the Boat was also observed and once a Partial Cone was produced. When R is an aryl compound, the Cone is not produced.

Altering the solvent has some effect on the product. When R=phenyl, the Chair is formed in a 3:1 mixture of dimethyl sulfoxide (DMSO) in equal parts methanol and acetonitrile. However, if only methanol is used as the solvent, the boat is formed. In the solid state, it has been observed that oxygenated aprotic solvents such as DMSO and dimethylformamide (DMF) have an obvious effect on the structure as they are able to hydrogen bond with the phenolic protons. This interaction causes the protons to rotate out of the plane of the pyrogallol subunit, thereby disrupting the stabilizing intra- and intermolecular hydrogen bonds. The solvent's ability, or inability, to interact with the hydroxyl groups of the macrocycle has an impact on which stereoisomer is formed.

Because pyrogallol[4]arene appears to exist in a Chair rather than a Cone conformation, it was a surprise to find that it still forms nanocapsules upon the addition of pentacoordinated zinc(II) complexes. Dimerization occurs in a solution of 3:1 methanol:acetonitrile with $ZnL_3(NO_3)_2$, where L = equatorial ligand. The formation of the capsule confirms that a conversion from the Chair to the Cone must occur. To gain a better understanding of the thermodynamics of this system, as well as the solvent interactions with the macrocycle, the present computational study was performed.

1.2 Methods

All calculations were done with the Gaussian03[26] and Gaussian09[27] suites. The 6-31G(d,p) basis set was used for all calculations. All geometries were optimized and frequencies calculated using the B3LYP[28-30] and wB97XD[31,32] functionals. Single-point MP2 calculations at the 6-31G(d,p) level were performed on both the B3LYP and wB97XD optimized structures. Intrinsic reaction coordinate (IRC) calculations were performed on transition states to determine the minima they connect. Atoms-in-molecules (AIM) calculations were performed to verify the presence of bond critical points between structures.

Single-point energies of the gas-phase optimized structures in a solvent shell were calculated using the Polarizable Continuum Model (PCM). Interactions of the solute with the solvent are modeled using a solvent reaction field rather than explicit solvent molecules. The solvent is considered to be a continuous medium represented by a solvent-specific dielectric constant with surface tension at the solute-solvent boundary. The Integral Equation Formalism (IEF)-PCM and Solvation Model Density (SMD)-PCM[33] methods were both employed. The IEF-PCM method creates a solute cavity formed of overlapping nuclear-centered spheres. The solvation free energy is based on the bulk electrostatic interaction between the solute and self-consistent reaction field of the solvent. The SMD-PCM method begins with the same treatment of the solute as the IEF-SMD method, but improves the solvation free

energy by adding a correction for short-range interactions (within the first solvation shell) between the solute and the implicit solvent field based on the quantum mechanical charge density. This contribution is proportional to the amount of surface area of solute atoms accessible to the solvent.

The solvents acetonitrile, DMSO, and methanol were chosen for the calculations because these are the solvents that are used experimentally for this system. The SMD method has been found to accurately reproduce experimental free energies of solvation of neutral small organic compounds[34] and macrocyclic sulfonates[35] at the B3LYP/6-31+G(d,p) level, outperforming the IEF-PCM method. The $\Delta G_{solvation}$ at 298 K is calculated by taking the difference in the gas-phase and SMD-PCM free energies.

Density Functional Theory uses functionals of the electron density to calculate the electronic structure of a system rather than a multi-electron wavefunction. Hybrid functionals are a combination of an exchange and a correlation functional. The exact exchange energy is calculated using the Hartree-Fock method. Both B3LYP and wB97XD are hybrid functionals. Early DFT methods, including B3LYP, do not include terms to calculate dispersion forces. Although dispersion forces can be relatively weak they become more important as the size of the system increases. Because the macrocycles are large compounds composed of nonpolar arenes with significant hydrogen bonding, these forces are important to take into consideration. MP2 theory can be used to include some dispersion effects. This method uses perturbation theory to calculate the correlation energy correction. However, it is not computationally feasible to perform MP2 optimizations on these systems. To address

this problem the wB97XD functional was used. This functional includes empirical atom-atom dispersion and long-range corrections. It was shown to perform significantly better than previous functionals on systems with non-bonding interactions. The long-range corrections increase the distance at which the non-coulomb part of the exchange functional is calculated. An ultrafine grid was used, specified by the Gaussian keyword option "integral=ultrafine" for all DFT calculations. This option specifies the use of a so-called pruned grid when evaluating the two-electron integrals. This was used to increase the accuracy of the calculations.

1.3 Results and Discussion

1.3.1 Gas-Phase Calculations of *C*-phenylpyrogallol[4]arene, R=ph

1.3.1.1 Geometries of C-phenylpyrogallol[4]arene

There are three different types of orientations to consider when investigating the stable geometries of pyrogallol[4]arene. First is the position of the pyrogallol subunit in relation to the plane of the macrocycle. It can be either in the plane or roughly perpendicular to it, directed above or below. The position of the pyrogallol subunits determines the stereoisomer of the arene. All the structures are conformational stereoisomers of each other in that they all have the same connectivity. When the R-group is not hydrogen, the possibility of an axial or

equatorial R-group orientation creates a group of diastereomers of a particular stereoisomer.

The orientation of the hydroxyl groups determines the conformational isomer. The most stable form of pyrogallol is with all three hydroxyl groups pointing in the same direction. Another stable form of pyrogallol contains the medial hydroxyl group rotated 90° out-of-plane [oop] of the molecule. In this structure both side hydroxyl groups remain in-the-plane pointing towards the oxygen of the medial hydroxyl group. These are the two forms of pyrogallol found in the macrocycle (see Figure 1.8). The only exception to this is when a hydrogen from an edge hydroxyl group slightly rotates out of the plane, by 30° to 40°, to interact with nearby parts of the macrocycle. However, this geometry is not a stable conformation of the individual pyrogallol molecule.

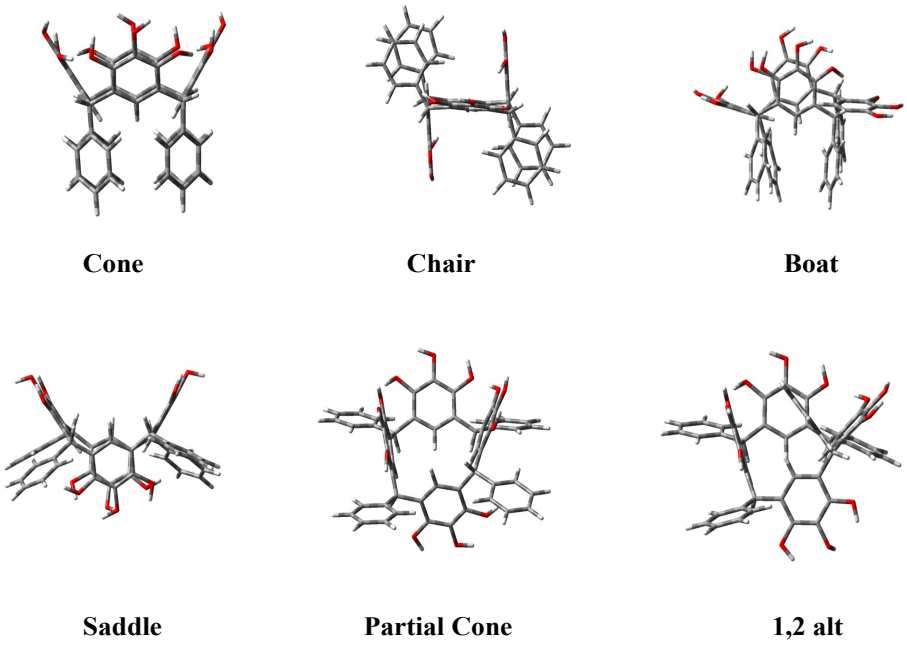

All structures optimized at the B3LYP/6-31g(d,p) level.

Figure 1.3. Stereoisomers of C-phenylpyrogallol[4]arene

The main structures are descriptively labeled the Cone, Chair, Boat, Saddle, Partial Cone, and 1,2 Alternate (Figure 1.3). The geometries for each stereoisomer were very similar whether B3LYP- or wB97XD-optimized. The cone structure has all four pyrogallol subunits pointing the same direction, which allows the hydroxyl groups to form a ring of internal hydrogen bonding along the upper rim of the Cone. It has C_4 symmetry, and the dihedral angle between adjacent pyrogallol subunits is ~ 0° (see Figure 1.11 for C-C-C-C angle description). This geometry is of great interest because it is the form of the macrocycle that assembles into dimeric and hexameric capsules. If a capsule is formed, then this geometry is ultimately achieved. To understand capsule complexation, the interconversion between the different minima

must be understood. While capsule formation from Cone structures makes intuitive sense, capsules also assemble from pyrogallol[4]arenes in the Chair conformation when R is an aryl group. The Chair is the only other isomer that is competitive with the Cone. Although similar in energy and experimentally observed in both the solvent and crystalline phases, the geometry of the Chair is quite disparate from that of the Cone. In the Chair, one pyrogallol subunit, the "back" of the Chair, is directed above the plane of the macrocycle while the opposing pyrogallol goes in the opposite direction, facing down below the plane of the macrocycle forming the "legs" of the chair. The two pyrogallol subunits between the "back" and "legs" lie flat in the plane of the macrocycle constituting the "arms" of the chair. Two stable Chairs were found, one with C_1 symmetry and the other with C_i symmetry. In the C_1 Chair all the hydroxyl hydrogens are in the plane of the pyrogallol while in the C*i* Chair the middle hydroxyl hydrogen is rotated out-of-plane on the "back" and "legs" pyrogallol subunits. The dihedral angle between pyrogallol subunits of Chair structures is 60° - 65°. In order for the Chair to convert to the Cone, three of the four subunits must change their orientation, two by ~90° and one by ~180°. Such rearrangement does not appear to be possible without breaking and reforming bonds due to the hindrance of bulky aryl groups between each pyrogallol.

The Boat is the other minimum that has been experimentally observed. The "sides" of the boat consist of two opposing pyrogallol subunits facing each other in the same direction above the plane of the macrocycle. The two subunits between the "sides" are in the plane of the macrocycle forming the "bottom" of the boat. These "bottom" pyrogallol subunits could rotate unhindered by the R-groups since all four

subunits are already in the same hemisphere of the macrocycle. The Partial Cone is a cone with one pyrogallol pointing the opposite direction as the three others. This is a stable minimum that can easily convert to the cone by the rotation of the wayward pyrogallol. Unlike in the chair, the R-groups do not appear to hinder this rotation. Three of the phenyl rings are in the equatorial position. One adjacent to the down-facing pyrogallol is in a distorted axial position. The R-group prevents the pyrogallol from rotating up to form the Cone. The 1,2 Alternate refers to the fact that there are two adjacent pyrogallol subunits directed up and two directed down. However, this structure can be distorted with one pyrogallol twisted in an opposite direction. This creates a geometry that is somewhat of a cross between the Chair and Partial Cone. The Saddle is actually similar to a 1,3 Alternate geometry with two opposing pyrogallol subunits facing each other, with oop hydrogen atoms, both directed above the plane of the macrocycle while the other two opposing pyrogallol subunits are directed below the plane of the macrocycle, near the phenyl groups. The phenyl groups are technically in an axial position, but the distorted geometry angles them more towards an equatorial position. The pyrogallol subunits are so splayed that the stereoisomer looks like a saddle.

1.3.1.2 Geometries of the Diastereomers of the Cone

There are diastereomers of the macrocycle based on the orientation of the R-groups. In some conformers, such as the chair, the position of the R-groups is

restricted by their geometry. For others such as the Cone and Boat, in which all the pyrogallol subunits are in one hemisphere of the macrocycle, it is possible for the R-groups to be in either the axial or equatorial position. The R-groups also have this freedom of position when the macrocycles join to form a capsule. The diastereomers of the Cone are depicted in Figure 1.4. The *rccc* axial Cone has all phenyl groups in the axial position. Moving one of these groups to the equatorial position creates the *rcct* Cone. The "*t*" indicates that one R-group is trans to the others. Switching two groups to the equatorial position forms the *rtct* and *rctt* Cones. In the *rtct* Cone the equatorial R-groups are opposite each other, while in the *rctt* Cone they are adjacent to each other. In the *rttt* Cone three phenyl groups are equatorial, or trans, to the one axial phenyl ring. If all four rings are in the equatorial position, that structure is denoted *rccc* [equatorial] Cone.

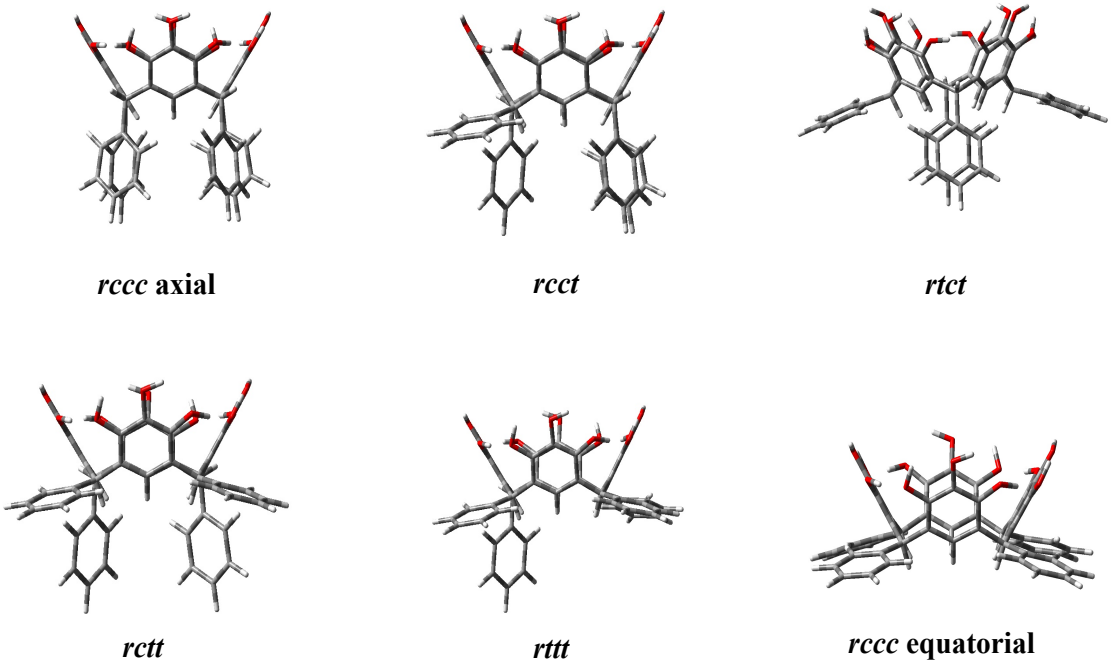

All structures optimized at the B3LYP/6-31G(d,p) level.

Figure 1.4. Diastereomers of the Cone

Solid-state experiments suggest that while it might not be important for the formation of the capsule, the R-group position is important to the arrangement of and communication between capsules in the crystal structure. Although all six geometries were found to be stable minima, the only observed orientations in both the crystal structure of the capsule and the solvated molecule are *rccc* [axial], *rctt*, and *rcct*. This apparent restriction of possible orientation of the R-groups could indicate what conformers are involved in forming capsules.

1.3.1.3 Energetics of C-phenylpyrogallol[4]arene

The relative enthalpies and free energies of the conformers of *C*-phenylpyrogallol[4]arene are listed in Table 1.1. Between the two functionals the results show that the relative energies from the wB97XD optimization more closely approach the MP2 single-point relative energies than do those from the B3LYP optimization. The wB97XD optimizations produced trends that match those of both the MP2//B3LYP and MP2//wB97XD single-point energies. The B3LYP optimization did not produce results similar to the other methods. The most important discrepancy is that, in terms of both ΔH and ΔG, the *rtct* Cone is calculated to be the most stable geometry, and thus the B3LYP calculations do not support the experimental observation that the C_1 Chair is the preferred structure. In fact, the *rtct* Cone is not even one of the experimentally observed Cone diastereomers. All three of the other gas-phase methods predict both the all-axial Cone and the C_1 Chair to be more stable than the *rtct* Cone (Table 1.1). Not only are they predicted to be more stable, but at all three levels the *rccc* (axial) Cone is preferred with respect to ΔH, but the C_1 Chair is preferred with respect to ΔG. The results of the MP2 single-point calculations correspond to the experimental results that the Chair is the observed structure.

Table 1.1 Gas-phase relative enthalpies and free energies of *C*-phenylpyrogallol[4]arene[a]

	B3LYP[b]		wB97XD[c]		MP2//B3LYP[d]		MP2//wB97XD[e]	
Structure	ΔH	ΔG	ΔH	ΔG	ΔH	ΔG	ΔH	ΔG
Cone [R=axial]	4.0	7.8	0.0	0.9	0.0	11.2	0.0	18.1
Cone [R=equatorial]	5.4	8.1	35.4	30.1	23.8	34.0	34.2	46.2
Chair C_1	29.2	9.3	20.7	0.0	12.5	0.0	3.5	0.0
Chair C_i	73.9	50.1	75.2	45.7	68.8	52.5	62.9	50.7
Boat	54.6	32.7	51.6	31.7	43.1	28.7	39.7	37.0
Saddle	82.8	66.6	91.9	77.1	73.7	64.9	78.8	81.1
Partial cone	31.0	20.7	53.6	38.8	39.7	36.7	47.5	49.8
1,2 alta	28.5	17.0	34.2	22.5	24.0	20.0	58.4	43.6
rtct Cone[f]	0.0	0.0	25.7	20.5	15.1	22.6	25.6	37.4

[a] All values in kJ/mol. [b] B3LYP/6-31G(d,p) optimized. [c] wB97XD/6-31G(d,p) optimized. [d] MP2/6-31G(d,p)//B3LYP/6-31G(d,p) single-point energy + B3LYP thermal correction terms. [e] MP2/6-31G(d,p)//wB97XD/6-31G(d,p) single-point energy + wB97XD thermal correction terms. [f] See Figure 2 for all cone stereoisomers.

The other notable difference about the B3LYP results from the others is that the spread of relative energies is much less than that of any of the other relative energies, even the MP2 single-point relative energies based on the B3LYP optimized geometries. The B3LYP method seems to overemphasize the relative stability of the stereoisomers. Not only are the magnitudes of the relative energies different but also the order of stability is more similar among the wB97XD and MP2 sets of data than for the B3LYP set.

The gap in ΔH between the global minimum all-axial Cone and the C_1 Chair decreases as more electron correlation is included in the calculation. At the B3LYP level this gap is 25.2 kJ/mol and it decreases to 3.5 kJ/mol at the MP2/wB97XD level. The ΔG data predicts the C_1 Chair to be more stable than the all-axial Cone, but their differences in relative energies increase as more electron correlation is included in the

calculations. Inclusion of dispersion forces stabilizes the C_1 Chair with respect to the Cone.

There is a surprisingly large difference in energy between the C_1 Chair and C_i Chair. Across all methods the C_i Chair is less stable by 40.8 – 59.4 kJ/mol. This cannot be completely due to the main geometrical difference between the structures, which is rotation of the medial hydrogen atom oop on two pyrogallol subunits, because that only accounts for less than 20 kJ/mol (Figure 1.6). Preliminary calculations show the same trend is also seen for the 1,2 Alternate structure. In both cases, the pyrogallol subunits are not close enough to interact with the adjacent pyrogallol subunits, so rearrangement of their hydroxyl groups does not affect other hydrogen bonding interactions within the macrocycle. The stability of the Cone can be explained as being from the result of so much internal hydrogen bonding within the arene. However, the Chair lacks such obvious hydrogen bonding between its pyrogallol subunits and yet is still very stable. A partial explanation might be that even though the Chair's pyrogallol subunits are not close to each other, there is enough interaction to cause an outer hydroxyl group on each pyrogallol subunit to rotate slightly, ~30°, out of the plane towards the neighboring pyrogallol. This type of interaction not as strong in the C_i Chair because on the "back" and "legs" of the chair the 90° oop medial hydrogen rotation causes the adjacent hydrogen atoms to orient themselves towards the medial oxygen to preserve internal hydrogen bonding. The 30° oop rotation is also present on the other two pyrogallol subunits that form the "arms" of the chair.

This same type of interaction is even more pronounced in the Boat. The hydroxyl groups on top of both "sides" of the boat are oriented in the same direction. The pyrogallol that the hydrogen atoms are directed towards is flat in the plane of the macrocycle. However, the opposing pyrogallol that forms the rest of the "bottom" of the boat does not have hydrogen atoms coming towards it but rather faces oxygen atoms. The result is a ~40° oop rotation of the outer hydrogen that is not part of an intra-pyrogallol hydrogen bond towards the closest oxygen. This interaction is further facilitated by the fact that the pyrogallol, with the oop hydrogen, is itself rotated up out of the plane of the macrocycle towards the "side" of the boat and its hydroxyl groups.

All four gas-phase methods predict the Saddle to be the least stable minimum. In this structure all four pyrogallol subunits are spread as far apart from each other as possible, with the result that two of the pyrogallol subunits are very close to the R-groups. The only opportunity for a stabilizing non-covalent interaction is C-H…O hydrogen bonding between pyrogallol and phenyl.

1.3.1.4 Energetics of the Diastereomers of the Cone

The relative energies of the cone diastereomers depend greatly on the method used [**Table 1.2**]. As is the case with the other conformers, the results of the wB97XD optimizations and MP2 single-point calculations are very similar, in magnitude and trend, but differ from the results of the B3LYP optimization. The

greatest disparity is still that at the B3LYP level the *rtct* diastereomer is the most stable, in terms of both enthalpy and free energy, with a decrease of stability by only a couple of kilojoules per a mol as the structures progress to all phenyl rings being in either the axial or equatorial position. Despite the B3LYP preference for the *rtct* Cone, only the *rccc* [axial], *rctt*, and *rcct* Cones have been experimentally observed. At all levels in the gas- and solvent-phase, except for the B3LYP optimization and PCM-B3LYP, these are the three most stable forms of the cone (with the *rctt* and *rtct* Cones being approximately equivalent).

Table 1.2 Relative energies of cone diastereomers

Cone	B3LYP[b]		wB97XD[c]		MP2//B3LYP[d]		MP2//wB97XD[e]	
Diastereomer	ΔH	ΔG	ΔH	ΔG[f]	ΔH	ΔG[f]	ΔH	ΔG[f]
rccc axial	4.0	7.8	0.0	0.9	0.0	11.2	0.0	18.1
rcct	3.2	1.8	16.5	11.6	9.4	15.5	16.7	28.9
rtct	0.0	0.0	25.7	20.5	15.2	22.6	25.6	37.4
rctt	3.8	2.0	25.3	19.5	15.9	21.5	25.5	36.9
rttt	3.2	1.9	31.3	26.4	20.1	26.2	30.7	43.0
rccc equatorial	5.4	8.1	35.4	30.1	23.8	34.0	34.2	46.2

[a] All values in kJ/mol. [b] B3LYP/6-31G(d,p) optimized. [c] wB97XD/6-31G(d,p) optimized. [d] MP2/6-31G(d,p)//B3LYP/6-31G(d,p) single-point energy + B3LYP thermal correction terms. [e] MP2/6-31G(d,p)//wB97XD/6-31G(d,p) single-point energy + wB97XD thermal correction terms. [f] All values are relative to the C_1 Chair, which is the global minimum at this level.

The inclusion of dispersion forces in the wB97XD functional and MP2 method is evident as both the relative ΔH and ΔG increase as the R-groups become more separated. The most stable form corresponds to all phenyl rings being in the axial position. This arrangement allows for the most intramolecular interaction. As each ring is moved one-by-one into the equatorial position, and therefore farther away

from the other phenyl groups, the stability of the macrocycle decreases. The B3LYP results do not produce this trend. At that level there is no correlation between an increasing number of R-groups in the equatorial position and a decrease in stability.

At the B3LYP level all Cone conformers are within 10 kJ/mol of each other, while at the other levels that range is expanded to 35.5 kJ/mol. The energies are closest for the structures with half the rings in the axial position, *rtct*, in which the two rings are facing each other, and *rctt*, in which the rings are ortho to each other. At all but the B3LYP/6-31G(d,p) level, these two structures' energies are within 1 kJ/mol of each other. The B3LYP functional, rather than increasing the closeness of relative energies compared to the other methods, actually increases that difference slightly to 3.8 and 2.0 k J/mol for ΔH and ΔG respectively.

1.3.1.5 MP2//B3LYP versus MP2//wB97XD for C-phenylpyrogallol[4]arene

That the MP2 single-point values show relatively the same trends whether based on the B3LYP or wB97XD geometries is not surprising because there is not a large difference in the geometries of the structures optimized at these two levels. The range of values is wider at the MP2/wB97XD level then at the MP2/B3LYP level, but the order of stability is similar. The data produced by the wB97XD method resembles the MP2 results very well, whether the MP2 single-point is based on the B3LYP- or wB97XD-optimized geometry. Comparing the values of the MP2 energies [Table

1.3], the single-point energies that are based on the structures that were wB97XD optimized are lower than those for the B3LYP optimized structures.

Table 1.3 MP2/B3LYP versus MP2/wB97XD//MP2 for *C*-phenylpyrogallol[a]

	Relative MP2 Energy	
Stereoisomer	B3LYP	wB97XD
rccc Cone [axial]	9.9	0.0
rcct Cone	5.2	0.0
rtct Cone	1.4	0.0
rctt Cone	3.1	0.0
rttt Cone	1.4	0.0
rccc Cone [equatorial]	1.4	0.0
Chair C_1	20.8	0.0
Chair C_i	16.2	0.0
Boat	14.6	0.0
Saddle	7.1	0.0
Partial Cone	3.4	0.0
1,2 Alternate	11.5	0.0

[a] All values in kJ/mol.

1.3.2 Gas-Phase Calculations of Pyrogallol[4]arene

1.3.2.1 Geometries of Pyrogallol[4]arene

There are several stable conformers of the pyrogallol[4]arene that correspond to the *C*-phenylpyrogallol[4]arene Cone, Chair, Boat, and Partial Cone (Figure 1.5). These all have the same basic structures as their R=ph counterparts. The lack of large R-groups eliminates the possibility of having diastereomers of the species. This decrease in the number of possible species makes this system more amenable to the investigation into the effects of hydroxyl group orientation on the macrocycle. There

is a C_4 version of the Cone, Cone A, with all the hydroxyl groups oriented the same direction creating a hydrogen-bonding network around the top of the pyrogallol subunits. Cone B is a regular cone with a peculiar hydrogen-bonding motif. In this structure two of the pyrogallol subunits have their hydroxyl groups facing the same direction and the hydroxyl groups on the other two pyrogallols face the opposite direction. At the intersection of same-facing hydroxyl groups, the unfavorable proximity of the hydrogen atoms results in one of these rotating oop. This structure was found by optimizing a boat geometry with the hydroxyl groups on two adjacent pyrogallol subunits pointing the same direction and the hydroxyl groups on the other two adjacent pyrogallol subunits pointing the opposite direction. Without the interference of a bulky R-group, all pyrogallol subunits rotated without barrier to form Cone B, either up from the "bottom" of the boat or out from the "sides" of the boat. Surprisingly, the hydroxyl groups did not re-orient to all face the same way but instead remained in a less stable geometry.

There are four different Chairs that all have the same basic pyrogallol orientation but different hydroxyl group orientations. Chair A is the R=H counterpart to the C_1 Chair in that all the hydrogen atoms are in the same plane as the pyrogallol and all point in the same direction. The dimensions of Chair A are similar to those of the C_1 Chair. The dihedral angle between adjacent pyrogallol subunits is 60° - 65°, like the R=ph Chairs. Chair B and Chair C both have two oop hydrogens, one on the "back" and one on the "legs" of the chair. These two chairs are very similar, both having a distorted 1,2 Alternate geometry in that the pyrogallol arms are tilted, one toward the upward pyrogallol (the "back" of the Chair) and the other toward the

downward pyrogallol (the “legs” of the Chair”). The dihedral angle between pyrogallol subunits facing the same direction is ~18°, which is not quite the same as for a 1,2 Alternate, ~0° (same as the Cone) and also not the -60° typical of Chair geometries.

The difference between these structures is that in Chair B the two oop hydrogens are pointing towards the inside of the macrocycle, while in Chair C they are pointing towards the outside of the macrocycle. Chair B is a transition state at the B3LYP level and Chair C is a transition state at both levels. IRC calculations on these transition states have been inconclusive, at best yielding the starting structure (still bearing an imaginary frequency) and a new 1,2 Alternate geometry. These calculations are ongoing, as the potential energy surface at this location is very flat and subsequent IRC calculations consistently produce similar saddle points rather than minima. Chair D has an oop hydroxyl group on every pyrogallol. This structure has sharp ~90° angles between the pyrogallol subunits, unlike the slanted Chairs B and C or the typical ~60° of Chair A.

Cone A, C_4

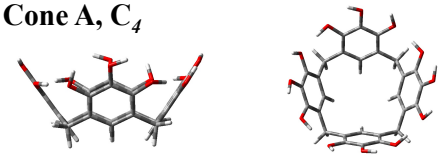

Cone B, C_2

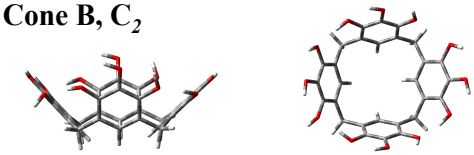

-

Chair A, C_i

Chair B, C_i

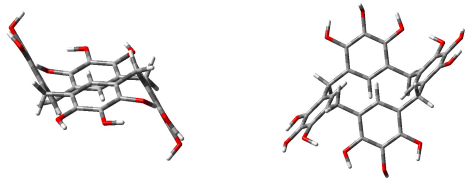

Chair C, C_i

Chair D, C_s

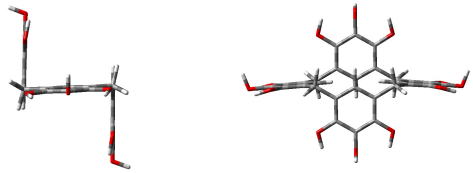

-

Boat A, C_1

Boat B, C_2

-

Partial cone, C_1

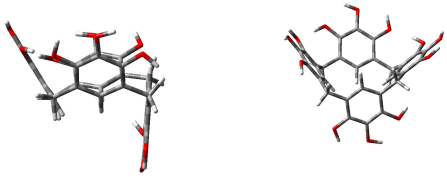

All structures optimized at the B3LYP/6-31G(d,p) level.

Figure 1.5 Stereoisomers of pyrogallol[4]arene

The only stereoisomer that was not found for the R=H system is the Saddle. This structure was searched for by starting with the R=ph Saddle geometry and replacing the phenyl groups with hydrogens. This structure optimized to Boat B when the opposing, facing pyrogallol subunits moved closer to allow a hydrogen bonding interaction between the hydroxyl groups and the pyrogallol subunits that comprise the "sides" of the Saddle moved to the plane of the macrocycle. The medial hydroxyl groups remain oop (as they began) in the Saddle structure. Boat A has the same geometry as the R=ph Boat with all hydroxyl groups in the plane, with the exception of the subtle oop rotation to accommodate a hydrogen bonding interaction across the top of the two "sides" of the Boat. The only difference between the two Boats is the oop hydrogen on the "bottom" pyrogallol subunits. The distances between the "side" pyrogallol subunits differ by only .003 Å.

The Partial Cone geometry is strikingly similar to the R=ph Partial Cone. Finding the stable form of this stereoisomer, without the large, obstructive phenyl groups to prevent the rotation of the one opposing pyrogallol subunit into a cone geometry, shows that this is a stable minimum in the absence of steric hindrance from the R-groups and that conversion to the Cone from this geometry is not barrierless. A transition state was found that connects these minima with a barrier of 17.2 kJ/mol.

1.3.2.2 Energetics of Pyrogallol[4]arene

The gas-phase results for the optimization of pyrogallol[4]arene, R=H, Table 1.4, are noticeably different from the R=ph system in that across every method the predicted global minimum is Cone A by 42.6-84.3 kJ/mol. Unlike the R=phenyl conformers, the addition of the thermal correction terms does not alter the identity of the global minimum. This result strongly correlates with the experimental observation that, unless R=ph, the preferred structure is the Cone.

Table 1.4 Gas-phase relative energies of pyrogallol[4]arene

	B3LYP[b]		wB97XD[c]		MP2/B3LYP[d]		MP2/wB97XD[e]	
Stereoisomer	ΔH	ΔG	ΔH	ΔG	ΔH	ΔG	ΔH	ΔG
Cone A	0.0	0.0	0.0	0.0	0.0	0.0	0.0	0.0
Cone B	63.5	53.0	64.5	54.3	66.2	55.7	66.9	56.3
Chair A	62.2	42.6	82.4	60.0	66.7	47.1	84.3	61.0
Chair B	86.2[f]	79.8[f]	89.2	74.5	91.8	85.4	95.2	79.9
Chair C[f]	87.1	79.6	88.5	84.8	94.0	86.5	94.7	90.9
Chair D	146.3	121.6	141.4	120.0	152.0	127.3	151.1	126.4
Boat A	85.9	65.8	59.0	47.1	61.1	41.0	58.4	43.6
Boat B	102.9	86.0	76.4	64.2	79.6	62.7	75.8	63.2
Partial Cone	55.4	39.2	51.1	38.4	52.0	35.8	51.5	38.3

[a] All values in kJ/mol. [b] B3LYP/6-31G(d,p) optimized. [c] wB97XD/6-31G(d,p) optimized. [d] MP2/6-31G(d,p)//B3LYP/6-31G(d,p) single-point energy + B3LYP thermal correction terms. [e] MP2/6-31G(d,p)//wB97XD/6-31G(d,p) single-point energy + wB97XD thermal correction terms. [f] This structure is a transition state.

The odd orientation of the hydroxyl groups in Cone B accounts for the lack of stability compared to Cone A. This is the only difference between the structures, and the disruption of two hydrogen bonds and the awkward, forced oop hydrogen account for a decrease of stability by ~55 – 65 kJ/mol, depending on the method used.

The progressive destabilization of the energy of the Chair geometries as the number of oop hydrogens increases is clearly evident in the data. Chair A is the lowest-energy Chair and is comparable to Cone B in energy. The gap in stability between Cone A and Chair A is much greater when R=H than when R=ph. As stated above, the addition of thermal correction terms, while stabilizing Chair A relative to Cone A, is not enough to change the identity of the global minimum.

The relative energy between pyrogallol and pyrogallol with an oop hydrogen is 6.2 – 8.9 kJ/mol, depending on the method (See

Table 1.10). The average difference in energy between Chair A and Chair B is 22.0 kJ/mol. There is also a slight change in geometry, as described in the previous section, which would account for the remaining energy difference. Recall that the only difference between Chair B and Chair C is the rotation of the oop hydrogen either inside the macrocycle or outside of the macrocycle, respectively. This is reflected in the very similar relative energies. It is slightly less stable for the oop hydrogen to point outside of the macrocycle, the greatest decrease in stability due to this rotation being found at the MP2//wB97XDlevel. Unlike a typical transition state that is noticeably higher in energy than the minima it connects, the Chair transition state structures are not much higher in energy compared to similar minima. The barrier for conversion between stereoisomers is not very high.

Chair D is by far the least stable Chair geometry and is the least stable of all the R=H structures. All pyrogallol subunits have the medial hydrogen oop. The geometry overall is far more rigid with 90° angles between subunits, instead of the typical 45° - 60°, which prevents stabilizing hydrogen bonding between the subunits.

When the medial hydrogen is oop, the other two outer pyrogallol hydrogen atoms also rotate to interact with the oxygen of the oop hydroxyl group and thus cannot interact with the hydroxyl groups of nearby pyrogallol subunits. This structure shows the importance of the barely noticeable ~30° oop rotation of the edge hydroxyl groups of the pyrogallol subunits to the overall stability of the macrocycle.

A similar trend is seen for the two Boats. The only difference between Boat A and Boat B is in the two pyrogallol subunits that constitute the "bottom" of Boat. Boat A has all in-plane hydrogen atoms, but Boat B, on the "bottom" pyrogallol subunits, has oop hydrogen atoms. The average difference in stabilities across the different levels is similar for the Boats, 18.6 kJ/mol, as compared to the average difference between Chair A and Chair B of 22.0 kJ/mol. These sets of structures are similar in that the only difference between them is two oop hydrogen rotations. These differences in energy are fairly close to the difference in energies for the same rotation in independent pyrogallol molecules. Neither of the Boat structures has enhanced stabilization from interacting pyrogallol subunits like the Chair does, so there is not such a dramatic difference in energies between the Boats as there is between Chairs B and C and Chair D. The Partial Cone is the most stable structure after Cone A. However, the average difference in stability between the two stereoisomers is slightly larger for the R=H Partial Cone, 45.2 kJ/mol, than for the R=ph structure, 34.5 kJ/mol. Possibly this is because when R=ph the downward-facing pyrogallol subunit has something to interact with to help stabilize the molecule. These numbers roughly reflect what is occurring in the geometrical difference between the Cone and Partial Cone, which is the breaking of two hydrogen bonds.

1.3.2.3 MP2//B3LYP versus MP2//wB97XD for pyrogallol[4]arene

The MP2 relative energies for the R=H structures are different from those for the R=ph system in that the wB97XD optimizations did not produce the most stable macrocycle at the MP2 level (Table 1.5). However, the difference is sufficiently small that these MP2 energies can be considered equivalent. Only Chair C and Boat B are slightly more stable when optimized with wB97XD, but that difference is still only 3.3 and 0.5 kJ/mol, respectively. The only incongruity in these results is that wB97XD Cone B is far less stable, by 19.7 kJ/mol, than its B3LYP counterpart. Cone B has an odd hydrogen-bonding motif in which the hydroxyl groups on two adjacent pyrogallol subunits are facing the same way, and this forces one of the hydroxyl groups oop. This highly unfavorable conformation could be the reason for the higher MP2 energy. The higher energy might be an example wherein the B3LYP level's neglect of dispersion forces results in a geometry that is more stable than it should be.

Table 1.5 MP2//B3LYP versus MP2//wB97XDfor pyrogallol[4]arene[a]

Stereoisomer	B3LYP	wB97XD
Cone A	0.0	2.1
Cone B	0.0	19.7
Chair A	0.0	0.05
Chair B	0.0	1.3
Chair C[d]	3.3	0.0
Chair D	0.0	0.2
Boat A	0.0	0.5
Boat B	0.5	0.0
Partial Cone	0.0	3.3

[a] All values in kJ/mol.

1.3.3 Macrocycle-Solvent Interactions

1.3.3.1 Solvent-Phase Calculations of C-phenylpyrogallol[4]arene

Two factors that contribute to the stability of the macrocycle are the internal hydrogen bonding within and between the pyrogallol moieties and the interaction of the structure with the solvent. In general, when a hydroxyl group rotates 90° out of the plane of the pyrogallol, there is a decrease in the amount of internal hydrogen bonding. Often a hydroxyl group will rotate out of the plane by less than 40° in order to interact with another component of the same macrocycle. This sacrifice of internal stability is compensated for when the oop hydroxyl group is now able to interact with the solvent. Polarizability by implicit solvent stabilizes the macrocycles. The PCM method addresses two types of polarizability, orientation and electronic. The orientation polarizability is due to permanent dipole moments, such as those of the hydroxyl groups, while electronic polarizability is the distortion of the electron distribution, which is important in the nonpolar regions.

The gas-phase trends are generally reproduced in the solvent-phase results, although the structures are all more stable relative to the global minimum (Table 1.6-Table 1.9). At the B3LYP level, for both the IEF and SMD methods, the *rtct* Cone is generally still the most stable structure. The exceptions are at the SMD-B3LYP level. In acetonitrile and methanol the structure favored enthalpically is the *rccc* (equatorial) Cone. That is the only time the *rccc* (equatorial) Cone is a global minimum.

However, in methanol at the SMD-B3LYP and SMD-wB97XD levels, the C_i Chair is the thermodynamically favored product.

The PCM-wB97XD results also reproduce gas-phase trends. The *rccc* (axial) Cone has the most stable enthalpy, but then the C_1 Chair has the most stable free energy. Again, there is the exception of the methanol-SMD results. As mentioned for the B3LYP results, the methanol-SMD-wB97XD level predicts the C_i Chair to be the thermodynamically favored product rather than the C_1 Chair. Unlike the other levels, the enthalpically favored product is the C_1 Chair rather than the C_i Chair by 6.6 kJ/mol.

The IEF results show that this method does not appear to discriminate between the different solvents very well. The relative energies of the stereoisomers across the three solvents differ by less than 1 kJ/mol. The two exceptions are the IEF-B3LYP C_1 Chair in acetonitrile and IEF-wB97XD C_i Chair in acetonitrile. These structures are less stable in acetonitrile by ~3 kJ/mol and ~5 kJ/mol, respectively.

One reason that the C_1 Chair might be favored over the C_i Chair is that even though the C_i Chair has oop hydroxyl groups to interact with the solvent, when this happens the other two hydroxyl groups, on either side of the oop one, are interacting with that medial oop hydroxyl oxygen. In the pyrogallol subunits on the C_1 Chair, both of those outer hydroxyl groups can interact with the solvent; one is already directed towards the solvent field while the other can rotate away from the medial hydroxyl group to also interact with the solvent. Model calculations show that on an individual pyrogallol molecule the rotation energy is 17.6 kJ/mol in the gas-phase, or about the amount of energy needed to break a hydrogen bond.

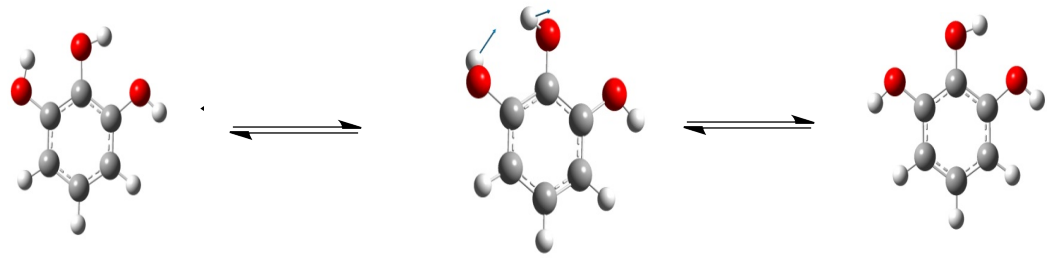

Figure 1.6 Transition state for hydroxyl rotation

The barrier to this rotation would be less in the solvent. The C_i Chair is more stable than the C_1 Chair only in methanol at the SMD-wB97XD level, and it is more stable by only 2.1 kJ/mol. This small difference is significant considering that at the other solvent levels the ΔG gap in stability between the two Chairs is 29.0 – 33.3 kJ/mol. This reversal is not because methanol stabilizes all the structures; rather, compared to the stabilization by the other solvents, everything is destabilized relative to the C_1 Chair except the C_i Chair and the Saddle.

Regarding the experimental question about the lack of capsule formation in DMSO, there is no enhanced stability of the Chair in DMSO at any level. The experimentally preferred Chair is relatively less stable in DMSO compared to the other solvents. There is no evidence here that stabilization of the Chair by the solvent is what prevents capsules from forming in DMSO. A structure modeling the interaction of an explicit DMSO molecule with 2 pyrogallol molecules, in a Chair-like conformation and connected by a C(H)(ph) linker group, showed the DMSO molecule interacting with, or bridging, both pyrogallol molecules (Figure 1.7). AIM

calculations showed the presence of bond critical points between the hydroxyl groups of one pyrogallol and the DMSO oxygen, while the hydrogen atoms on the DMSO methyl groups interacted with the hydroxyl groups of the other pyrogallol. The stabilization due to this interaction was only 5.1 kJ/mol. Again, this does not seem enough to explain why the Chair does not convert to form capsules.

Figure 1.7 DMSO interacting with two pyrogallol molecules

The dielectric constants of acetonitrile and methanol are closer in value to each other, 35.9 and 32.6, respectively, than to that of DMSO, 46.8. One might expect greater similarity between the data for acetonitrile and methanol, but this is not the case. The acetonitrile and DMSO SMD-PCM values are similar to each other and different from those obtained for methanol. As stated above, the results of the IEF calculations produce the same relative energies independent of the solvent. Both SMD calculations, using B3LYP and wB97XD, predict the C_i Chair to be the free energy global minimum in methanol. Crystal structure images show methanol bonding to the oop hydrogen (Figure 1.9), so this is known to be a favorable interaction.

Table 1.6 IEF-PCM/B3LYP[a] solvent-phase relative energies of C-phenylpyrogallol[4]arene

	acetonitrile		DMSO		methanol	
Stereoisomer	ΔH	ΔG	ΔH	ΔG	ΔH	ΔG
rccc Cone (axial)	5.1	10.7	5.0	10.7	5.1	10.7
rcct Cone	2.4	4.2	3.3	5.2	2.4	4.2
rtct Cone	0.0	0.0	0.0	0.0	0.0	0.0
rctt Cone	2.4	3.0	2.3	2.9	2.4	3.0
rttt Cone	2.3	2.3	2.3	2.3	2.4	2.4
rccc Cone (equatorial)	2.1	6.6	2.0	6.5	1.8	6.3
Chair C_1	25.1	6.9	22.2	4.1	22.4	4.3
Chair C_i	35.2	13.3	34.6	12.7	35.4	13.5
Boat	36.1	16.1	35.7	15.7	36.2	16.2
Saddle	50.0	35.7	49.5	35.2	50.2	35.8
Partial Cone	28.5	20.0	28.5	20.0	28.6	20.0
1,2 Alternate	25.8	16.1	25.7	16.1	25.8	16.2

[a] IEF-PCM B3LYP/6-31G(d,p)//B3LYP/6-31G(d,p) single-point energies in kJ/mol.

Table 1.7SMD-PCM/B3LYP[a] solvent-phase relative energies of C-phenylpyrogallol[4]arene

	acetonitrile		DMSO		methanol	
Stereoisomer	ΔH	ΔG	ΔH	ΔG	ΔH	ΔG
rccc Cone (axial)	8.7	14.2	7.0	12.7	9.4	21.9
rcct Cone	3.8	5.4	3.3	5.2	5.4	14.0
rtct Cone	0.2	0.0	0.0	0.0	0.9	7.7
rctt Cone	2.7	3.1	2.3	2.9	4.0	11.4
rttt Cone	0.8	0.6	1.4	1.4	2.1	8.9
rccc Cone (equatorial)	0.0	4.4	0.4	5.0	0.0	11.4
Chair C_1	21.5	3.2	20.8	2.7	14.6	3.3
Chair C_i	33.6	11.5	38.3	16.4	15.1	0.0
Boat	34.3	14.2	35.9	15.9	25.9	12.8
Saddle	49.3	34.8	53.8	39.4	61.7	54.2
Partial Cone	26.7	18.0	25.7	17.2	24.8	23.1
1,2 Alternate	24.0	14.2	24.0	14.4	20.3	17.5

[a] SMD-PCM B3LYP/6-31G(d,p)//B3LYP/6-31G(d,p) single-point energies in kJ/mol.

Table 1.8 IEF-PCM/wB97XD[a] solvent-phase relative energies of C-phenylpyrogallol[4]arene

	acetonitrile		DMSO		methanol	
Stereoisomer	ΔH	ΔG	ΔH	ΔG	ΔH	ΔG
rccc Cone (axial)	0.0	9.4	0.0	9.5	0.0	9.4
rcct Cone	15.2	18.8	15.3	19.0	15.2	18.8
rtct Cone	24.2	27.5	24.3	27.6	24.2	27.4
rctt Cone	22.9	25.6	22.9	25.8	22.9	25.6
rttt Cone	28.0	31.6	28.0	31.7	28.0	31.5
rccc Cone (equatorial)	29.9	33.2	29.9	33.3	29.9	33.2
Chair C_1	12.2	0.0	12.1	0.0	12.2	0.0
Chair C_i	34.3	13.4	28.0	7.3	28.1	7.1
Boat	31.5	20.1	31.2	19.9	31.6	20.1
Saddle	55.6	49.3	55.2	49.0	55.8	49.4
Partial Cone	50.0	43.7	50.0	43.8	50.0	43.6
1,2 Alternate	31.6	28.5	31.7	28.7	31.6	28.5

[a] IEF-PCM wB97XD/6-31G(d,p)//wB97XD/6-31G(d,p) single-point energies in kJ/mol.

Table 1.9 SMD-PCM/wB97XD[a] solvent-phase relative energies of C-phenylpyrogallol[4]arene

	acetonitrile		DMSO		methanol	
Stereoisomer	ΔH	ΔG	ΔH	ΔG	ΔH	ΔG
rccc Cone (axial)	0.0	14.7	0.0	13.2	5.3	29.0
rcct Cone	11.4	20.2	13.7	21.1	18.2	36.1
rtct Cone	17.7	26.2	21.3	28.3	24.5	42.0
rctt Cone	16.4	24.3	19.7	26.2	24.2	41.2
rttt Cone	19.6	28.4	24.1	31.4	27.0	44.8
rccc Cone (equatorial)	20.4	29.0	25.2	32.3	27.5	45.1
Chair C_1	6.9	0.0	8.4	0.0	0.0	2.1
Chair C_i	27.4	11.8	33.2	16.1	6.6	0.0
Boat	24.7	18.5	27.5	19.8	20.6	23.5
Saddle	49.2	48.1	57.0	54.4	29.0	37.0
Partial Cone	41.7	40.7	44.9	42.4	45.4	53.4
1,2 Alternate	25.6	27.8	28.0	28.7	25.9	37.0

[a] SMD-PCM wB97XD/6-31G(d,p)//wB97XD/6-31G(d,p) single-point energies in kJ/mol.

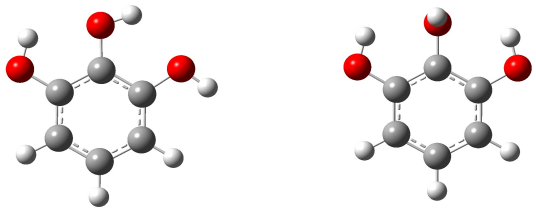

Figure 1.8 Pyrogallol and out-of-plane pyrogallol

Table 1.10 Relative instability of H oop pyrogallol with respect to pyrogallol

	B3LYP[a]				wB97XD[b]			
	ΔH		ΔG		ΔH		ΔG	
Gas-phase	**7.0**		**8.9**		**6.2**		**8.1**	
Solvent-phase	**IEF**		**SMD**		**IEF**		**SMD**	
	ΔH	ΔG	ΔH	ΔG	ΔH	ΔG	ΔH	ΔG
acetonitrile	**3.2**	**5.1**	**4.6**	**6.5**	**2.5**	**4.4**	**4.2**	**6.0**
DMSO	**3.6**	**5.5**	**5.2**	**7.1**	**2.5**	**4.3**	**4.7**	**6.5**
methanol	**3.3**	**5.2**	**2.7**	**4.6**	**2.6**	**4.4**	**1.8**	**3.7**

All values in kJ/mol. [a] IEF- and SMD-B3LYP/6-31G(d,p) [b] IEF- and SMD-wB97XD/6-31G(d,p)

1.3.3.1.1 Solvent-phase calculations of cone diastereomers

As noted above, reproducing gas-phase trends, both the IEF- and SMD-B3LYP methods predict the *rtct* Cone to be the most stable diastereomer, indeed the global minimum in most solvents. Both B3LYP solvent calculations predict the

experimentally observed *rccc* (axial) Cone to be the least stable of all the Cone diastereomers by 5.0 - 21.9 kJ/mol. Continuing this trend of not favoring the experimentally observed structures, the next least stable cones at the B3LYP level are the *rcct* and *rctt* Cones. However, the differences from the global minimum are less than 5 kJ/mol, except that the ΔG of *rctt* Cone in methanol-SMD is 11.4 kJ/mol.

The results of the wB97XD calculations are different from the B3LYP results in that the experimentally observed diastereomers are also the most stable computationally. The *rccc* (axial) cone is enthalpically the most stable, it is even the solvent-wB97XD global minimum of all the *C*-phenylpyrogallol[4]arenes, except in methanol at the SMD level. It is also the most stable cone diastereomer, though it is replaced by the Chairs as the most stable structures overall. In terms of stability the *rccc* (axial) cone is followed by the *rcct* and *rctt* Cones. The Cones that are not experimentally observed, *rtct*, *rttt,* and *rccc* (equatorial), are all the highest in energy. This reflects the wB97XD gas-phase trend of decreasing stability as more R-groups are moved into the equatorial position.

1.3.3.2 Solvent-Phase calculations of pyrogallol[4]arene

The most striking feature of the solvent-phase results for pyrogallol[4]arene is that the most stable structure, across all methods and all solvents, is Cone A. These results correlate very well with the experimental observation that when the R-group is alkyl rather than aryl, the Cone is the preferred stereoisomer. The implicit solvent

stabilizes all the structures relative to Cone A but, in contrast to the R=ph system, the Chair never comes close to consideration for the global minimum. The difference in free energy between Cone A and Chair A is at best 23.3 kJ/mol (methanol-SMD-B3LYP and at worst 52.8 kJ/mol (all solvents, IEF-wB97XD). With respect to enthalpy, Chair A is 42.8 kJ/mol (methanol-SMD-B3LYP) to 76.1 kJ/mol (all solvents, IEF-wB97XD) from being as stable as Cone A.

As seen in the *C*-phenylpyrogallol[4]arene results, the IEF method for the pyrogallol[4]arene yields essentially the same relative energies of the stereoisomers, independent of the identity of the solvent. Another repeated trend is seen when the identity of the solvent does make a difference. The SMD results yield values for acetonitrile and DMSO that are very similar to each other, whereas methanol stabilizes everything relative to the other two solvents.

Like the gas-phase results, the Chairs decrease in stability as more hydrogen atoms rotate oop, but in the solvent phase the spread in relative energies decreases, to ~40 kJ/mol from ~70 kJ/mol. The same trend is seen between the Boats at the B3LYP level. In the gas-phase Boats A and B are ~19 kJ/mol apart in energy. In the solvent-phase the difference in energy caused by the oop hydrogen decreases to 1.1 – 11.3 kJ/mol.

There is a strange turn-around in the relative energies of the Boats. Boat A is more stable than Boat B in the gas-phase and in B3LYP solvent-phase calculations. However, the wB97XD values rearrange this trend. If there is an error in these values, it has not yet been determined.

Table 1.11 IEF-PCM/B3LYP[a] solvent-phase relative energies of pyrogallol[4]arene

	acetonitrile		DMSO		methanol	
Stereoisomer	ΔH	ΔG	ΔH	ΔG	ΔH	ΔG
Cone A	0.0	0.0	0.0	0.0	0.0	0.0
Cone B	37.7	27.2	37.4	26.9	37.9	27.3
Chair A	54.1	34.5	54.1	34.5	54.1	34.5
Chair B[b]	57.2	50.8	56.9	50.5	57.3	50.9
Chair C[b]	57.9	50.4	57.6	50.1	58.0	50.5
Chair D	93.5	68.8	92.9	68.2	93.8	69.1
Boat A	78.3	58.2	78.3	58.2	78.3	58.2
Boat B	79.7	62.8	79.5	62.5	79.8	62.8
Partial Cone	48.5	32.2	48.5	32.2	48.5	32.3

[a] IEF-PCM B3LYP/6-31G(d,p)//B3LYP/6-31G(d,p) single-point energies in kJ/mol. [b] This structure is a transition state.

Table 1.12 SMD-PCM/B3LYP[a] solvent-phase relative energies of pyrogallol[4]arene

	acetonitrile		DMSO		methanol	
Stereoisomer	ΔH	ΔG	ΔH	ΔG	ΔH	ΔG
Cone A	0.0	0.0	0.0	0.0	0.0	0.0
Cone B	36.1	25.5	39.6	29.0	23.1	12.6
Chair A	47.9	28.3	50.0	30.4	42.8	23.2
Chair B[b]	55.5	49.1	60.0	53.6	41.7	35.2
Chair C[b]	56.4	48.9	60.7	53.2	42.7	35.2
Chair D	91.7	67.0	100.4	75.7	62.6	37.9
Boat A	75.0	55.0	76.1	56.0	61.2	41.1
Boat B	80.3	63.4	84.2	67.3	59.1	42.2
Partial Cone	44.8	28.6	46.3	30.1	38.8	22.5

[a] SMD-PCM B3LYP/6-31G(d,p)//B3LYP/6-31G(d,p) single-point energies in kJ/mol. [b] This structure is a transition state.

Table 1.13 IEF-PCM/wB97XD[a] solvent-phase relative energies of pyrogallol[4]arene

	acetonitrile		DMSO		methanol	
Stereoisomer	ΔH	ΔG	ΔH	ΔG	ΔH	ΔG
Cone A	0.0	0.0	0.0	0.0	0.0	0.0
Cone B	40.7	30.1	40.4	29.8	40.8	30.2
Chair A	76.1	52.8	76.1	52.8	76.1	52.8
Chair B	62.8	47.6	62.5	47.3	62.9	47.7
Chair C[b]	61.7	58.0	61.5	57.7	61.9	58.1
Chair D	95.6	70.9	95.0	70.3	95.9	71.2
Boat A	115.8	101.0	115.7	100.9	115.9	101.1
Boat B	57.6	44.9	57.4	44.8	57.6	45.0
Partial Cone	46.3	33.1	46.2	33.0	46.3	33.1

[a] IEF-PCM wB97XD/6-31G(d,p)//wB97XD/6-31G(d,p) single-point energies in kJ/mol. [b] This structure is a transition state.

Table 1.14 IEF-PCM/wB97XD[a] solvent-phase relative energies of pyrogallol[4]arene

	acetonitrile		DMSO		methanol	
Stereoisomer	ΔH	ΔG	ΔH	ΔG	ΔH	ΔG
Cone A	0.0	0.0	0.0	0.0	0.0	0.0
Cone B	39.7	29.1	42.6	32.0	25.9	15.2
Chair A	72.1	48.8	72.7	49.4	59.6	36.3
Chair B	61.8	46.6	66.3	51.1	45.8	30.6
Chair C[b]	60.7	56.9	65.2	61.5	45.0	41.3
Chair D	95.6	70.8	103.8	79.1	61.8	37.1
Boat A	111.4	96.6	115.9	101.1	88.1	73.3
Boat B	60.2	47.5	63.7	51.1	36.9	24.3
Partial Cone	43.3	30.1	44.6	31.4	36.6	23.4

[a] SMD-PCM wB97XD/6-31G(d,p)//wB97XD/6-31G(d,p) single-point energies in kJ/mol. [b] This structure is a transition state.

1.3.3.3 ΔG of Solvation

The $\Delta G_{solvation}$ was calculated (Table 1.15) in order to add another component to our understanding of why certain structures are observed in certain solvents rather than others. In general, the magnitude of the values of $\Delta G_{solvation}$ correlate with the number of hydroxyl groups available to interact with the solvent. These sites offer the opportunity for the most direct interaction with the solvent field. Following this trend, the Cones have the least favorable $\Delta G_{solvation}$ of all the stereoisomers while the Chairs have the most favorable solvent interaction. The C*i* Chair has a lower $\Delta G_{solvation}$ than the C_1 Chair by 27.1 – 47.8 kJ/mol. The Saddle and Boat have the next lowest values. These are the structures with the most oop hydroxyl groups as well as room for solvent interactions. The structures with higher $\Delta G_{solvation}$ values, the Partial Cone, 1,2 Alternate, and Cones, all have pyrogallol-pyrogallol interactions that limit the number of solvation sites.

Table 1.15 $\Delta G_{solvation}$ of C-phenylpyrogallol[4]arene [a]

	B3LYP[b]			wB97XD[c]		
Stereoisomer	acetonitrile	DMSO	methanol	acetonitrile	DMSO	methanol
rccc Cone (axial)	-133.3	-110.9	-145.1	-138.8	-119.3	-153.7
rcct Cone	-136.1	-112.4	-146.9	-143.9	-122.2	-157.3
rtct Cone	-139.7	-115.7	-151.4	-146.8	-123.8	-160.3
rctt Cone	-138.7	-114.8	-149.7	-139.8	-125.0	-160.2
rttt Cone	-141.0	-116.3	-152.2	-144.6	-126.6	-163.4
rccc Cone (equatorial)	-143.5	-118.9	-155.8	-153.7	-129.4	-166.8
Chair C_1	-145.8	-122.4	-165.1	-152.5	-131.6	-179.7
Chair C_i	-178.4	-149.5	-209.3	-186.5	-161.3	-227.5
Boat	-158.3	-132.6	-179.1	-165.7	-143.5	-190.0
Saddle	-171.5	-142.9	-171.5	-181.5	-154.3	-221.9
Partial Cone	-142.4	-119.2	-156.7	-150.6	-128.1	-167.2
1,2 Alternate	-142.6	-118.4	-158.6	-147.3	-125.5	-167.3

[a] All values in kJ/mol. [b] SMD-PCM B3LYP/6-31G(d,p)//B3LYP/6-31G(d,p) single-point energies. [c] SMD-PCM wB97XD/6-31G(d,p)//wB97XD/6-31G(d,p) single-point energies

Looking at the *C*-phenylpyrogallol[4]arene data, one might be tempted to think that the $\Delta G_{solvation}$ values can help predict which stereoisomers will be experimentally observed. However, the data for the pyrogalllol[4]arene system does not support such a correlation. All of the calculations thus far have strongly supported the global minimum status of the Cone when R=H but it has the highest $\Delta G_{solvation}$.

Table 1.16 $\Delta G_{solvation}$ of pyrogallol[4]arene, R=H[a]

	B3LYP[b]			wB97XD[c]		
Stereoisomer	acetonitrile	DMSO	methanol	acetonitrile	DMSO	methanol
Cone A	-90.9	-85.0	-112.3	-96.1	-90.8	-118.8
Cone B	-118.3	-109.0	-152.7	-123.4	-115.2	-160.0
Chair A	-105.1	-97.2	-131.8	-109.6	-103.7	-144.9
Chair B	-121.5[d]	-111.2[d]	-156.8[b]	-126.9	-117.1	-165.7
Chair C[d]	-121.5	-111.4	-156.7	-127.3	-117.5	-165.7
Chair D	-145.5	-130.9	-196.0	-149.9	-136.4	-206.4
Boat A	-101.7	-94.8	-137.1	-48.5	-38.6	-94.5
Boat B	-113.5	-103.7	-156.1	-115.3	-106.4	-161.3
Partial Cone	-101.5	-94.1	-129.0	-105.9	-99.3	-135.3

[a] All values in kJ/mol. [b] SMD-PCM B3LYP/6-31G(d,p)//B3LYP/6-31G(d,p) single-point energies. [c] SMD-PCM wB97XD/6-31G(d,p)//wB97XD/6-31G(d,p) single-point energies. [d] This structure is a transition state.

Among the Chairs, the higher number of oop hydroxyl groups correlates with a lower $\Delta G_{solvation}$, as it is with the *C*-phenylpyrogallol[4]arene Chairs. This trend is seen for all of the geometries, supporting the observation that the ease of solvation best correlates with available solvation sites. However, the thermodynamic stability of the cone outweighs its lack of free hydroxyl groups and corresponding relatively unfavorable $\Delta G_{solvation}$.

1.3.4 Gas-phase Calculations of *C*-phenylpyrogallol[4]arene with Explicit Solvent

Gas-phase calculations of the macrocycle interacting with explicit solvent molecules show that these interactions stabilize the system. Reasons for this are that when the solvent is bound to hydroxyl protons on the independent pyrogallol groups in the chair and boat there is no disruption of the internal hydrogen bonding between the subunits of the macrocycle. In the cone configuration, such solvent bonding would disrupt the intramolecular hydrogen bonding as the outer pyrogallol hydroxyl proton has the opportunity to hydrogen bond to the hydroxyl groups on the adjacent pyrogallol subunits.

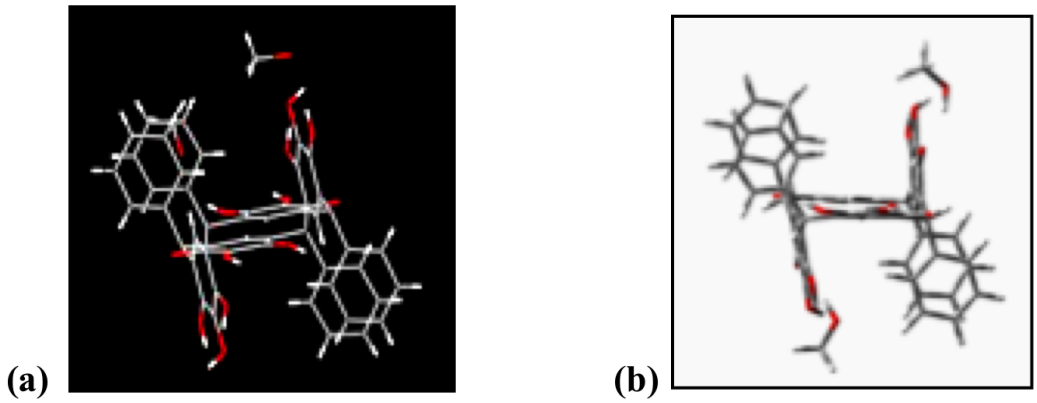

Crystal structure courtesy of Andrew Maerz.

Figure 1.9 (a) Crystal Structure of C_i Chair with methanol (b) B3LYP/6-31G(d,p) optimized crystal structure geometry

In the crystal structure of the Chair, individual methanol molecules are seen bound to the oop hydrogen on the Chair's "back" and "legs." The solid-state geometry was optimized at the B3LYP/6-31G(d,p) level and was found to be stable with the methanol hydrogen-bonded to the oop hydroxyl groups, as they are in the crystal structure (Figure 1.9). Among the models of this interaction between an individual pyrogallol molecule and an explicit methanol molecule, this was found to be one of the most stable methanol-pyrogallol geometries. Computationally, adding two methanol solvent molecules stabilizes the C_i Chair by 38.5 kJ/mol. This is a reasonable amount considering that two hydrogen bonds have been added. In contrast, this interaction only stabilizes the C_1 Chair by 2.3 kJ/mol. It is not beneficial to the C_1 Chair to form this interaction, because intramolecular hydrogen bonds must be broken to form this bond with the solvent. A crystal structure geometry of the Boat, R=4-propoxybenzene, with two bridging methanol groups was also optimized (Figure 1.10). The same addition of two methanol solvent molecules to the Boat stabilizes that structure by 14.3 kJ/mol. As with the C_1 Chair, the sacrifice of internal hydrogen bonding decreases the amount of stabilization by the solvent.

(a) 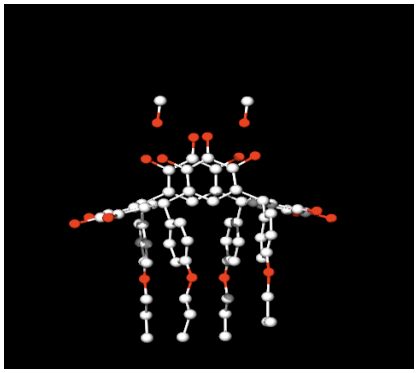 (b) 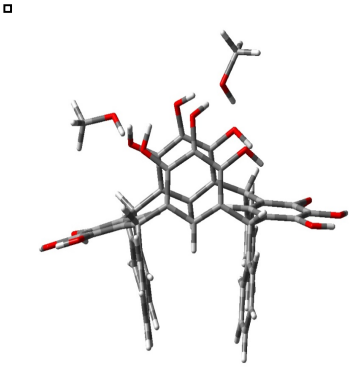

Crystal structure courtesy of Andrew Maerz.

Figure 1.10 (a) Crystal Structure of the Boat with methanol, R=4-propoxybenzene (b) B3LYP/6-31G(d,p) optimized crystal structure geometry

1.3.5 Transition States

A gas-phase transition state was found that involves the rotation of pyrogallol from a chair-type geometry to that of a cone without the assistance of solvent or metal complexes. A structure consisting of two pyrogallol molecules connected by C(H)(ph) was used to model the connectivity of two pyrogallol units in the macrocyle. This structure is stable in both Cone- and Chair-like geometries, with the dihedral angle between the pyrogallol molecules CCCC = ~4.3° and CCCC = ~45.3°, respectively. The same angle in the transition state is -53.2° (depicted in yellow Figure 1.11). The imaginary frequency is for an oop wag of the hydrogen that is directed towards the other pyrogallol (depicted by the blue arrow in Figure 1.11). The barrier for this transition is only 11 kJ/mol.

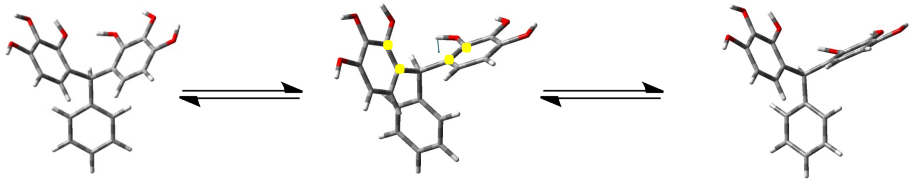

Figure 1.11 Transition state connecting cone and chair model geometries

Thus far a similar transition state has not been found for the structure's R=H counterpart. If no such transition state exists then the rotation of the pyrogallol subunits from a chair-like geometry to a cone-like can be considered to be barrierless. Barrierless interconversion can help explain why the Cone is consistently preferred over the Chair, both experimentally and computationally, for R=alkyl.

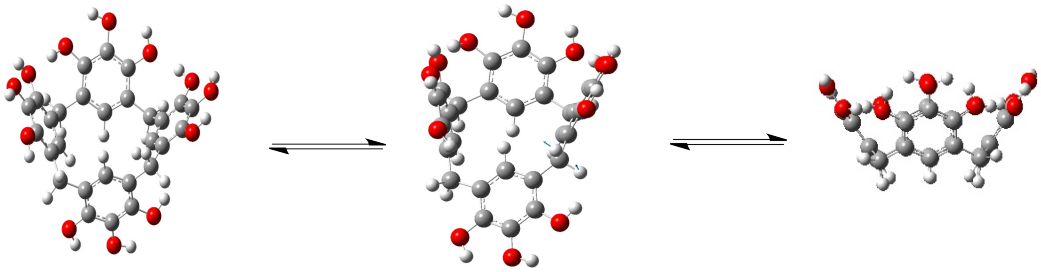

Partial Cone **Cone A**

Figure 1.12 Transition state connecting the partial cone and cone

A macrocyclic transition structure was found connecting the R=H Cone A and Partial Cone (Figure 1.12). The imaginary frequency is for a H-C-H rocking bend on the linker group between the downward pyrogallol and adjacent upward pyrogallol. The barrier for this transition is only 14 kJ/mol. At the wB97XD level this transition structure optimized to the Cone. A similar structure has not been found for the R=ph stereoisomers.

1.4 Conclusions

To answer the question of why do Chairs rather than Cones form when R=ph, both the gas- and solvent-phase results at the wB97XD and MP2 levels generally predict the Chair to be the most stable structure. The *rccc* (axial) Cone is enthalpically preferred and is second to the Chair in overall stability. The gap between the free energy of the C_1 Chair and the Cone widens as the level of theory increases.

The wB97XD functional appears to be a better choice for the R=ph system. In the gas- and solvent-phases it predicts the experimentally observed structures to be the most stable while the B3LYP results favor the unobserved *rtct* Cone. The B3LYP functional only predicts a Chair, C_i not C_1, to be a global minimum at the SMD-B3LYP level in methanol. The wB97XD functional is also better than the B3LYP functional at producing trends similar to those of the MP2 calculations.

For R=H, the Cone is by far, 42.6-84.3 kJ/mol, the most energetically favorable conformation, with respect to both enthalpy and free energy, in both the gas- and solvent-phases. Unlike for the R=phenyl conformers, the addition of the thermal correction terms does not alter this trend. This result nicely supplements the experimental observation that, when R=alkyl, the Cone is the preferred product of the formation of pyrogallol[4]arene. The interactions of a large aromatic R-group may be necessary to produce or stabilize the Chairs that are formed. It can be stated for certain that a lack of the phenyl groups produces a very different thermodynamic profile of the stereoisomers. Even with the inclusion of thermal correction terms, the

chair is no longer a viable global minimum. At almost every level, no structure lies within 20 kJ/mol of the Cone. The only structure that gets close is the structure that geometrically most closely resembles the cone, the Partial Cone. If the Partial Cone does form, only 14.2 kJ/mol is required to convert it to the cone.

The results of the MP2 single-point calculations show that when R=ph, the wB97XD functional produces an optimized structure that is more stable than the B3LYP-optimized structure. Although the MP2 energy is lower for the wB97XD-optimized structure when R=ph, this is not the case when R=H. For that set of structures the B3LYP functional yields geometries that are either slightly more stable than or equivalent to the wB97XD version of those conformers. Because dispersion forces are more significant in larger molecules and in those with more arene groups, these results appear to highlight the wB97XD functional's ability to account for these intramolecular forces.

The relative instability in the gas-phase calculations between stereoisomers of the same conformer can be explained by a decrease in internal stability due to rearrangements of the intramolecular hydrogen bonding. The changes in energy correspond to the amount of energy that is lost when a hydrogen bond is broken or rearranged, 10 – 25 kJ/mol. However, the relative energies of these structures rearrange in the solvent phase. The lack of available internal hydrogen bonding is compensated for by the presence of the solvent. When all available solvation sites can interact favorably with the polarizable solvent continuum, the difference in energy is mainly due to the difference in geometries. When there is not a large difference in

geometries, the solvent-phase relative energies are also very similar between conformers of the same stereoisomer.

The solvent-phase data for the Cone diastereomers also shows that the results generated by the wB97XD functional are more accurately predictive than those generated by the B3LYP functional. The wB97XD solvent methods calculate the experimentally observed Cone diastereomers to be the most stable. In contrast, the B3LYP method does not perform as well, predicting a preference for structures that are not observed to be the most energetically favorable.

The IEF method was very disappointing in that it barely distinguishes between the different solvents whether the B3LYP or wB97XD method is used. Because of this the IEF results do not seem very reliable in general. The SMD method favors the C_i Chair in methanol. This is the only method and solvent in which the C_i Chair is predicted to be the most stable. The solvent-phase calculations on individual pyrogallol and oop pyrogallol show that methanol stabilizes the two rotamers relative to each more do than the other solvents. Methanol, not DMSO, was found to favor the Chair. Explicit solvent calculations with an individual pyrogallol molecule show that methanol preferentially interacts with the hydroxyl groups of pyrogallol in a C_i Chair geometry. Although implicit DMSO did not strongly favor the Chair geometry, bridging DMSO solvent between the R-groups and hydroxyl groups may yield a stabilizing interaction and should be investigated further.

1.5 References

[1] Dalgarno, S. J.; Power, N. P.; Atwood, J. L. *Org. Nanostruct.* **2008**, 317.

[2] Dalgarno, S. J.; Power, N. P.; Atwood, J. L. *Coord. Chem. Rev.* **2008**, *252*, 825.

[3] Heaven, M. W.; Cave, G. W. V.; McKinlay, R. M.; Antesberger, J.; Dalgarno, S. J.; Thallapally, P. K.; Atwood, J. L. *Angew. Chem., Int. Ed.* **2006**, *45*, 6221.

[4] Cave, G. W. V.; Ferrarelli, M. C.; Atwood, J. L. *Chem. Commun.* **2005**, 2787.

[5] Antesberger, J.; Cave, G. W. V.; Ferrarelli, M. C.; Heaven, M. W.; Raston, C. L.; Atwood, J. L. *Chem. Commun.* **2005**, 892.

[6] Maerz, A. K.; Fowler, D. A.; Mossine, A. V.; Mistry, M.; Kumari, H.; Barnes, C. L.; Deakyne, C. A.; Atwood, J. L. *New J. Chem.* **2011**, *35*, 784.

[7] Cave, G. W. V.; Dalgarno, S. J.; Antesberger, J.; Ferrarelli, M. C.; McKinlay, R. M.; Atwood, J. L. *Supramol. Chem.* **2008**, *20*, 157.

[8] Salgarno, S. J.; Bassil, D. B.; Tucker, S. A.; Atwood, J. L. *Angew. Chem., Int. Ed.* **2006**, *45*, 7019.

[9] Bassil, D. B.; Dalgarno, S. J; Cave, G. W. V.; Atwood, J. L.; Tucker, S. A. *J Phys Chem B* **2007**, *111*, 9088.

[10] Dalgarno, S. J.; Szabo, T.; Siavosh-Haghighi, A.; Deakyne, C. A.; Adams, J. E.; Atwood, J. L. *Chem. Commun.* **2009**, 1339.

[11] Cave, G. W. V.; Antesberger, J.; Barbour, L. J.; McKinlay, R. M.; Atwood, J. L. *Angew. Chem., Int. Ed.* **2004**, *43*, 5263.

[12] Iyer, K. S.; Norret, M.; Dalgarno, S. J.; Atwood, J. L.; Raston, C. L. *Angew. Chem., Int. Ed.* **2008**, *47*, 6362.

[13] Dalgarno S. J.; Power N. P.; Atwood J. L. *Chem. Commun.* **2007**, 3447.

[14] Dalgarno S. J.; Power N. P.; Antesberger, J.; McKinlay R. M.; Atwood J. L. *Chem Commun* **2006**, 3803.

[15] Jin, P.; Dalgarno, S. J.; Barnes, C.; Teat, S. J.; Atwood, J. L. *J. Am. Chem. Soc.* **2008**, *130*, 17262.

[16] Jin, P.; Dalgarno, S. J.; Warren, J. E.; Teat, S. J.; Atwood, J. L. *Chem. Commun.* **2009**, 3348.

[17] Jin, P.; Dalgarno, S. J.; Atwood, J. L. *Coord. Chem. Rev.* **2010**, *254*, 1760.

[18] Fowler, D. A.; Mossine, A. V.; Beavers, C. M.; Teat, S. J.; Dalgarno, S. J.; Atwood, J. L. *J. Am. Chem. Soc.* **2011**, *133*, 11069.

[19] Dalgarno, S. J.; Power, N. P.; Warren, J. E.; Atwood, J. L. *Chem. Commun.* **2008**, 1539.

[20] Atwood, J. L.; Brechin, E. K.; Dalgarno, S. J.; Inglis, R.; Jones, L. F.; Mossine, A.; Paterson, M. J.; Power, N. P.; Teat, S. J. *Chem. Commun.* **2010**, *46*, 3484.

[21] Mayer, C. *Int J Artif Organs* **2005** *28*, 1163.

[22] Miyazaki, S.; Takahashi, A.; Kubo, W.; Bachynsky, J.; Löbenberg, R. *J Pharm Pharmaceut Sci* **2003**, *6*, 238.

[23] Maerz, A. K.; Thomas, H. M.; Power, N. P.; Deakyne, C. A.; Atwood, J. L. *Chem. Commun.* **2010**, *46*, 1235.

[24] Podyachev, S. N.; Syakaev, V. V.; Sudakova, S. N.; Shagidullin, R. R.; Osyanina, D. V.; Avvakumova, L. V.; Buzykin, B. I.; Latypov, S. K.; Bauer, I.; Habicher, W. D.; Konovalov, A. I. *J. Inclusion Phenom. Macrocyclic Chem.* **2007**, *58*, 55.

[25] Funck, M.; Guest, D. P.; Cave, G. W. V. *Tetrahedron Lett.* **2010**, *51*, 6399.

[26] Gaussian 03, R. C., Frisch, M. J.; Trucks, G. W.; Schlegel, H. B.; Scuseria, G. E.; Robb, M. A.; Cheeseman, J. R.; Montgomery, J., J. A.; Vreven, T.; Kudin, K. N.; Burant, J. C.; Millam, J. M.; Iyengar, S. S.; Tomasi, J.; Barone, V.; Mennucci, B.; Cossi, M.; Scalmani, G.; Rega, N.; Petersson, G. A.; Nakatsuji, H.; Hada, M.; Ehara, M.; Toyota, K.; Fukuda, R.; Hasegawa, J.; Ishida, M.; Nakajima, T.; Honda, Y.; Kitao, O.; Nakai, H.; Klene, M.; Li, X.; Knox, J. E.; Hratchian, H. P.; Cross, J. B.; Bakken, V.; Adamo, C.; Jaramillo, J.; Gomperts, R.; Stratmann, R. E.; Yazyev, O.; Austin, A. J.; Cammi, R.; Pomelli, C.; Ochterski, J. W.; Ayala, P. Y.; Morokuma, K.; Voth, G. A.; Salvador, P.; Dannenberg, J. J.; Zakrzewski, V. G.; Dapprich, S.; Daniels, A. D.; Strain, M. C.; Farkas, O.; Malick, D. K.; Rabuck, A. D.; Raghavachari, K.; Foresman, J. B.; Ortiz, J. V.; Cui, Q.; Baboul, A. G.; Clifford, S.; Cioslowski, J.; Stefanov, B. B.; Liu, G.; Liashenko, A.; Piskorz, P.; Komaromi, I.; Martin, R. L.; Fox, D. J.; Keith, T.; Al-Laham, M. A.; Peng, C. Y.; Nanayakkara, A.;

Challacombe, M.; Gill, P. M. W.; Johnson, B.; Chen, W.; Wong, M. W.; Gonzalez, C.; and Pople, J. A.; Gaussian, I., Wallingford CT, 2004.

[27] Gaussian 09, R., Frisch, M. J.; Trucks, G. W.; Schlegel, H. B.; Scuseria, G. E.; Robb, M. A.; Cheeseman, J. R.; Scalmani, G.; Barone, V.; Mennucci, B.; Petersson, G. A.; Nakatsuji, H.; Caricato, M.; Li, X.; Hratchian, H. P.; Izmaylov, A. F.; Bloino, J.; Zheng, G.; Sonnenberg, J. L.; Hada, M.; Ehara, M.; Toyota, K.; Fukuda, R.; Hasegawa, J.; Ishida, M.; Nakajima, T.; Honda, Y.; Kitao, O.; Nakai, H.; Vreven, T.; Montgomery, J., J. A.; Peralta, J. E.; Ogliaro, F.; Bearpark, M.; Heyd, J. J.; Brothers, E.; Kudin, K. N.; Staroverov, V. N.; Kobayashi, R.; Normand, J.; Raghavachari, K.; Rendell, A.; Burant, J. C.; Iyengar, S. S.; Tomasi, J.; Cossi, M.; Rega, N.; Millam, N. J.; Klene, M.; Knox, J. E.; Cross, J. B.; Bakken, V.; Adamo, C.; Jaramillo, J.; Gomperts, R.; Stratmann, R. E.; Yazyev, O.; Austin, A. J.; Cammi, R.; Pomelli, C.; Ochterski, J. W.; Martin, R. L.; Morokuma, K.; Zakrzewski, V. G.; Voth, G. A.; Salvador, P.; Dannenberg, J. J.; Dapprich, S.; Daniels, A. D.; Farkas, Ö.; Foresman, J. B.; Ortiz, J. V.; Cioslowski, J.; Fox, D. J. G., Inc., Wallingford CT, 2009.

[28] Becke, A. D. *J. Chem. Phys.* **1993**, *98*, 5648.

[29] Lee, C.; Yang, W.; Parr, R. G. *Phys. Rev. B Condens. Matter* **1988**, *37*, 785.

[30] Stephens, P. J.; Devlin, F. J.; Chabalowski, C. F.; Frisch, M. J. *J. Phys. Chem.* **1994**, *98*, 11623.

[31] Chai, J.-D.; Head-Gordon, M. *Phys. Chem. Chem. Phys.* **2008**, *10*, 6615.

[32] Chai, J.-D.; Head-Gordon, M. *J. Chem. Phys.* **2008**, *128*, 084106.

[33] Marenich, A. V.; Cramer, C. J.; Truhlar, D. G. *J. Phys. Chem. B* **2009**, *113*, 6378.

[34] Rayne, S.; Forest, K. Nature Proceedings, **2010**.

[35] Kucharski, T. J.; Yang, Q.-Z.; Tian, Y.; Boulatov, R. *J. Phys. Chem. Lett.* **2010**, *1*, 2820.

2 The Addition of H_2O and O_2 to Ligated Vanadyl Cations

The unique catalytic, biological, and electrical properties of vanadium oxides have generated interest from many fields. These systems can be induced to either donate or accept electron density through control of the ligand field and charge on the metal center. The Van Stipdonk group and our group have been using electrospray ionization mass spectrometry, DFT and conventional ab initio calculations to study the addition and ligand-exchange reactions of vanadium oxide cations. The topic of the current chapter is the computational modeling of the addition of H_2O and O_2 to vanadyl complexes of the form $[VOX(NCCH_3)]^+$ where X = F^-, Cl^-, Br^-, I^-, and OH^-. In addition to determining the PES and thermochemistry of these reactions, the immediate questions are 1) how does electron density on the metal center influence whether H_2O or O_2 is added, and 2) how does the identity of X affect the reaction? The results of different DFT methods suggest the need for higher-level single-point calculations. The results of CCSD and CCSD(T) single-point calculations indicated the strong multi-reference character of the system.

2.1 Introduction

Oxides of the transition metal vanadium have demonstrated diverse chemical activity. The most common use is as a powerful oxidative catalyst. The most common form, vanadium (V) oxide, V_2O_5, is the most effective catalyst for the

oxidation of sulfur dioxide to sulfur trioxide for the production of sulfuric acid. It catalyzes the reduction of nitrogen oxides in power plant emissions[1-3]. Vanadium is comparable to iron in that it is involved at the active sites of many enzymes in biochemical processes, binds with O_2, and binds with proteins[4]. In marine animals vanadium is found sequestered in the cells, vanadocytes, bound to proteins called vanabins[5].

As a material, vanadium oxide has advantageous semiconducting and optical properties. Vanadium oxide has a uniquely high temperature coefficient of resistance; the compound's electrical resistance changes greatly with very little change in temperature. At the semiconductor-metal phase transition its resistivity changes 5-10 times more than other metals[6]. These features make it the material of choice for uncooled IR sensors, or microbolometers, which use changes in electrical resistance to detect changes in temperature. Because they do not need to be cooled, vanadium oxides have many thermal imaging applications as small, hand-held sensors and night cameras[7]. Subtle changes of temperature can also create large changes in optical properties, such as transmittance. One application of VO_2 is as a coating for energy efficient windows that, depending on temperature, can control the amount of light or heat transmitted through the window. These properties can be manipulated by altering the structure of the material[8].

Acid-base properties have been used to describe the catalytic oxidation of hydrocarbons by transition metal oxides[1]. Vacant coordinate positions on the metal centers function as acidic sites, while nearby O^{2-} ions act as basic sites. An important feature of the Lewis acid vanadium oxide is that by control of coordination and

charge, its can be induced to function as a Lewis base. Catalytic active sites often involve a Lewis acid, Lewis base, and a metal. Catalysis is facilitated by the changes in the oxidation state of the metal. Transition metals are especially useful in chemical reactions because they easily change oxidation state and coordination modes, making them flexible active site participants.

Much of the important chemistry of these systems comes from the V-O interactions. Thus, understanding this relationship is crucial to understanding vanadium's industrial, biological, and electronic applications. Several theoretical studies have used gas-phase vanadium oxide clusters as models for active sites[3,9-13]. The properties of this system are highly influenced by the variable structure of $[V_xO_y]^+$; however, neither the molecular nor the electronic structure is well understood. This lack of understanding hinders the otherwise promising development of vanadium oxides for the design of new catalysts, nanomaterials, and other applications. Experimentally the structural qualities are very difficult to elucidate, so more theoretical studies are needed[2]. Many studies on larger oxovanadium gas-phase clusters report that often there is a terminal vanadyl group where, it is theorized, much of the important chemistry, such as transferring oxygen, abstracting hydrogen, or oxidizing an alkene, occurs[9,12,19]. In gas-phase studies of ethylene reacting with $V_xO_y^+$, it was found that the unpaired electron is shared between the vanadium d-orbitals and a terminal oxygen. In these systems, where there are several oxygen and vanadium atoms and most have multiple bonds, they found that the unpaired electron was on the terminal (least coordinated) vanadium and its singly bound oxygen. The CASSCF results predict the same location for the unpaired electron.

Zemski reports[13] that when $[V_xO_y]^+$ reacts with ethane or ethylene, atomic oxygen is transferred from the metal cation to the hydrocarbon and then lost. The reason, it is believed, that the hydrocarbon is involved in this reaction is because the loss of atomic oxygen is not observed during collision-induced dissociation studies or when it is mixed with an inert gas. When butane or 1,3-butadiene was used, dehydration was also observed. Bell and Castleman also found water to be product of $[V_xO_y]^+$ ions with 1,3-butadiene and isomers of butane[23]. Their conclusion is that the hydrogen is abstracted at a single vanadyl site and not at a bridged oxygen site. This site also is believed to be involved in the oxygen transfer between vanadium oxides and hydrocarbons. For the other group V transition metal oxides there was little or no evidence that such reactions occurred. One theory as to why vanadium works better than the element below it on the Periodic Table, niobium, is tht V-O bonds are weaker than Nb-O bonds and, therefore, are more easily broken in the catalytic cycle. Justes at al.[9] find that oxygen is reversibly bound and released easily from vanadium oxide cations.

More evidence to support these conclusions comes from the IR and DFT studies of $[V_xO_y]^+$-ethene fragmentation[19]. When reacting $[V_2O_5]^+$ with ethene, ethane is lost, but for $[V_2O_6]^+$-ethene, ethane and O_2 are lost. This lack of fragmentation of the overall complex is interpreted as evidence that the vanadyl site is involved in the reaction as opposed to a centrally located, bridged, oxygen atom. It was also found in this study of $[V_xO_y]^+$ clusters with ethene that the molecule's unpaired electron is localized to a terminal V-O group. It was determined that the ethane binds to the lowest-coordinated vanadium atom in the cluster, once again

indicating that the terminal vanadium sites are where the reaction takes place. It was concluded that it is the positive charge on the complex that drives the addition of the hydrocarbon to the metal center. Furthermore, Janssens reports[17] that for $[V_2O_y]^-$, the unpaired electron is delocalized over both vanadium atoms, but in larger clusters the electron stays on one vanadium atom. Asmis and co-workers[10] also found, in their study of transition metal oxide clusters, that charge localization is size dependent.

Experimentalists have used mass spectrometry and IR to study reactions of V_xO_y with hydrocarbons. Many mechanisms and active sites are still unknown[13]. The experimentalists working on the current study have been using mass spectrometry, ESI, and FELIX IR to investigate gas-phase addition and ligand-exchange reactions of vanadium oxide compounds[14]. This work began as an extension of their previous work on uranyl oxides[15]. Their results on these systems show that the oxidation state and ligand field of the metal center are very important to determining what addition reactions the complex will undergo.

Depending on the amount of electron density donated to the positive metal center by coordinated species, the acidic (electron-accepting) vanadium cation can be induced to act as a base (electron donating) in addition and ligand-exchange reactions. In the present study, the addition of one molecule of H_2O or one molecule of O_2 to 3-coordinate vanadium oxide cations of the form $[VOX(NCCH_3)]^+$ where X is OH^-, F^-, Cl^-, Br^-, or I^-, has been computationally examined. Our group is interested in what effect the identity of the anion has on the addition reactions. Experiments in which additional H_2O, O_2, or $NCCH_3$ either adds to or replaces a ligand on the vanadium

center have also been performed to study the effects of neutral ligands on the complex.

The experimental results suggest that the amount of charge transfer from the anion to the metal center does influence whether water or molecular oxygen will bind to the complex. When highly electronegative fluorine is the anion, H_2O is easily added but not O_2. When the complex includes the very polarizable iodine, O_2 is easily added, but not H_2O (Figure 2.10 - Figure 2.13). These trends suggest that when a strongly electron-withdrawing ligand is present, the vanadium center is more positive and more likely to bond with water (accept electrons). When a more electron-donating ligand is attached, the metal center is more negative and more likely to add O_2 (donate electrons). Examining these trends is the main subject of this project.

Experimentally, the addition of a second water molecule is also observed. Although the addition of a second O_2 molecule to these systems was not observed, molecular oxygen will add to the vanadium after a water molecule has been added. There are also ligand exchange reactions in which H_2O is replaced by O_2 and vice-versa. Finally, water addition is also observed for compounds containing more than one acetonitrile group. In this scenario, when the anion is F^- or Cl^-, the loss of one of the acetonitrile groups and HX is observed. The explanation is that the water molecule separates and a hydroxyl group replaces the halogen on the vanadium. The remaining water H attaches to the anion and is lost as HF or HCl.

2.2 Methods

The initial goal of this work was to find the theoretically possible products of the H_2O and O_2 addition reactions. All calculations were performed using the Gaussian 03 and 09 programs[5]. Possible products of the addition reactions were searched for using the DFT methods B3LYP and G96LYP to optimize geometries and calculate vibrational frequencies. Using the B3LYP functional with a triple-zeta basis set is a common level of theory used to study vanadium oxides.[9-13,17-19]. These methods were chosen because preliminary calculations done by our collaborators suggest that the B3LYP functional produces more reliable frequencies, while G96LYP produces more accurate energies. The decision of which basis set to use was difficult because of the limited number of basis sets available for vanadium and iodine. The LANL2DZ and 6-311+G(d,p) basis sets were chosen. A 6-311+G(d,p) basis set that was developed for iodine was obtained from the literature[20]. The search for minima was done at the B3LYP/6-311+G(d,p), G96LYP/6-311+G(d,p), wB97XD//6-311+G(d,p), and G96LYP/LANL2DZ levels. Both doublet and quartet ground electronic states were examined; however, the quartet states were consistently much higher in energy and only the results for the doublet states will be reported here. The Atoms in Molecules (AIM) method[21] was used to determine the presence of bond critical points and rings. IRC calculations were used to determine the minima that the transition states identified connect.

2.3 Results and Discussion

2.3.1 Minima

2.3.1.1 Water addition

The addition of water to vanadium is a typical metal center - ligand interaction. A lone pair of electrons is donated from the water oxygen to form a coordinate-covalent bond with a vanadium p-orbital. In this way the metal acts like an acid. Several minima were found to be possible products of the water addition to the vanadium complex (Figure 2.1). After the H_2O bonds to the vanadium center, either the water molecule remains intact or one hydrogen atom is transferred from the water to another ligand. The two main isomers are very close in energy. The identity of the global minimum depends on which method is used (Figure 2.2). One product results from the binding of the intact water molecule to the vanadium center. In the other main product, one of the hydrogen atoms transfers to the lone oxygen on the vanadium, resulting in two hydroxyl groups attached to the vanadium, in addition to the anion and acetonitrile group. These two structures are very close in energy and vie to be the global minimum at all levels and for all halogens.

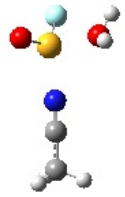

$[VOX(H_2O)(NCCH_3)]^+$

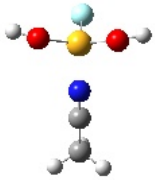

$[VX(OH)_2(NCCH_3)]^+$

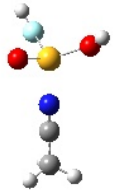

$[VO(OH)(XH)(NCCH_3)]^+$

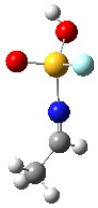

$[VOX(OH)(NC(H)CH_3)]^+$

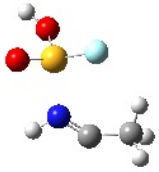

$[VOX(N(H)CCH_3)]^+$

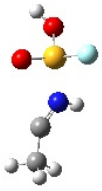

$[VOX(NCCH_3)]^+$ (X = F only)

In order of decreasing stability. V = yellow, O = red, N = blue, C= grey, X = light blue, H = white
All geometries are B3LYP/6-311+G(d,p) optimized.

Figure 2.1 Water addition products

The third-most-stable isomer of the water addition products is consistently much higher in energy, independent of the method and the identity of the anion. In this structure, a hydrogen atom from the water molecule transfers to the anion. These structures are interesting because in some of the mass spectrometry experiments, HF and HCl are observed products of water addition (see below). Finally, the other possible isomers involve transfer of the hydrogen from the water to the acetonitrile group. The loss of a protonated acetonitrile group has been experimentally observed. The hydrogen can bond to the carbon or nitrogen of the acetonitrile group. This bonding motif changes the geometry of the ligand and in some cases a ring is formed, composed of the acetonitrile and the vanadium center. Calculations performed using

the AIM method[21] confirm the presence of this ring. For all isomers in which a hydrogen transfers from the water, the remaining hydroxyl group remains attached to the vanadium.

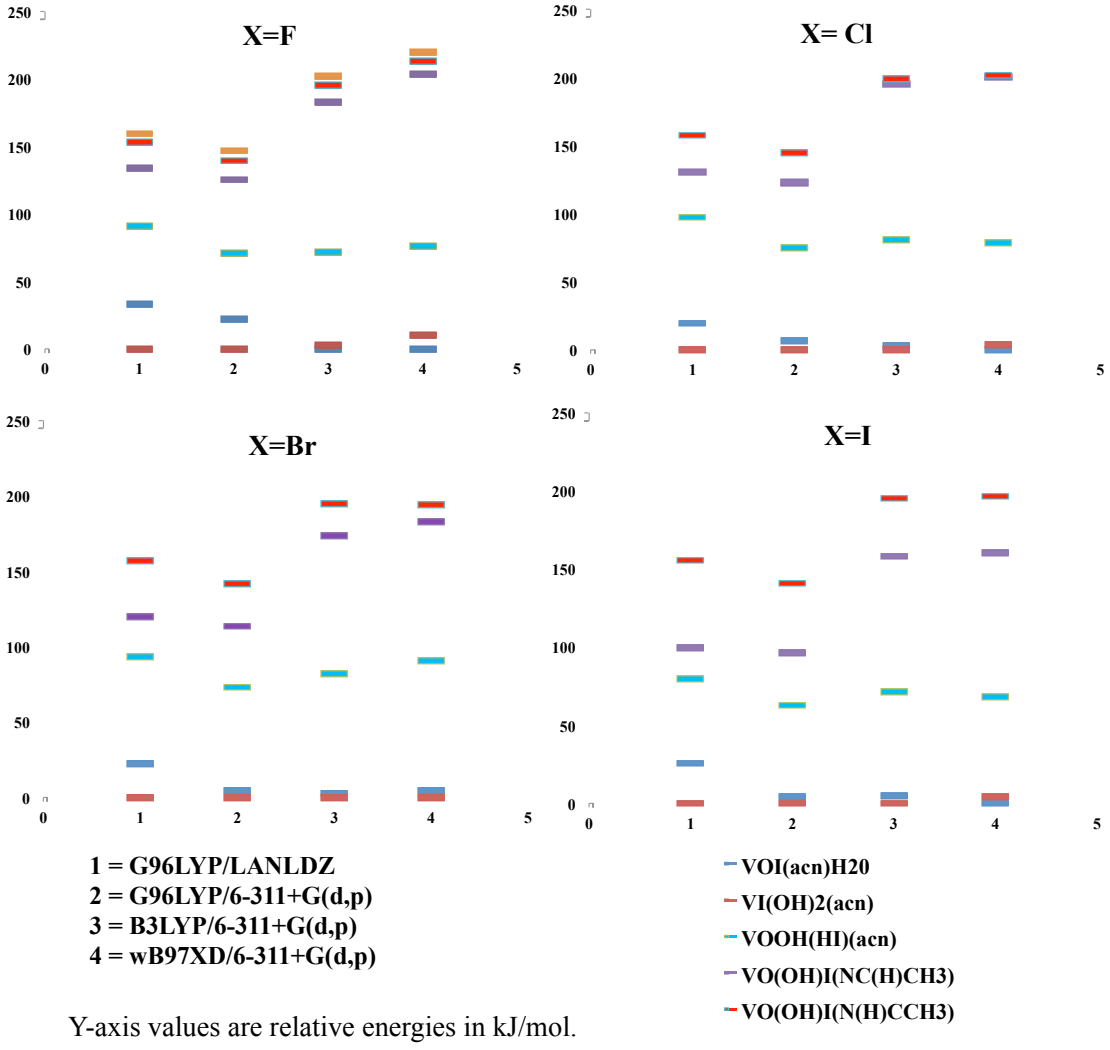

Y-axis values are relative energies in kJ/mol.

Figure 2.2 Relative energies of H_2O addition

2.3.1.2 O_2 addition

When molecular oxygen is added to the metal center, the vanadium acts like a base donating electron density to unfilled π-orbitals on the molecular oxygen. All three methods yielded different results for the relative energies of the O_2 addition products (Figure 2.4).

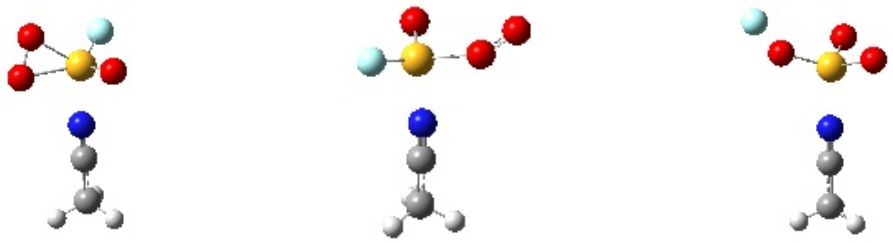

$[VOX(NCCH_3)(O_2)]^+$ bidentate | **$[VOX(NCCH_3)(O_2)]^+$ monodentate** | **$[V(O)_2(OX)(NCCH_3)]^+$**

In order of decreasing stability. V = yellow, O = red, N = blue, C= grey, X = light blue, H = white
All geometries are B3LYP/6-311+G(d,p) optimized.

Figure 2.3 Products of O_2 addition

Three minima for the O_2 addition reaction were found (Figure 2.3). When O_2 bonds to vanadium it either remains intact, bonding in a bidentate (side-on) or monodentate (end-on) way or the oxygen atoms separate and both bond individually. It seems that the most stable complex is the bidentate one, where both oxygen atoms bind to the vanadium, occupying two coordinate locations. The AIM analysis confirms the presence of a three-membered ring consisting of the vanadium center and the two molecular oxygen atoms. The next-most-stable predicted product of the

O_2 addition is the monodentate form in which the O_2 forms a single bond to the vanadium through only one of the oxygen atoms. Finally, a third and higher-energy minimum is the one in which the bond between the molecular oxygen is broken and the two oxygen atoms attach singly and separately to the vanadium center. When this happens the anion transfers from the vanadium to one of the lone oxygen atoms. Most methods predict this isomer to be much higher in energy than the others. A study of VO_2 anions and neutral species found that their most stable geometry is the one in which the O_2 bonds as separate oxygen atoms to the vanadium, instead of side-on or end-on[18]. Present calculations do not seem to forecast a similar situation for their cationic cousins.

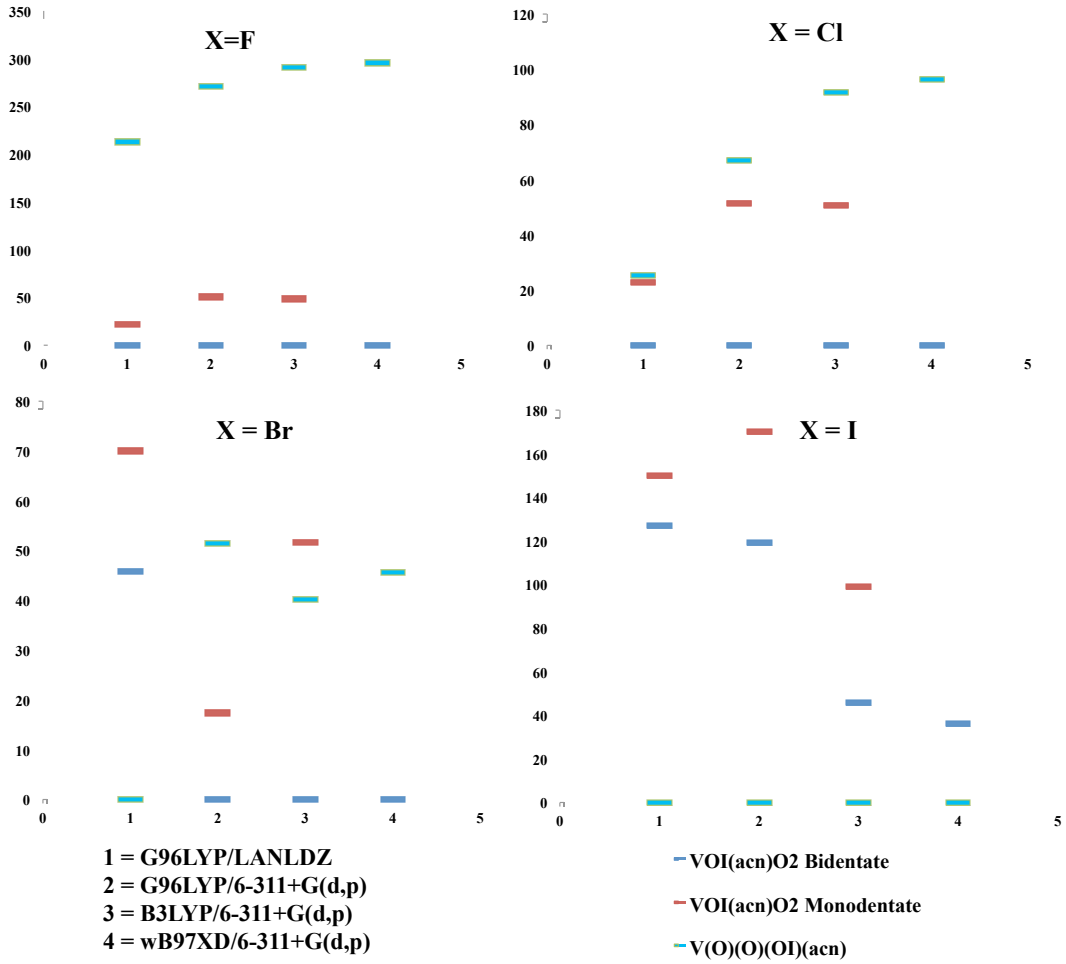

Figure 2.4 Relative energies of O_2 addition

Initial calculations produced highly varied relative energies for these three structures. Using a different DFT method or basis set produced different relative energies. When a triple-zeta basis set is used, the bidentate isomer is predicted to be the most stable. Further higher-level single-point calculations also indicate that the most stable molecular oxygen addition occurs in a bidentate fashion.

2.3.1.2.1 Aromaticity of V-O-O ring

Steiner and co-workers[24] used a coupled Hartree-Fock ipsocentric method to examine the delocalization pathway of the π current in a porphyrin macrocycle around a central metal cation. Using coupled HF molecular orbital theory they were able to map the total current density and changes in the charge on the metal center. Changes in the central cation cause changes in the delocalized electron current around the macrocycle. This method might be useful to the study of larger vanadyl systems, especially in enzymatic or biological applications where the cation is enmeshed in a larger organic species or surface. Another interesting way to study the electronic behavior of this system is to calculate NMR shifts using the Nucleus-Independent Chemical Shifts (NICS) method. In this process, an NMR calculation is done using Gauge Independent Atomic Orbitals (GIAO). Ghost atoms are then used as sites to calculate magnetic shieldings in places that cannot be measured by experiment, such as the center of a ring or along a bond[25]. This method provides a measure of cyclic electron delocalization. Negative values indicate diatropic (aromatic) ring currents and positive values indicate paratropic (anti-aromatic) currents. Preliminary calculations of this type at the B3LYP/LANL2DZ level were performed to see if the V-O-O rings of the bidentate O_2 addition products possess any aromaticity. The geometries were optimized at this level before the NMR shifts were computed. The bidentate species were found to have significant aromatic character. Interestingly, a simple V-O-O ring, with no other ligands, is strongly anti-aromatic. When another oxygen atom is added to the vanadium center, the molecule becomes very strongly

aromatic. The value at the center of the ring is very high, and there is also a smaller amount of aromaticity along the bonds. If a halogen replaces the lone oxygen, then the molecule is still very aromatic, but the chemical shift is slightly less in the center and slightly more along the V-X bond. This method does not delineate between σ- and π- aromaticity. If NMR shifts are to be used, then a NICS method that separates the types of aromaticity is needed. At lower levels of theory the data is not reliable and varies greatly depending on basis set size. If this method is to be used, then the basis set needs to be at least 6-311+G(2d,p) in size[26]. This is a computationally inexpensive method to examine how different ligands and oxidation states alter the flow of electron density between vanadium, oxygen, and other species.

2.3.1.3 Bond lengths

Although the effect of the anion is one of the main points of interest in this project, there is not much change in bond lengths when different anions are present. Table 2.2 shows that for other than the V – X bond, the bond lengths depend more on the identity of the isomer than on the identity of the anion.

There is slight variation in the change in V - X bond length upon water addition. When the water molecule binds to the vanadium and remains intact, the V - X bond lengthens by .02 Å for F and .03 Å for the others. When the hydrogen splits from the water to form a second hydroxyl group, the V - X bond does not change for F but increases by 0.01 for Cl, 0.02 for Br, and 0.03 for I. As the anion becomes less electron withdrawing, the addition of the water ligand lengthens the V - X bond.

Table 2.1 Bond lengths for $[VOX(acn)]^+$

	V-O	V-X	V-NCH_3
$[VOF(acn)]^+$	1.55	1.74	2.03
$[VOCl(acn)]^+$	1.54	2.14	2.03
$[VOBr(acn)]^+$	1.55	2.28	2.03
$[VOI(acn)]^+$	1.55	2.50	2.04

All bond lengths are reported in angstroms.

The greatest influence the anion has on the V–X bond length is when the water ligand separates and the hydrogen bonds with the anion. The change in V-X bond length is more related to the identity of the anion when it is part of a V-XH bond. The V-XH bond increases by 22.4% for X = F, by 17.9% for Cl, by 15.8% for Br and only by 13.6% for I. In contrast, the V-X bond only lengthens by 1.1% at most for the other water addition products when X=F and by 2.4% when X=I. This increased lengthening of the V-XH bond correlates with the breaking of that same bond to produce HX.

Table 2.2 Bond lengths for H_2O addition

Water Addition Product	V-X	V-N	V-O	V-OH	V-OH	V-H2O	V-XH
VO(OH)(acn)	1.75	2.04	1.55				
VO(OH)(acn)(H_2O)	1.77	2.06	1.56			2.08	
V$(OH)_3$(acn)	1.76	2.04		1.73	1.73		
VO$(OH)_2$(acn)H	1.73	2.00	1.55	1.73			
VO$(OH)_2$H(acn)	1.74	2.06	1.55	1.74			
VOF(acn)	1.74	2.03	1.55				
VOF(acn)(H_2O)	1.76	2.05	1.55			2.06	
VF$(OH)_2$(acn)	1.74	2.02		1.72	1.72		
VO(OH)(HF)(acn)		2.05	1.56	1.76			2.13
VOF(OH)(acn)H	1.72	1.98	1.55	1.72			
VOF(OH)H(acn)a	1.73	2.06	1.55	1.72			
VOCl(acn)	2.14	2.03	1.54				
VOCl(acn)(H_2O)	2.17	2.06	1.55			2.06	
VCl$(OH)_2$(acn)	2.15	2.02		1.72	1.72		
VO(OH)(HCl)(acn)		2.05	1.56		1.76		2.51
VOCl(OH)(acn)H	2.13	1.98	1.55	1.72			
VOCl(OH)H(acn)	2.13	2.06	1.55	1.73			
VOBr(acn)	2.28	2.03	1.55				
VOBr(acn)(H_2O)	2.31	2.06	1.55			2.06	
VBr$(OH)_2$(acn)	2.30	2.02		1.72	1.72		
VO(OH)(HBr)(acn)		2.06	1.56	1.76			2.64
VOBr(OH)(acn)H	2.29	1.96	1.55	1.72			
VOBr(OH)H(acn)	2.28	2.06	1.55	1.73			
VOI(acn)	2.5	2.04	1.55				
VOI(acn)(H_2O)	2.53	2.06	1.55			2.07	
VI$(OH)_2$(acn)	2.53	2.02		1.72	1.72		
VO(OH)(HI)(acn)		2.06	1.56	1.76			2.84
VOI(OH)(acn)H	2.56	1.89	1.55	1.73			
VOI(OH)H(acn)	2.50	2.06	1.55	1.74			

All bond lengths are reported in angstroms.

Table 2.3 Bond lengths for O_2 addition

O_2 Addition Product	V-X	V-N	V-O	V-O2		V-OX
VO(OH)(acn)O_2 bi	1.73	2.03	1.54	1.93	1.98	
VO(OH)(acn)O_2 m	1.74	2.03	1.55	1.89		
VO(F)(acn)O_2 bi	1.72	2.02	1.54	1.92	1.96	
VO(F)(acn)O_2 m	1.73	2.02	1.55	1.96		
VOO(OF)(acn)		2.02	1.56			1.78
VOCl(acn)O_2 bi	2.12	2.02	1.54	1.92	1.97	
VOCl(acn)O_2 m	2.14	2.03	1.55	1.94		
VOO(OCl)(acn)		2.05	1.58			1.98
VOBr(acn)O_2 bi	2.27	2.03	1.54	1.92	1.97	
VOBr(acn)O_2 m	2.28	2.03	1.55	1.93		
VOO(OBr)(acn)		2.05	1.58			1.96
VOI(acn)O_2 bi	2.50	2.03	1.54	1.92	1.97	
VOI(acn)O_2 m	2.51	2.03	1.55	1.91		
VOO(OI)(acn)		2.06	1.58			1.93

All bond lengths are reported in angstroms.

There is even less variation in the changes in bond lengths after O_2 addition. The V-X bond lengths change by only 0.00 - .01 Å. The most notable difference is the increase in the V-O distance after X binds to the O. This bond length is 1.555 Å in all the reactant structures, except when X is Cl for which the bond length is 1.54 Å. After a halogen transfers, the increase in bond length does not follow a periodic trend: 15% increase for X=F, 29% for Br, 27% for Cl, and 25% for I. The two V-O bond lengths in a bidentate geometry are not equal. The difference is 0.04 – 0.05 Å.

2.3.1.4 Charges on the vanadium

The charge on the metal center influences whether or not the metal will accept or donate electrons in bonding interactions with ligands.

Table 2.4 shows that when the most electronegative anion is present the charge on the vanadium is more positive. Beyond that there is not a strong correlation between the charge on the vanadium and periodicity for the Mulliken charges. This periodic trend is better reflected in the NBO charges, however.

Table 2.4 Charges on vanadium

$[VOX(acn)]^+$

X	Mulliken	NBO
F	0.993	1.648
Cl	0.636	1.416
Br	0.709	1.356
I	0.615	1.274

$[VOX(acn)(H_2O)]^+$

X	Mulliken	NBO
F	0.954	1.599
Cl	0.568	1.375
Br	0.634	1.302
I	0.545	1.232

$[VOX(acn)(O_2)]^+$

X	Mulliken	NBO
F	0.821	1.485
Cl	0.338	1.192
Br	0.357	1.120
I	0.355	1.094

2.3.1.5 Bond dissociation energies

The identity of the anion has very little influence on the addition reaction energies (Figure 2.5 and Figure 2.6). When looking at bond energies for the water addition complexes with different anions, we find that down the halogen group there is a very slight trend towards a decrease in stability. The OH^- anion is the least stable X. This trend is reversed for the addition of O_2. This trend is observed for the bidentate isomer, but it is less clear for the monodentate structure. These results support the experimental results that H_2O addition is easier for the more electronegative anions and O_2 addition is favored for the more polarizable anions. However, the numbers are very close and not very convincing at this level of theory. Multi-reference calculations are needed to resolve this issue.

X =	$[VOX(acn)(H_2O)]^+$	$[VX(OH_2)(acn)]^+$
OH	-156.5	-155.3
F	-171.9	-174.7
Cl	-169.2	-166.5
Br	-165.8	-162.4
I	-165.8	-157.1

B3LYP/6-311+G(d,p)

Figure 2.5 H_2O - V bond dissociation enthalpies (kJ/mol)

X =	bidentate	monodentate
OH	-123.0	-66.2
F	-113.9	-65.6
Cl	-114.7	-64.1
Br	-115.2	-63.5
I	-117.7	-64.3

B3LYP/6-311+G(d,p)

Figure 2.6 O_2 – V bond dissociation enthalpies (kJ/mol)

2.3.1.6 Loss of XH reaction

One of the interesting reactions observed in the ESI-Mass Spectrometry experiments was the unexpected loss of HF and HCl during isolation and storage of product ions (Figure 2.13). There is no evidence that HBr or HI is produced. No induced collisional activation was necessary to yield these products. In the presence of both H_2O and O_2, $[VOX(acn)]^+$ is generated by collision induced dissociation (CID) of $[VOX(acn)_2]^+$. When H_2O is present, the following reaction occurs:

$$[VOF(acn)_2]^+ + H_2O \rightarrow [VOF(acn)_2H_2O]^{+}* \leftrightarrow [VOOH(acn)_2HF]^{+}* \rightarrow [VOOH(acn)_2]^+ + XF$$

It might be supposed that this reaction is only observed for the structures that preferentially bind H_2O because water is necessary to form XH, whereas and it is not

observed for cations that preferentially bind O_2. However, even though the trend for halogens to preferentially bind O_2 increases down the group, water addition still takes place creating the reactants necessary for the loss of HX reaction. Calculation of ΔG for the loss of HX shows that, when there is only one acetonitrile group, this reaction is spontaneous for X = F^- and Cl^-, but it is not spontaneous for X = Br^- and I^- (Table 2.5). When there are two acetonitrile ligands, the reaction is spontaneous for all X.

Table 2.5 ΔG for loss of HX (kJ/mol)

	F^-	Cl^-	Br^-	I^-
1 acn	**-14.0**	**-12.0**	**4.3**	**7.0**
2 acn	**-32.0**	**-35.8**	**-30.8**	**-38.9**

B3LYP/6-311+G (d,p)

2.3.2 Multi-reference calculations

In order to determine which DFT results were the most reliable, CCSD and CCSD(T)/6-311+G(d,p) single-point energy calculations were done for B3LYP/6-311+G(d,p) optimized structures. Successful completion of the CCSD(T) calculations proved difficult for some of the structures. The T_1 diagnostic values from both types of calculations are well above the acceptable limit of 0.02 (see Table 2.6). These values indicate that the single-reference Hartree-Fock wavefunction used in the CCSD(T) calculations might be insufficient to describe these molecules. The

consistently high T_1 diagnostic values mean that the results from these calculations are unreliable and the system requires a multi-reference wavefunction. The T_1 diagnostics are lowest for the higher-energy isomers that have hydrogen transferred to the acetonitrile group. Unfortunately, it is the most stable isomers that have the highest T_1 diagnostics values.

Table 2.6 T1 Diagnostic Values

Water Addition Products	OH^-	F^-	Cl^-	Br^-	I^-
VOX(acn)	0.049	0.052	0.055	0.057	0.058
$VX(OH)_2$(acn)	0.031	0.030	0.031	0.032	0.032
VOX(acn)(H_2O)	0.040	0.039	0.040	0.040	0.038
VO(OH)(HX)(acn)	na	0.039	0.040	0.040	0.037
VOX(OH)(acn)H	0.037	0.039	0.037	0.039	0.042
VOX(OH)H(acn)a	0.035	0.035	0.035	0.036	0.036
VOX(OH)H(acn)b	na	0.034	na	na	na
O_2 Addition Products					
VOX(acn)O_2 Bidentate	0.050	0.073	0.077	0.079	0.054
VOX(acn)O_2 Monodentate	0.069	0.068	0.078	0.073	0.046
VOO(OX)(acn)	na	0.097	0.043	0.096	na

All values calculated at the CCSD/6-311+G(d,p) level.

To remedy this problem, future calculations must employ multi-reference methods. Complete Active Space Self-Consistent Field (CASSCF) calculations were performed with the MOLPRO program[22] to study the important minima. Early CASSCF results show that re-optimizing the DFT geometries at the CASSCF/LANL2DZ level does not dramatically change the structures but does greatly decreased the delocalization of the electron occupancy of the orbitals. The main structural change is the lengthening of all V-ligand distances. There had been

speculation about whether the 3-coordinate complex is trigonal planar or trigonal pyramidal. The single-reference calculations produced pyramidal structures, but a preliminary CASSCF calculation produced a planar geometry. However, that active space was smaller than the one recently used and also unbalanced [9,9] (nine electrons in five open HOMO's and four virtual LUMO's). The optimizations with an [11,12] active space (eleven electrons in six open HOMO's and six virtual LUMO's) have produced a pyramidal geometry. The active space that was used seems just large enough for this system. There is not a significant amount of electron density coming out of or being promoted into the lowest and highest orbitals in the active space. When an extra HOMO or LUMO orbital was added, although it was similar to the other active space orbitals, it was not used.

The single-point CASSCF calculations based on the single-reference geometries produced orbitals that were much delocalized around the entire molecule. After the CASSCF optimization the electron density was more uniformly distributed on a few important atoms. In the 3-coordinate complex, the unpaired electron is mainly found in vanadium d-orbitals. The occupancy of the virtual orbitals are similar to those for the addition products in that most of their electron density is in a vanadium d-orbital.

2.4 Unusual Structures

While searching for transition state structures several unique but stable geometries were found. They are the result of the water addition reaction when a hydrogen atom dissociates from the water molecule upon addition and ends up in an unexpected location. These are possibly just artifacts, and proper higher-level calculations are needed to determine this.

2.4.1 H on V

(a) 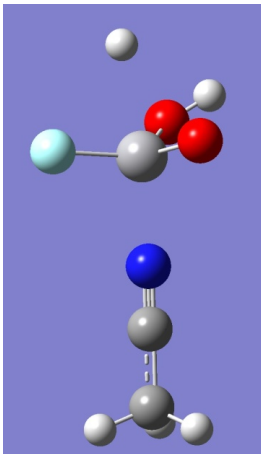 (b) 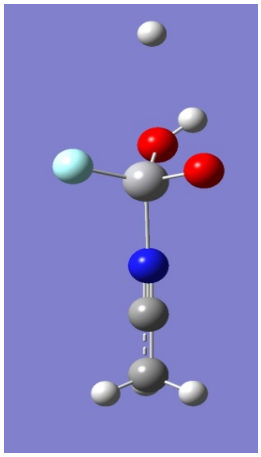

Figure 2.7 Two structures with V-H connectivity, B3LYP/6-311+G(d,p)

Two structures were found in which the dissociated hydrogen "binds" to the vanadium in an axial position opposite the acetonitrile, creating a slightly distorted bipyramidal geometry (Figure 2.7). The structures are the same except for the V-H bond length: 2.089 Å in (a) and 3.562 Å in (b). The charges on the vanadium are 0.735 e and 0.878 e, in structures (a) and (b) respectively. There are no imaginary

frequencies. This species is also stable at the wB97XD level. These structures are more stable with a relative energy of 123.7 kJ/mol then the higher-energy B3LYP structures.

(c) 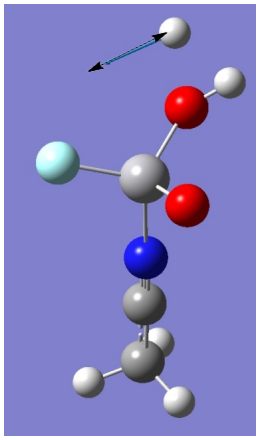 (d) 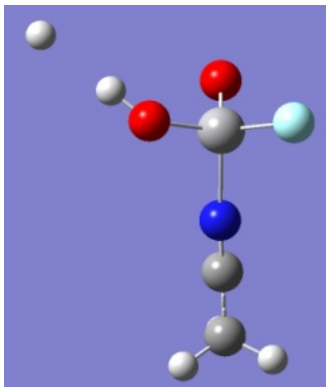

Figure 2.8 Transition state (c) that yielded (d), B3LYP/6-311+G(d,p)

Another unusual but commonly found binding site for the dissociated hydrogen atom is at the other hydrogen atom, not the oxygen atom, from the hydroxyl group that was also formerly part of the added water molecule. This structure, (d), was the product of an IRC calculation performed on (c), (Figure 2.8). Structure (c) is a transition state; the blue arrow indicates movement due to the imaginary frequency. This structure seems like a good candidate for a transition state connecting $[VOF(H_2O)(acn)]^+$ and $[VO(OH)(HF)(acn)]^+$. However, the IRC produced another similar transition state and a minimum with V-O-H-H connectivity (d). The H-H distance is 1.789 Å. The relative stability of structure (d) is 129.3 kJ/mol at the wB97XD/6-311+G(d,p) level and 286.2 kJ/mol at the B3LYP/6-311+G(d,p) level, relative to the global minimum. There is some experimental evidence for the loss of

H_2 and this structure displays a possible path to such a reaction. The PES that these structures lie along is very flat in that IRC calculations repeatedly yield new transition states that vary only slightly in energy and magnitude of the imaginary frequency rather than descending from the saddle point area of the PES. These odd transition states all seem to be very close to potentially useful transition states, if only the wandering hydrogen would just settle.

2.4.1.1 6-311++G(3df,3pd)

Figure 2.9 Stable structures 6-311++(3df,3pd)

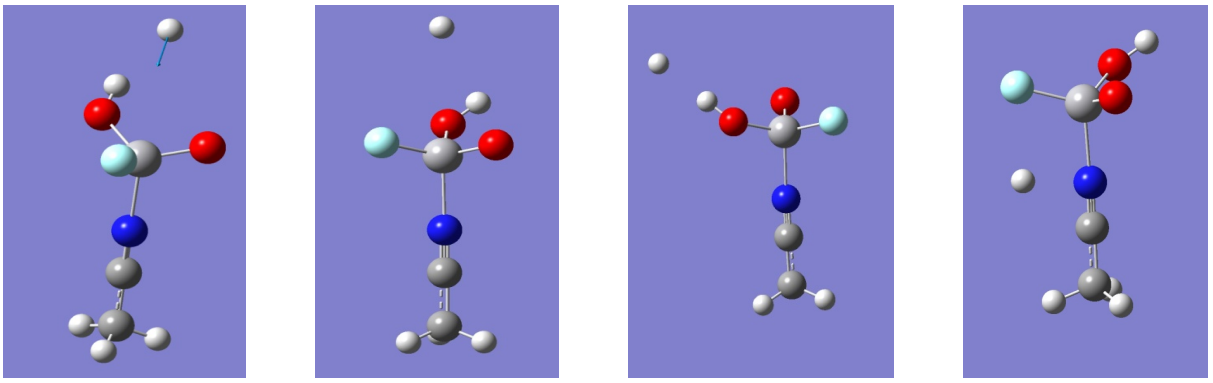

Because these structures possess such unusual geometries, they were reoptimized using a very large basis set, 6-311++(3df,3pd), and were still found to be stable minima. The concept of a "roaming hydrogen" has been seen before, but for small organic species. Higher-level calculations, perhaps multi-reference, should be employed to determine how realistic these geometries are. If these are valid structures, then they lend support to the theories that an individual vanadium metal center is active in the abstraction of hydrogen.

2.5 Conclusion

It remains to be seen if certain ligands are necessary to observe the dual Lewis nature of the metal center and how they compete as electron donors and acceptors. The results of the NBO calculations did not demonstrate any periodic trends for the donation of electron density between the metal and ligands. The experimentally observed trends were reproduced in the computational results. Water addition is preferred when the anion is more electron withdrawing, and molecular oxygen addition is more likely as the polarizability of the anion increases. Changes in the identity of the anion did very little to change the geometries of the product structures. The identity of the anion has the greatest impact on the increased lengthening of the V-XH bond with increased electronegativity of the anion. This change is conducive to the reaction in which HF and HCl are lost but not HBr and HI. In further support of the experimental data, the ΔG for this reaction was negative for HF and HCl but is positive for HBr and HI.

Several isomers of the water addition products were formed due to the ability of a hydrogen atom to separate from the water molecule and bond to every other atom in the system, except those of the methyl group. These structures have a wide range of relative stabilities, with the $[VOX(H_2O)(acn)]^+$ and $[VOX(OH)_2(acn)]^+$ species competitive to be the global minimum. It is preferential for the molecular oxygen to bind to the metal center in a bidentate rather than monodenate fashion. The fact that this binding occurs in two coordinate locations is shown not only by the bonds formed but also by verification of the aromaticity of the V-O-O three-membered ring.

Although there are no reported multi-reference studies on oxovanadium cations, the results of this study indicate that this system requires a multi-reference wavefunction. Similar to previous work on non-ligated vanadium oxide cations, the unpaired electron is located in a d-orbital on the vanadium. At this point, it is not certain that using B3LYP with a triple-zeta basis set is sufficient. The B3LYP and wB97XD methods yield similar results, while the double-zeta and triple-zeta G96LYP results are more similar to each other. CCSD(T) T_1 diagnostic values indicate the need for a multi-determinant wavefunction to properly describe the most stable species of this system.

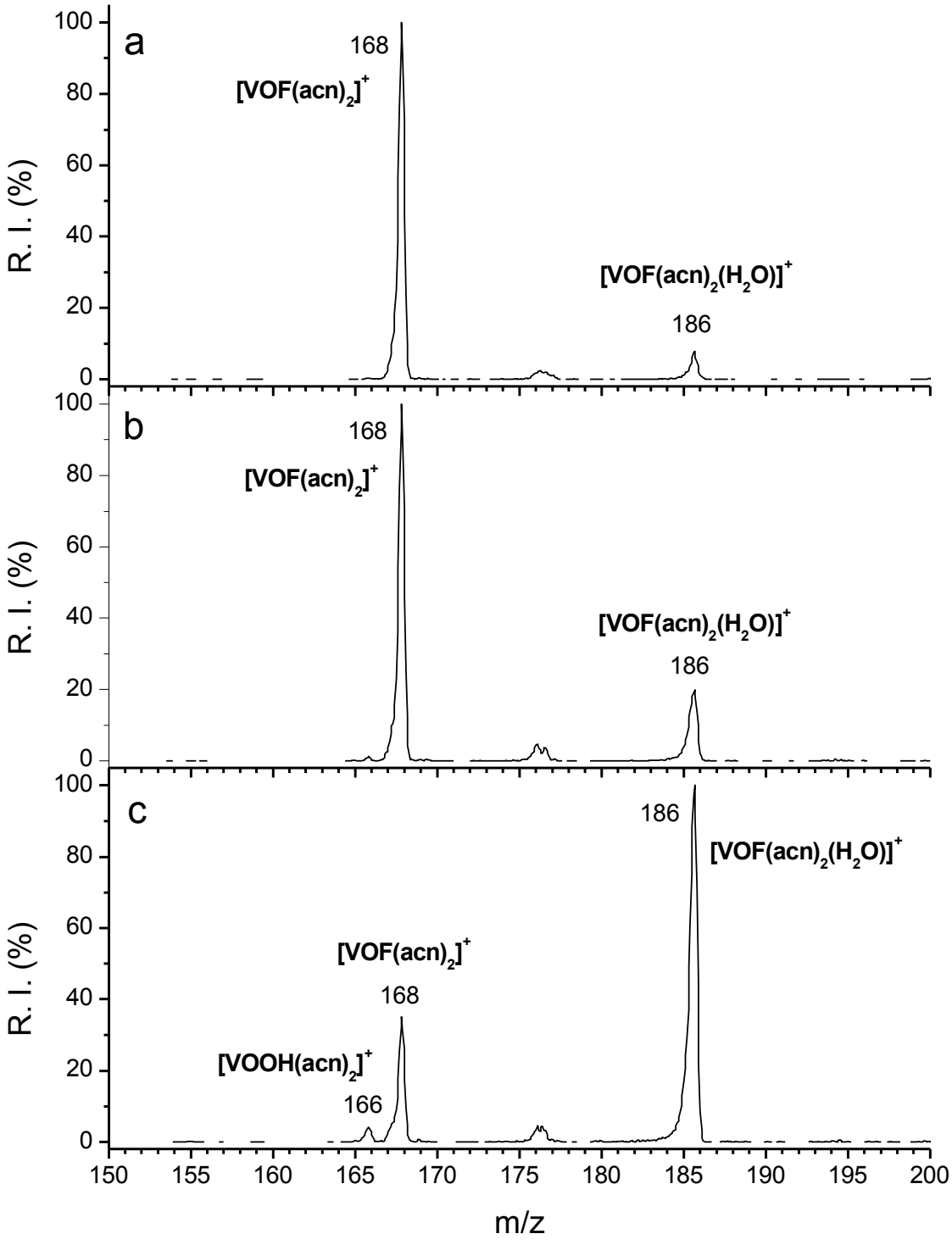

Figure 2.10 Product ion spectra generated by isolation and storage, without imposed collisional activation, of $[VOF(acn)_2]^+$ for (a) 10 ms, (b) 100 ms, (c) 1000 ms.

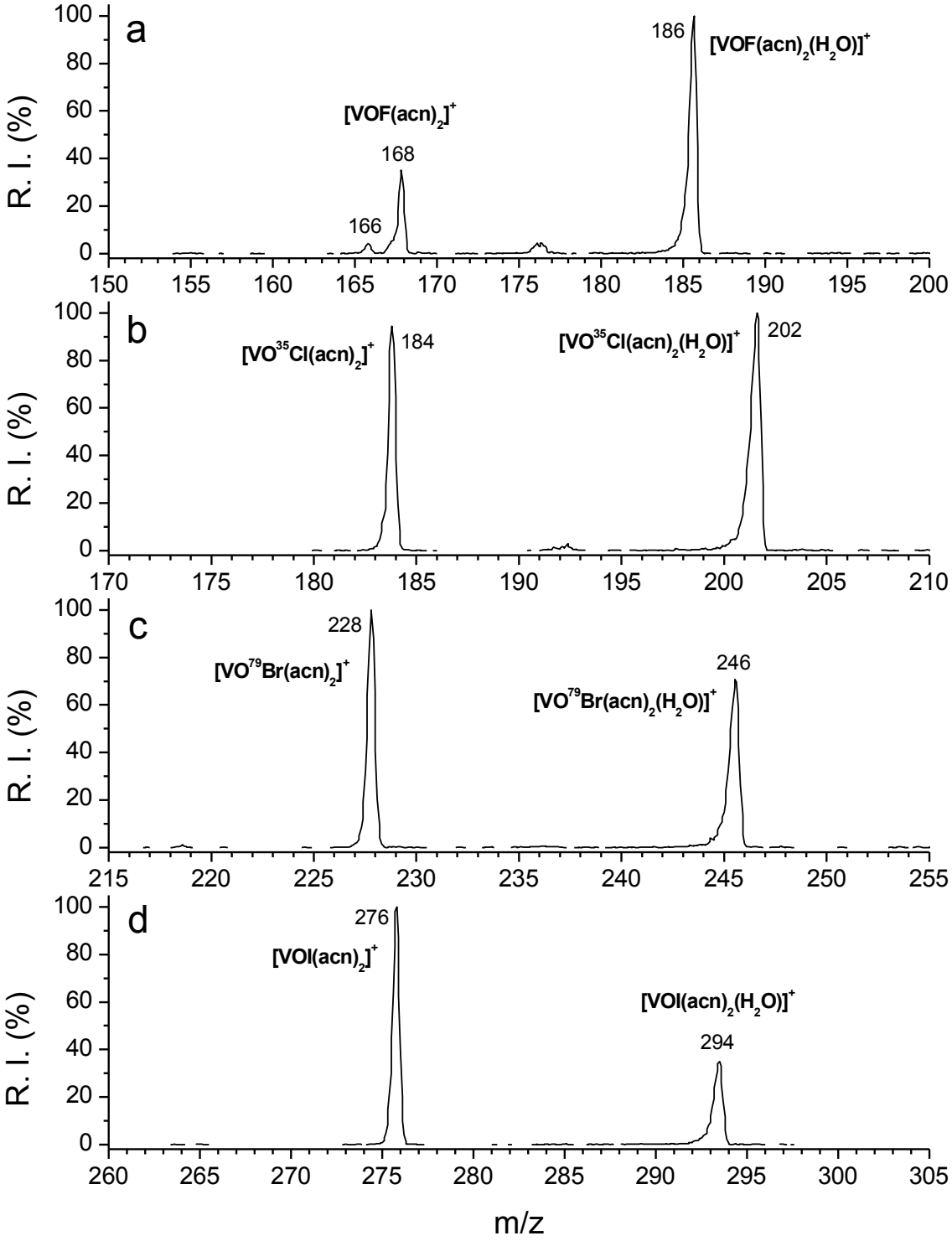

Figure 2.11 Product ion spectra generated by isolation and storage, without imposed collisional activation, of $[VOX(acn)_2]^+$, where X corresponds to (a) fluoride, (b) chloride, (c) bromide, (d) iodide. For each spectrum, the isolation time was 1000 ms.

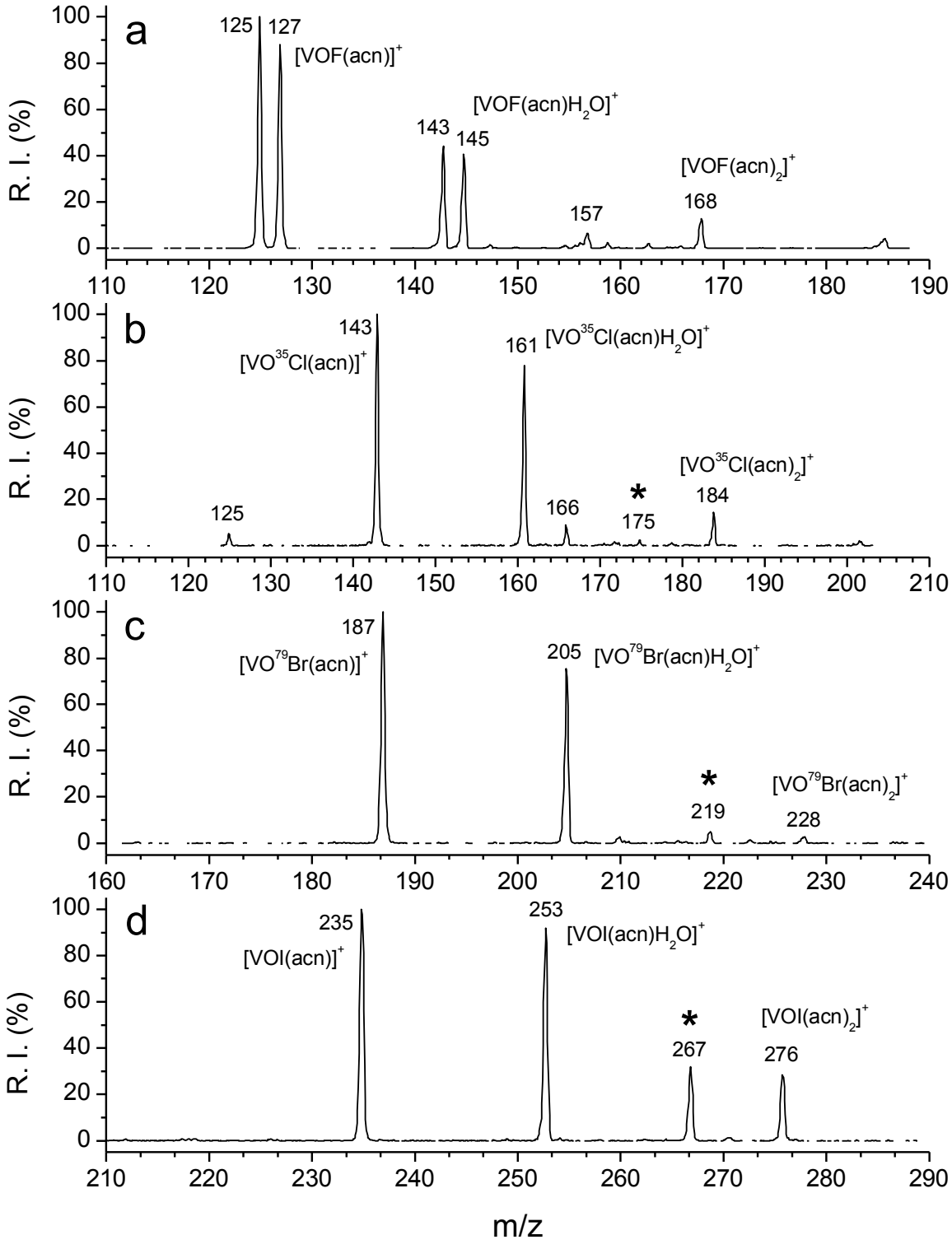

Figure 2.12 Collision-induced dissociation spectra of $[VOX(L)_2]^+$, where X corresponds to (a) fluoride, (b) chloride, (c) bromide, (d) iodide.

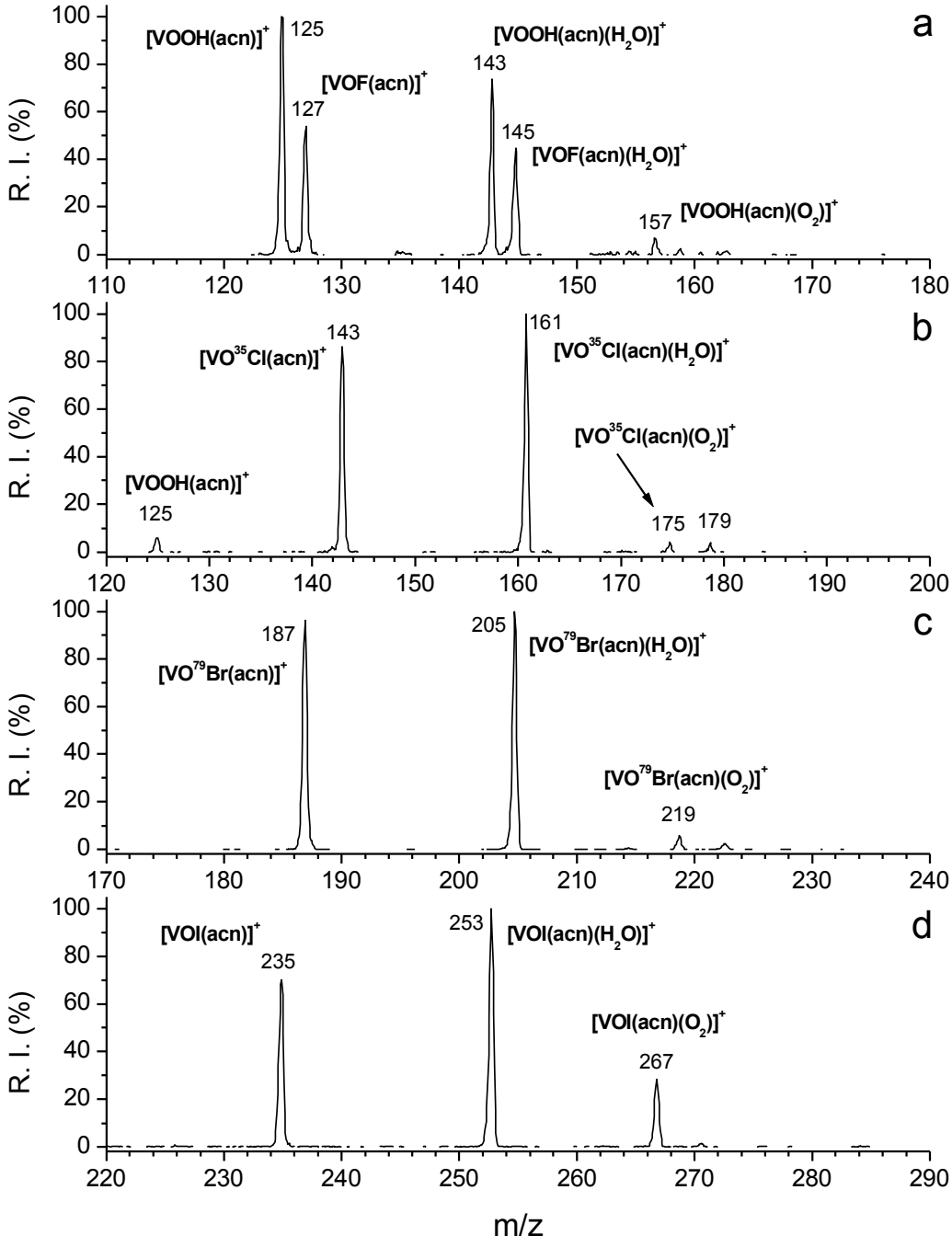

Figure 2.13 Product ion spectra generated by isolation and storage, without imposed collisional activation, of $[VOX(acn)]^+$ generated by CID of $[VOX(acn)_2]^+$ where X corresponds to (a) fluoride, (b) chloride, (c) bromide, (d) iodide.

2.6 References

[1] Corma, A.; Garcia, H; *Chem. Rev.* **2002**, *102*, 3837.

[2] Weckhuysen B. M.; Keller, D. E.; *Catal. Today* **2003**, *78*, 25.

[3] Vyboishchikov, S. F.; Sauer, J. Journal of Physical Chemistry A. **2001**, 105, 8588.

[4] Momenteau, M.; Reed, C. A. *Chem. Rev*. **1994**, *94*, 659.

[5] Yamaguchi, N.; Amakawa, Y.; Yamada, H.; Ueki, T.; Michibata, H. Zoological Science. **2006**, *23*, 909.

[6] Wang, H.; Yi, X.; Huang, G.; Xiao, J.; Li, X.; Chen, S. *Infrared Phys. Technol*. **2004**, *45*, 53.

[7] Nguyen, C.; Hyun-Joon, S.; KunTae, K; Yong-Hee, H.; Sung, M. *Sens. Actuators, A*. **2005**, *123*, 87.

[8] Mlyuka, N. R.; Kivaisi, R. T.; *J. Mater. Sci*. **2006**, *41*, 5619.

[9] Justes, D. R.; Mitric, R.; Moore, N. A.; Bonacic-Koutecky, V.; Castleman, A.W., Jr. *J. Am. Chem. Soc*. **2003**, *125*, 6289.

[10] Asmis, K. R.; Santambrogio, G.; Brummer, M.; Sauer, J. *Angew. Chem. Int. Ed. in English*. **2005**, *44*, 3122.

[11] Asmis, K. R.; Meijer, G.; Brummer, M.; Kaposta, C.; Santambrogio, G.; Woste, L.; Sauer, J. *J. Chem. Phys*. **2004**, *120*, 6461.

[12] Vyboishchikov, S. F.; Sauer, J. *J. Phys. Chem. A*. **2000**, *104*, 10913.

[13] Zemski, K. A.; Justes, D. R.; Castleman, Jr. A. W. *J. Phys. Chem. B*. **2002**, *106*, 6136.

[14] Parsons, Z.; Leavitt; C. Duong, T.; Groenewold, G. S.; Gresham, G.; Van Stipdonk, M. J. *J. Phys. Chem*. A. **2006**, *110*, 11627.

[15] Anbalagan, V.; Chien, W.; Gresham, G. L.; Groenewold, G. S.; Van Stipdonk, M. J. *Rapid Commun. Mass Spectrom*. **2004**, *18*, 3028.

[16] Gaussian 03, Revision D.01, M.J. Frisch, G. W. Trucks, H. B. Schlegel, G. E. Scuseria, M. A. Robb, J. R. Cheeseman, J. J. A. Montgomery, T. Vreven, K. N. Kudin, J. C. Burant, J. M. Millam, S. S. Iyengar, J. Tomasi, V. Barone, B. Mennucci, M. Cossi, G. Scalmani, N. Rega, G. A. Petersson, H. Nakatsuji, M. Hada, M. Ehara, K. Toyota, R. Fukuda, J. Hasegawa, M. Ishida, T. Nakajima, Y. Honda, O. Kitao, H. Nakai, M. Klene, X. Li, J. E. Knox, H. P. Hratchian, J. B. Cross, V. Bakken, C. Adamo, J. Jaramillo, R. Gomperts, R. E. Stratmann, O. Yazyev, A. J. Austin, R. Cammi, C. Pomelli, J. W. Ochterski, P. Y. Ayala, K. Morokuma, G. A. Voth, P. Salvador, J. J. Dannenberg, V. G. Zakrzewski, S. Dapprich, A. D. Daniels, M. C. Strain, O. Farkas, D. K. Malick, A. D. Rabuck, K. Raghavachari, J. B. Foresman, J. V. Ortiz, Q. Cui, A. G. Baboul, S. Clifford, J. Cioslowski, B. B. Stefanov, G. Liu, A. Liashenko, P. Piskorz, I. Komaromi, R. L. Martin, D. J. Fox, T. Keith, M. A. Al-Laham, C. Y. Peng, A. Nanayakkara, M. Challacombe, P. M. W. Gill, B. Johnson, W. Chen, M. W. Wong, C. Gonzalez, J. A. Pople, Gaussian, Inc., Wallingford, CT, **2004**.

[17] Janssens, E.; Santambrogio, E.; Brummer, M.; Woste, L.; Sauer, J.; Meijer, G.; Asmis, K. R. *Phys. Rev. Lett*. **2006**, *96*, 233401.

[18] Gutsev, G. L.; Rao, B. K.; Jena, P.; *J. Phys. Chem. A*. **2000**, *104*, 11961.

[19] Fielicke, A.; Mitric, R.; Meijer, G.; Bonacic-Koutecky. V.; von Helden, G. *J. Am. Chem. Soc*. **2003**, *125*, 15716.

[20] Glukhovtsev, M. N.; Pross, A.; McGrath, M. P.; Radom, L. *J. Chem. Phys*. **1995**, *103*, 1878.

[21] Bader, R. F. W.; Atoms in molecules: A quantum theory,2nd ed.; Oxford University Press: New York, 1994.

[22] MOLPRO, version 2006.1, a package of ab initio programs, H.-J. Werner, P. J. Knowles, R. Lindh, F. R. Manby, M. Schütz, P. Celani, T. Korona, G. Rauhut, R. D. Amos, A. Bernhardsson, A. Berning, D. L. Cooper, M. J. O. Deegan, A. J. Dobbyn, F. Eckert, C. Hampel and G. Hetzer, A. W. Lloyd, S. J. McNicholas, W. Meyer and M. E. Mura, A. Nicklass, P. Palmieri, R. Pitzer, U. Schumann, H. Stoll, A. J. Stone, R. Tarroni and T. Thorsteinsson, see http://www.molpro.net.

[23] Bell, R. C.; Castleman, Jr., A. W. *J. Phys. Chem. A*. **2002**, *106*, 9893.

[24] Steiner, E.; Soncini, A.; Fowler, P. W. *Org. Biomol. Chem*. **2005**, *3*, 4053.

[25] Chen, Z.; Chaitanya, S. W.; Corminboeuf, C.; Puchta, R.; von Rague Schleyer, P.; *Chem. Rev*. **2005**, *105*, 3842.

[26] Cheeseman, J. R.; Trucks, G. W.; Keith, T. A.; Frisch, M. J. *J. Chem. Phys*. **1996**, *14*, 5497.

3 The Structure and Energetics of Singlet, Closed-Shell [B, C, F, H_2]: Simplicity Resulting in Diversity

In the current chapter, we discuss our high-level quantum chemical results for the structure and energetics of singlet (closed-shell) isomers corresponding to the stoichiometry of one boron, carbon, and fluorine apiece, and two hydrogens. While the ketene- and diazomethane-like H_2C=B-F plausibly emerges as the most stable isomer, a variety of novel structural features emerge for the assembled energy minima. All of these species are compared as well as transition states that connect them. Comparison is also made with corresponding forms of the aforementioned ketene and diazomethane to which our species are isoelectronic, as well as with our earlier studied [B, C, F, H_3]$^+$ which may be recognized as the protonated counterparts of the species of direct interest in this study.

3.1 INTRODUCTION

The isomeric compounds with the formula [B, C, F, H_2] are formally the simplest (i.e. neutral, closed-shell) species containing each of the elements together: boron, carbon, fluorine and hydrogen. Each of these elements has compounds with diverse structures. Boron is commonly found in species with coordination numbers (number of bonding partners) 3 – 6, and occasionally lower and higher values are observed as well. (The higher values are typically found in boron hydrides, carboranes, and their derivatives.) Carbon is commonly found in species with coordination numbers 2 – 4, with 1 and 5 and 6 not uncommon. (The value of 1 has long been known in isonitriles, 5 in protonated alkanes and other nonclassical carbocations, and both 5 and 6 in the aforementioned carboranes and derivatives.) Fluorine has the common coordination number of 1, but 2 is increasingly found as well – we recognize both the species and the researcher in citing Žemva's diverse salts containing HF, AsF_3 and XeF_2 as ligands in the cation[1,2]. We might even dare to say that coordination number 0 and/or 6 and beyond is a commonplace occurrence in that these provide alternative descriptions of the fluorine as found in binary fluoride salts. Hydrogen is almost totally limited to coordination numbers 1 and 2 (forgetting about hydride salts) but here we find two significantly different electronic environments with 2 coordination. These are the so called 3 center/2-electron bonds or hydrogen bridges found in the above boron hydrides and their derivatives, and the commonly known hydrogen bonds as found in $[HF_2]^-$ and liquid HF, as well as proteins, DNA and (of course)

liquid water, which relatedly have also, albeit rarely, been called 3 center/4-electron bonds.

Returning to [B, C, F, H_2] the simplest structure we can write is CH_2~B~F, where the squiggles "~" indicate there is bonding between the carbon and boron, and boron and fluorine but no suggestion of bond order or bond strength is to be inferred. We wish to hedge, at least for the moment, about how much the resonance structures CH_2=B-F and $CH_2=B^-=F^+$ contribute to the description of the molecule. (This is neither laziness nor cowardice; even the well-known species BF_3 has such complications in its description. More precisely, while many – if not most – in the theoretical community argue against B-F π bonding, others have emphatically included it. See, for such a dissenting view, *Periodic Trends in Bond Dissociation Energies. A Theoretical Study*, O. Mó, M. Yáñez, M. Eckert-Maksić, Z.B. Maksić, I. Alkorta, J. Elguero, J. Phys. Chem. A 109 (2005) 4359-4365.) Except for the dicoordinated boron, this species looks rather unexceptional. After all, it is isoelectronic and isostructural to the long-known diazomethane, CH_2~N~N (with a related ambiguity $CH_2=N^+=N^-$ and CH_2^--$N^+\equiv$N) and ketene (rather definitively CH_2=C=O). Both of these latter compounds have classical isomers. For diazomethane, we have cyanamide (H_2N-C≡N), carbodiimide (HN=C=NH) and 1*H* and 3*H*-diazirine (with their strained three-membered ring containing the carbon and the two nitrogens, the latter isomer also antiaromatically destabilized). For ketene, we have ethynol (HC≡C-OH) and oxirene (with a likewise strained and antiaromatic ring with two carbons and an oxygen). In that the C~N and C~C bonds in diazomethane and ketene are well established to be quite weak and so easily broken, we expect

much the same for the C~B bond in CH_2~B~F. It is thus not unreasonable to assume that it will likewise have a variety of isomers, even if only CH_2=B-F (both connectivity and bond order now conveyed explicitly) has been seen so far in the laboratory. Some are these isomers are expected to mimic those of diazomethane and ketene.

However, by precedent of the simple ions composed of the same elements B, C, F and H, even greater diversity of structural type and electronic diversity may be expected. After all, we earlier showed by use of quantum chemical calculations that ions with the composition $[B, C, F, H_3]^+$ have ten isomeric minima[3]. The most stable is $[CH_3BF]^+$, isoelectronically and isostructurally paralleling the well understood $[CH_3N_2]^+$ and $[CH_3CO]^+$. Indeed, we recognize this stoichiometry as corresponding to protonated [B, C, F, H_2] in the form of CH_2BF much as these last two ions are protonated diazomethane and ketene, respectively. (We may also say that these species are methylated *B*F, N_2 and *C*O and so recall earlier discussions of F- and O-methylation of BF and CO, respectively.)

In the current study we will report the results of quantum chemical calculations on only closed shell species. We will thus describe studies on only the singlet, not triplet, state of the carbene BH_2CF as to parallel, and so exploit, the study of $[B, C, F, H_3]^+$. In the current study we will also not make any additional comparisons with diazomethane, ketene and their isomeric neutral and protonated counterparts. We likewise also wish to avoid explicit discussions of diradicals that parallel questions such as the importance of $CH_2^{\bullet}$-N=N• in the description of diazomethane, and even of

monoradicals as would be the case for the presumed plethora of ions with the description [B, C, F, H_2]$^+$ that arise from loss of electrons from our neutrals.

Previous computational investigations on [B, C, F, H_2] have been reported by Lanzisera and Andrews[4] and by Minyaev and Gribanova[5]. Minyaev and Gribanova performed the computations to assess the importance of π-bonding in carbon-halogen and other carbon-X bonds. In addition to the compounds H_2BCX and H_2CBX (X = F, Cl), H_2CX and H_2CCX (X = O, F^+, Ne^{2+}, S, Cl^+, Ar^{2+}) were also examined[5]. Lanzisera and Andrews performed the computations to complement their matrix isolation study of the reaction of laser-ablated boron atoms with CH_3X (X = F, Cl, Br)[4]. This study is one of a series of such studies from which Andrews and co-workers have identified a number of novel, small boron-containing molecules[4,6-10]. For example, reactions between atomic boron and mono- or dimethylamine yielded three new iminoboranes, CH_3BNH, CH_3NBH and CH_3BNCH_3, as well as the related isomer CH_2BNH_2[7]. Three major new species were also produced from the reaction of boron with methanol, namely CH_3BO, CHBO, and CHBOH[8].

Both of the earlier investigations on [B, C, F, H_2] considered only minima with connectivities H_2CBF, H_2BCF[4,5] and F(H)CBH[4]. We have mapped out the potential energy surface (PES) of this system more extensively by considering a number of alternative connectivities for the minima and by identifying transition states on isomerization pathways between the minima. Also, our results indicate that whether or not BH_2CF corresponds to a minimum on the PES is sensitive to the size of the basis set and the level of calculation.

3.2 CALCULATIONAL DETAILS

Conventional ab initio molecular orbital calculations were carried out with use of the Gaussian 98[11] and 03[12] suites of programs. Minima on the singlet PES of [B, C, F, H_2] were located using both Møller-Plesset second-order perturbation, MP2[13,14], calculations and quadratic configuration interaction, QCISD[15], calculations with the aug-cc-pVDZ basis set[16,17]. Transition states connecting the more stable minima, i.e. those for which fragmentation is not necessarily the most likely decomposition pathway, were determined at only the MP2/aug-cc-pVDZ level of calculation. Tight convergence criteria were utilized to optimize structures fully, and computed energies were then improved by evaluating coupled cluster CCSD(T)/aug-cc-pVXZ, X = D, T, and Q, and Brueckner double BD(T)/aug-cc-pVTZ single-point energies[18-20]. Single-point energies required for the cationic systems[3] have been reevaluated at the CCSD(T) level[19]. All stationary points were characterized by harmonic vibrational frequency calculations; the reported vibrational frequencies are unscaled. Intrinsic Reaction Coordinate, IRC[21-23], calculations were performed to verify the minima connected by each transition state.

In the truncated coupled cluster CCSD[24] and quadratic configuration interaction QCISD[15] methods, the electron correlation energy is taken into account by generating all singly and doubly excited determinants. Likewise, the CCSD(T)[19] and procedure calculates the singles and doubles contributions to the correlation energy directly but use perturbation theory to approximate the triples contribution. Brueckner theory[18,20]

is a variation of coupled cluster theory that involves optimizing the orbitals used in the Slater determinant such that the contribution from singles is constrained to be zero. The BD(T) approach can alleviate overestimations of the triples correction to the correlation energy associated with large singles amplitudes[25].

CCSD(T) total energies at the complete basis set (CBS) limit have been estimated with the function first introduced by Peterson et al. (equation 1) [ref]. In equation 1, X = 2 (DZ), 3 (TZ) or 4 (QZ) and E_{CBS} is the extrapolated energy as $X \rightarrow \infty$.

$$E(X) = E_{CBS} + A \exp[-(X - 1)] + B \exp[-(X - 1)^2] \quad (1)$$

The augmented correlation consistent basis sets of Dunning and coworkers are particularly well suited for estimating E_{CBS} values because this family of basis sets was constructed to converge systematically toward the basis set limit[16,17]. Only the CCSD(T)/aug-cc-pVXZ//MP2/aug-cc-pVDZ single point energies were utilized to evaluate E_{CBS}.

From this point we will use MP2 to signify MP2/aug-cc-pVDZ and QCISD to signify QCISD/aug-cc-pVDZ; CCSD(T)//MP2, CCSD(T)//QCISD and BD(T)//MP2 will be utilized to represent the CCSD(T)/aug-cc-pVTZ//MP2/aug-cc-pVDZ, CCSD(T)/aug-cc-pVTZ//QCISD/aug-cc-pVDZ and BD(T)/aug-cc-pVTZ//MP2/aug-cc-pVDZ single-point calculations, respectively. The CCSD(T) total energies at the CBS limit will be designated as CCSD(T)/CBS.

An NBO[26] analysis was performed for each of the minima to provide information on bonding. This type of analysis[27-31] considers deviations in the molecular electron

density from the best classical Lewis structure. It also associates the underlying localized orbitals with concepts such as hybrid orbitals, steric repulsion, resonance, and charge transfer. We have utilized NBO analysis of the Hartree-Fock molecular orbitals to elucidate the influence of hyperconjugative effects on the (MP2 optimized) structures and stabilities of the minima. The second-order perturbation approach was employed to evaluate energies of hyperconjugative interactions ($\Delta E^{(2)}$(donor→acceptor))[29]. For all of the minima, the Lewis NBOs describe about 99% of the total electron density.

3.3 RESULTS AND ANALYSIS

3.3.1 Minima and Transition States Identified

3.3.1.1 Minima

Linear, bent, cyclic and hydrogen-bonded arrangements of [B, C, F, H_2] were examined, but all of the cyclic arrangements considered converted to acyclic molecules. (This is not a surprise – rings containing fluorine are rare.) Ten acyclic connectivities are minima at the MP2 level of calculation, and only nine corresponding connectivities are minima at the QCISD level. The isomers have been numbered in order of decreasing stability, based on the MP2 geometries, and are illustrated in Figure 3.1. Table 3.1 provides bond lengths, bond angles and dihedral

angles. As expected, one of the classical covalently bound structures is H_2CBF **1**, isoelectronically and isostructurally related to H_2CCO and H_2CNN. Combination of borane(1) with FCH yields isomer **2** H(F)CBH and the weak F-B bonding heterodimer **10** HCF...BH. Two of the minima have a two-coordinate fluorine atom, the unbranched HCBFH **6**, analogous to ethynol, and the carbyne H(C)BFH **7**, analogous to hydroxyvinylidene, with its 1-coordinated carbon. Only one structure $BC(H)_2F$ **3** has a 4-coordinate carbon atom – this species shows no tendency to "collapse" to form a ring isoelectronically related to 3*H*-diazirine. Complexes HCH…BF **4** and HCH…FB **5** are describable as having unconventional C–H…B and C–H…F hydrogen bonds, respectively. Unconventional or improper hydrogen bonds have the unusual features of decreasing X–H bond length, increasing X–H stretching frequency and decreasing IR intensity upon complexation[32]. This type of hydrogen bonding has been observed primarily when carbon is the proton-donating atom X[33-38] but has been reported for other proton donors as well, e. g. Si and P[39]. Isomers **8** and **9** are van der Waals complexes between a hydrogen molecule and triatomic FCB species. Complex **8** H_2...C(F)B is linked through the carbon atom, whereas complex **9** H_2...FCB is linked through the fluorine atom. At the QCISD level of calculation **9** rearranges to **8** without any activation barrier.

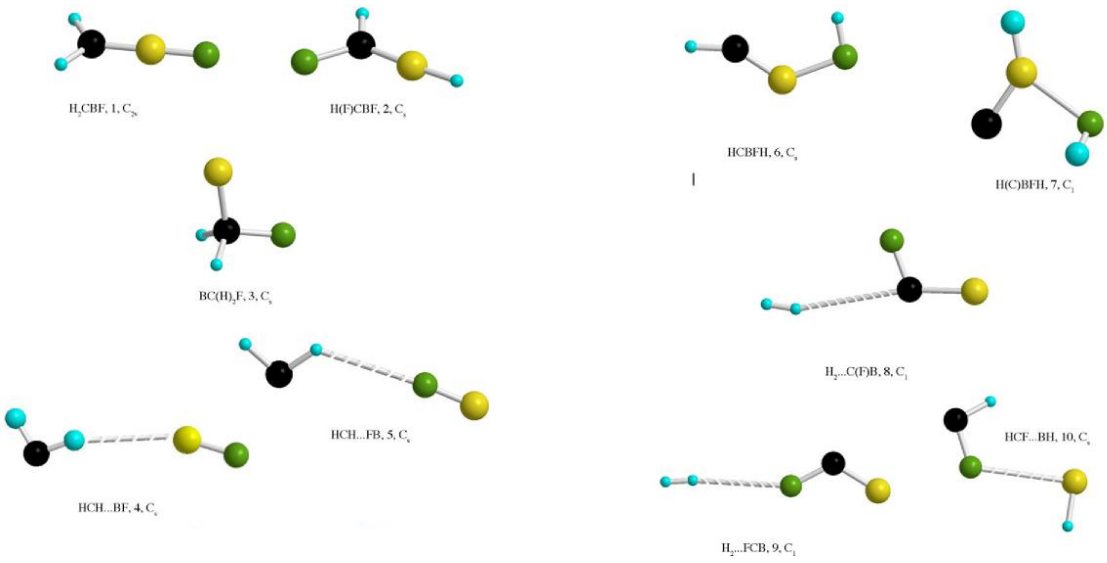

Figure 3.1 Ball and stick representations of the nine isomers located on the singlet potential energy surface of [B, C, F, H_2]. The degrees of grayness are: C > F > B > H.

We have seen many species on the singlet potential energy surface of [B, C, F, H_2], many with novel connectivities and bonding patterns; nevertheless, the connectivities identified for [B, C, F, H_2] are not as diverse as those identified for [B, C, F, H_3]$^{+3}$ with its additional H atom and charge. In particular, there are no neutral structures corresponding to the cationic structures with CFB or CFH fluorine bridges. Two other singlet species that are missing are borylfluoromethylene, H_2BCF and (fluoroboryl)methylene H(F)BCH with their tricoordinate boron, dicoordinate carbon, and singly coordinated fluorine description. These species appear quite normal, in that organoboranes and dicoordinated carbon as found in carbenes are both well chronicled in both the experimental and theoretical literature. However, our quantum chemical calculations show that neither species is a minimum when studied as a

singlet, as were all the other compounds discussed above. This is, perhaps, disconcerting given the variety of other structures that enjoy stability, i. e. that lie in local or global minima. We understand this seeming omission by noting the empty p (or should we say low lying empty π) orbital on B. To maximize stabilization in this isomer the H_2B (HBF) group may be expected to rotate perpendicular to the B-C-F (B-C-H) plane allowing for maximal B-H (and B-F) bond donation and hyperconjugation. Barrierless hydrogen migration, just like found in $[H_3BCF]^+$, results in even more stabilization. Equivalently, H_2BCF and H(F)BCH fail to exist, even for the theoretical chemist.

It should be noted that borylfluoromethylene is a minimum on the PES of [B, C, F, H_2] when studied at lower levels of theory and/or with smaller basis sets. H_2BCF equilibrium structures with no imaginary frequencies have been reported by Lanzisera and Andrews[4] (BP86/6-311G(d)) and by Minyaev and Gribanova[5] (B3LYP/6-311+G(d,p) and CCD(full)/6-311+G(d,p)). In order to confirm our conclusion that H_2BCF is not stable, we extended our calculations on this structure to the BP86/aug-cc-pVDZ, BP86/aug-cc-pVTZ and MP2/aug-cc-pVTZ levels of theory. In each case the results indicate that H_2BCF is no longer a minimum.

Clearly, the structures at minima for [B, C, F, H_2] are sensitive to the level of calculation. However, those minima observed at both the MP2 and QCISD levels have similar optimum geometries (Table 3.1). Most of the equilibrium bond distances differ by less than 0.01Å for the two methods. The exceptions occur for the long, weaker bonds, such as the H…F bond in **5**, for which the deviations are as large as 0.1 Å. In general, the QCISD values are elongated compared to the MP2 values. The

largest difference in the MP2 and QCISD bond angles is 12° (isomer **5**) but most vary by less than 2°. With the exception of HH…C(F)B **8**, the results for the dihedral angles are similar. The symmetry of **8** changes from C_1 to C_s as the level of theory improves. This is the only isomer for which such a change occurs. Despite these rare discrepancies in the two sets of geometries, the two sets of CCSD(T) single-point energies and relative thermochemical values are generally in good agreement (see below). For this reason, we examined the reaction pathways between isomers only at the MP2 level.

Table 3.1 Geometric parameters for minima, transition states, and fragmentation products[a]

Structure	Bond Lengths			Bond Angles			Dihedral Angles		
CH_2BF	CB	1.399	[1.401]	HCB	121.1	[121.3]			
1, $\mathbf{C_{2v}}$	BF	1.313	[1.313]	HCH	117.3	[117.4]			
	CH	1.092	[1.093]						
H(F)CBH	CB	1.418	[1.420]	FCB	124.0	[123.2]			
2, $\mathbf{C_s}$	CF	1.382	[1.383]	HCF	113.2	[112.8]			
	CH	1.095	[1.096]	HCB	122.8	[123.9]			
	BH	1.180	[1.183]	HBC	176.0	[176.5]			
$BC(H)_2F$	CB	1.603	[1.691]	FCB	107.0	[107.2]	HCBF	118.8	[118.8]
3, C_s	CF	1.422	[1.421]	HCF	108.5	[108.3]	HCBH	122.3	[122.5]
	CH	1.106	[1.108]	HCB	112.0	[112.2]			
$H_1CH…BF$	BF	1.302	[1.307]	HCH	101.8	[101.3]	$H_1CH…B$	180.0	[180.0]
4, C_s	CH	1.118	[1.124]	CH…B	161.3	[163.4]			
	CH_1	1.119	[1.126]	H…BF	162.7	[164.9]			
	H…B	3.007	[3.089]						

$H_1CH…FB$	BF	1.303	[1.308]	HCH	101.7	[101.3]	$H_1CH…F$	180.0	[180.0]
5, C_s	CH	1.119	[1.125]	CH…F	114.5	[126.1]			
	CH_1	1.119	[1.125]	H…FB	172.7	[174.9]			
	H…F	2.863	[2.793]						
HCBFH	CB	1.356	[1.367]	CBF	134.4	[127.1]	HCBF	180.0	[180.0]
6, C_s	BF	1.593	[1.629]	HCB	151.7	[149.8]	CBFH	0.0	[0.0]
	CH	1.083	[1.085]	HFB	97.0	[98.8]			
	FH	0.949	[0.941]						
H(C)BFH	CB	1.475	[1.478]	HBC	167.0	[169.0]	HBFH	136.2	[133.3]
7, C_1	FB	1.912	[1.996]	HBF	105.1	[103.1]	CBFH	-44.0	[-46.8]
	BH	1.185	[1.188]	HFB	99.5	[101.7]			
	FH	0.941	[0.934]						
$H_2…C(F)B$	CB	1.455	[1.682]	FCB	120.9	[111.9]	HH…CF	40.1	[0.0]
8, C_1 [C_s]	CF	1.334	[1.337]	H…CF	82.3	[79.4]	HH…CB	160.1	[180.0]
	HH	0.756	[0.762]	HH…C	165.3	[164.2]			
	H…C	2.885	[2.990]						
$H_2…FCB$	CB	1.454		FCB	120.8				
9, C_s	CF	1.336		H…FC	148.9				
	HH	0.755		HH…C	173.6				
	H…F	2.737							
HCF…BH	CF	1.342	[1.345]	CFB	112.8	[113.4]	HCF…B	0.0	[0.0]
10, $\mathbf{C_s}$	CH	1.125	[1.133]	HCF	101.2	[101.3]	CF…BH	180.0	[180.0]
	BH	1.241	[1.249]	HBF	86.8	[86.3]			
	F…B	2.836	[2.963]						
TS1-2	CB	1.389		HCB	178.7		HCBH	180.0	
C_s	CH	1.080		HBC	169.3				
	BH	1.180		C…F…B	49.1				
	C…F	1.672							
	B…F	1.668							

TS1-3	BC	1.531	HCB	122.2	HC…F…B	±117.3
C_s	CH	1.099	HCH	115.6		
	C…F	1.919	HC…F	107.8		
	B…F	1.568	B…F…C	50.9		
TS1-6	BC	1.362	CBF	122.2	HCBF	180.0
C_s	BF	1.596	HCB	152.5	CBFH	0.0
	CH	1.083	HFB	76.7		
	FH	0.996	HC…H	154.7		
	H…C	2.099				
TS2-3	BC	1.493	FCB	130.2	FC…H…B	120.9
C_1	CF	1.350	HCB	117.0	HC…H…B	-114.0
	CH	1.106	B…H…C	61.8		
	C...H	1.557	H…CF	117.8		
	B…H	1.325	H…CH	103.5		
FCB	CB	1.455	FCB	130.2		
	CF	1.334				
HCB	CB	1.402	HCB	75.8		
	CH	1.183				
HBC	CB	1.490	HBC	180.0		
	BH	1.184				
HCF	CF	1.333	HCF	101.6		
	CH	1.128				
CH_2	CH	1.120	HCH)	101.5		
BF	BF	1.304				
BH	BH	1.244				
HF	HF	0.925				
H_2	HH	0.755				

[a]MP2/aug-cc-pVDZ and QCISD/aug-cc-pVDZ (in brackets) data. [b]Bond lengths in angstroms, bond angles and dihedral angles in degrees.

3.3.1.2 Multiple Bond Character

In their study of H_2CBF and H_2CBCl, Minyaev and Gribanova[5] noted that the B-X bond lengths obtained calculationally for these molecules, about 1.29 Å and 1.69 Å respectively, were considerably shorter than those obtained experimentally[40] for BF_3 and BCl_3, about 1.31 Å and 1.74 Å respectively. On the basis of delocalized molecular orbital and NBO analyses of H_2CBX, they attributed these bond length differences to B-X double bonding. The analyses also revealed C=B bonds for these molecules and C=X bonds for H_2CX and H_2CCX (X = O, F^+, Ne^{2+}, S, Cl^+, Ar^{2+})[5]. The highest occupied molecular orbital (HOMO) for H_2CBF **1** has a bonding π-interaction between carbon and boron, with coefficients of similar magnitude on the two atoms. In contrast, the B-F overlap in the occupied bonding π-orbitals is not only much weaker, it is offset, at least partially, by that in a corresponding occupied antibonding orbital. Therefore, although we agree that there is evidence for C=B bonding in H_2CBF **1**, we find the evidence for B=F bonding less clear-cut. As has been pointed out by Gillespie and Popelier[41], there is seemingly no need to invoke fluorine back-bonding to rationalize short, strong B-F bonds. They can be understood from the high electron density in the internuclear region and the strong attraction between the large atomic charges.

C-B double bonding is also indicated in isomers H(F)CBH **2**, HCBFH **6** and H(C)BFH **7**. The HOMO for each of these molecules has the same characteristics as the HOMO for **1**. The C-F bond in **2**, however, is unlikely to have significant double bond character as the π-orbital pattern for these atoms is similar to that observed for the boron and fluorine in **1**.

3.3.1.3 Transition Structures

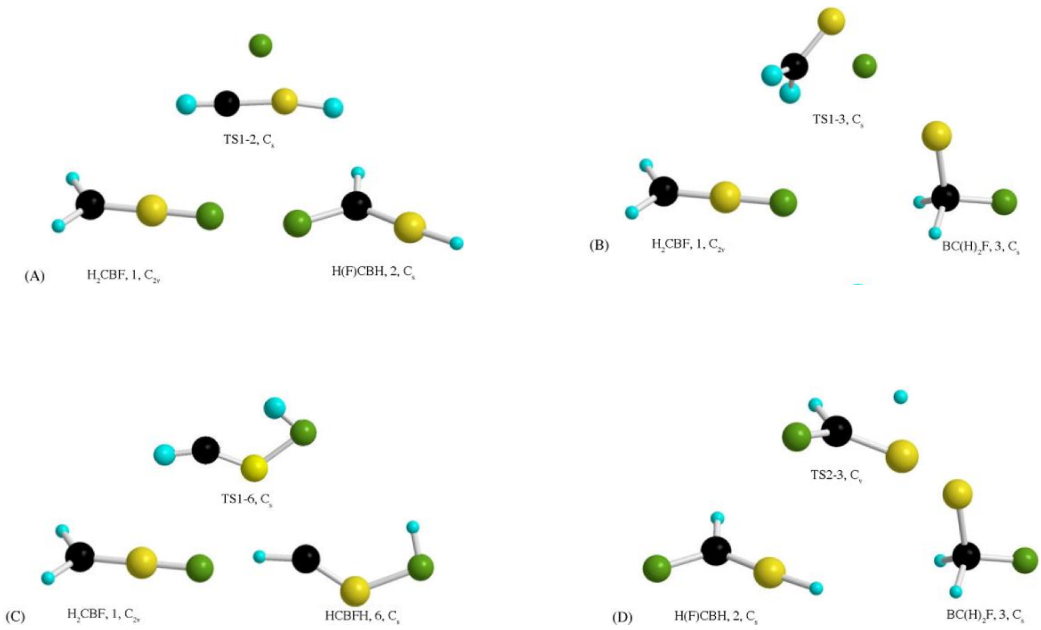

Figure 3.2 Ball and stick representations of transition states and connected minima on the singlet potential energy surface of [B, C, F, H_2]. The degrees of grayness are: C > F > B > H.

The four most relevant transition structures located on the PES of [B, C, F, H_2] are shown in Figure 3.2. Bond lengths, bond angles and dihedral angles are listed in Table 3.1. For convenience, each transition structure is labeled to denote the minima it connects. We focused on the reaction pathways between **1** and **2**, **1** and **3**, **1** and **6**, and **2** and **3** because these are the molecules that are more likely to rearrange rather than merely fragment. In addition, on the basis of the bond-insertion mechanism preferred by Andrews and coworkers[4,7-9,42] these are the most likely isomers to be formed in the reaction between laser ablated boron and methyl fluoride.

As presented in the figure, all of the isomerizations are endothermic and, thus, obey the Leffler-Hammond's postulate[43,44], as all of the transition structures resemble the product more closely than the reactant. **TS1-3** and **TS2-3** have structures analogous to what would be expected on the basis of chemical intuition (Figure 3.2(B) and Figure 3.2(D)). Conversion of **1** to **3** requires a shift of the fluorine atom from the boron to the carbon, whereas conversion of **2** to **3** requires a shift of the hydrogen atom from the boron to the carbon. For each of these reactions, the transition structure has the relevant atom transferring across the B–C bond.

The remaining two transition structures in Figure 3.2 have more unexpected features (Figure 3.2(A) and Figure 3.2(C)). Transition structure **TS1-2** indicates that the requisite interchange of hydrogen and fluorine atoms occurs in a stepwise manner. The transfer of the hydrogen from the carbon to the boron is essentially complete before the fluorine begins to move from the boron to the carbon. In fact, the B–H bond length is 1.180 Å in both **TS1-2** and **2**. Likewise, in transition

structure **TS1-6**, the requisite movement of a hydrogen atom from the carbon to the fluorine is nearly complete. In this case, the hydrogen is displaced by only 5% from its equilibrium distance in **6**.

As noted in the previous section, the carbene H_2BCF is a transition state on the PES of [B, C, F, H_2] for both levels of calculation utilized in this work. H_2BCF does not lie on an isomerization pathway; rather, it is the transition structure for the hydrogen exchange process between carbon and boron for isomer **2**.

3.4 Energetics

Although standard coupled cluster (CC) theory is more tolerant of a poor reference wave function than is MP theory, the results do depend on the quality of the zeroth-order wave function. The T_1 diagnostic of Lee and Taylor[45] is one measure of the quality of the CCSD wave function, and our calculated values for this diagnostic are reported in Table 3.2. A value of $T_1 > 0.02$ is indicative of multi-reference character in the wave function and of a possible need for caution in interpreting the CCSD(T) results.

Only H_2…C(F)B **8**, H_2…FCB **9**,**TS1-3**, FCB and HCB have T_1 values significantly greater than 0.02, but the values for some of the other transition states are marginal (Table 3.2). Given the T_1 value for FCB and the conflicting MP2 and QCISD results for **9**, the observed magnitudes of T_1 for **8** and **9** are not unexpected. Multi-reference calculations are currently underway in our laboratory to quantitate our

understanding of these at best weakly bound complexes and their triatomic components.

A comparison of the BD(T)/MP2 and CCSD(T)/MP2 results demonstrates that there is no glaring triples overcorrection for any of the [B, C, F, H_2] systems. The BD(T)/MP2 and CCSD(T)/MP2 thermochemical data deviate by no more than 6 kJ/mol, and most of the discrepancies in the data are considerably smaller. More specifically, isomers **8** and **9** are destabilized by 6 kJ/mol with respect to isomer **1** at the BD(T)/MP2 level of calculation compared to the CCSD(T) level. Likewise, **TS1-3** is destabilized by 3.5 kJ/mol with respect to both **1** and **3**. Otherwise, the discrepancies in the two sets of results are all $\leq$ 1 kJ/mol. Therefore, only the CCSD(T)/MP2 data are tabulated.

3.4.1 Minima

Thermochemical data for the isomers relative to the data for CH_2BF **1** are collected in Table 3.3. Only the CCSD(T)/QCISD and CCSD(T)/MP2 values are tabulated because the trends in the MP2/MP2 and QCISD/QCISD data reproduce those reported for the CCSD(T)/QCISD data. The placement of the high-lying isomers H_2…C(F)B **8** and HCF…BH **10** is the only difference between the two sets of stability trends. At the CCSD(T) level of calculation, the MP2 equilibrium geometry for **8** is about 60 kJ/mol more stable than the corresponding QCISD equilibrium geometry. Consequently, **8** is destabilized by about 25 kJ/mol with respect to **10** for the CCSD(T)/QCISD results (Table 3.3). Otherwise, the single-point energies are

quite insensitive to which set of geometrical parameters is utilized; therefore, the CCSD(T)/MP2 thermochemical data will be used in the remainder of this section. Converting energies to enthalpies and Gibbs free energies stabilizes the other structures with respect to **1**, but significant differences are observed only for the weakly bound structures. Although the contribution of the TΔS term (T = 298 K) to the free energy is as large as 30 kJ/mol, the trends in relative free energy and enthalpy are identical for the current set of molecules. Similar results were found in our earlier work on the cationic system $[B, C, F, H_3]^+$.

Table 3.2 T_1 Values for Neutral and Corresponding Protonated Minima, Fragmentation Products and Transition Structures.[a]

Isomer	T_1	Transition Structure	T_1	Fragment	T_1	Cation[b]	T_1
H_2CBF	0.014	**1** TS1-2	0.020	BF	0.017	$[H_3CBF]^+$	0.014
1	[0.014]					**1′**	
H(F)CBH	0.014	**2** TS1-3	0.064	BH	0.014	$[F(H)CBH_2$	0.019
2	[0.014]					**2′**	
$BC(H)_2F$	0.014	**3** TS1-6	0.019	CH_2	0.0095	$[H_2CBFH]^+$	0.016
3	[0.014]					**4′**	
HCH…BF **4**	0.014	**4** TS2-3	0.021	FCB	0.065	$[HF(H)CBH]^+$	0.015
	[0.014]					**5′**	
HCH…FB **5**	0.014	**5**		HBC	0.016	$[HFC(H)_2B]^+$	0.015
	[0.015]					**8′**	
HCBFH	0.019			HCB	0.037		
6	[0.020]						
H(C)BFH	0.016			HCF	0.019		

7	[0.016]		
H_2…C(F)B **8**	0.061	HF	0.010
	[0.053]		
H_2…FCB	0.060	H_2	0.0056
9			
HCF…BH **10**	0.018		
	[0.018]		

[a]CCSD(T)/aug-cc-pVTZ//MP2/aug-cc-pVDZ and CCSD(T)/aug-cc-pVTZ//QCISD/aug-cc-pVDZ (in brackets) data. [b]Minima on the $[B, C, F, H_3]^+$ PES [3] with neutral $[B, C, F, H_2]$ counterparts.

Table 3.3 Relative Thermochemical Data for the Minima Identified.[a,b]

Isomer	ΔE	Δ(E + ZPE)	$\Delta_{298}H$	$\Delta_{298}G$
H_2CBF	0.0	0.0	0.0	0.0
1	(0.0)	(0.0)	(0.0)	(0.0)
	[0.0]	[0.0]	[0.0]	[0.0]
	0.0	**0.0**	**0.0**	**0.0**
H(F)CBH	249.5	247.3	246.8	244.6
2	(249.8)	(247.5)	(247.1)	(244.8)
	[249.6]	[246.9]	[246.5]	[244.2]
	251.6	**249.4**	**248.9**	**246.7**
$BC(H)_2F$	347.5	349.3	348.6	346.1
3	(347.5)	(349.3)	(348.7)	(346.2)
	[347.5]	[349.1]	[348.4]	[346.1]
	355.9	**357.7**	**357.0**	**354.5**
HCH…BF	474.6	454.2	461.8	433.8
4	(474.5)	(454.1)	(461.7)	(433.7)
	[475.4]	[453.7]	[461.6]	[432.1]
	484.9	**464.5**	**472.1**	**444.1**
HCH…FB	477.0	455.9	464.0	433.5

5	(476.9)	(455.8)	(463.9)	(433.4)
	[477.8]	[455.6]	[463.8]	[432.8]
	486.9	**465.8**	**473.9**	**443.4**
HCBFH	498.8	494.1	495.5	490.2
6	(499.8)	(495.1)	(496.6)	(491.3)
	[498.3]	[493.0]	[494.6]	[489.0]
	501.0	**496.3**	**497.8**	**492.5**
H(C)BFH	601.9	590.2	592.6	584.0
7	(602.0)	(590.4)	(592.8)	(584.2)
	[602.9]	[590.6]	[593.5]	[583.8]
	608.1	**596.5**	**598.9**	**590.3**
H_2…C(F)B	709.7	681.1	688.2	664.4
8	(715.5)	(686.9)	(694.0)	(670.3)
	[767.5]	[734.9]	[743.1]	[717.1]
	718.0	**689.4**	**696.5**	**672.7**
H_2…FCB	710.4	681.0	688.8	661.7
9	(716.2)	(686.9)	(694.7)	(667.5)
	718.4	**689.1**	**696.8**	**669.6**
HCF…BH	740.0	716.5	722.7	702.1
10	(740.1)	(716.6)	(722.8)	(702.2)
	[740.7]	[715.4]	[722.1]	[699.2]
	753.9	**730.4**	**736.5**	**716.0**

aCCSD(T)/MP2, BD(T)/MP2 (in parentheses), CCSD(T)/QCISD (in brackets), and CCSD(T)/CBS (in boldface) data. All values in kJ/mol. b CCSD(T)/MP2 values (in hartrees) for isomer 1 are E = -163.7559702, E + ZPE = -163.7274492, H298 = -163.7226172, and G298 = -163.7509352. BD(T)/MP2 values for 1 are E = -163.7557556, E + ZPE = -163.7272346, H298 = -163.7224026, and G298 = -163.7507206. CCSD(T)/QCISD values for 1 are E = -163.7558711, E + ZPE = -163.7273641, H298 = -163.7225471, and G298 = -163.7508431. CCSD(T)/CBS values for 1 are E = -163.8217944, E + ZPE = -163.7932734, H298 = -163.7884414, and G298 = -163.8167594.

3.4.1.1 Isomer 1 versus Isomer 2

That isomer **1** is so much more stable than even isomer **2** (Table 3.3) can be rationalized in several ways. The two qualitative analyses considered here involve comparing the Lewis acidities and basicities of the fragments of **1** and **2** and comparing the bonds broken and formed in the interconversion of **1** and **2**. Structure **1** can be split into the Lewis acid (electron pair receptor) BF and the Lewis base (electron pair donor) singlet CH_2, whereas structure **2** can be split into the Lewis acid BH and the Lewis base C(F)H. BF is expected to be a better Lewis acid than BH because fluorine withdraws electrons better than hydrogen; CH_2 is expected to be a better Lewis base than C(F)H for the same reason. Although the differences in the electron densities are small, the NBO analyses of BF, BH, CH_2 and C(F)H support our expectations. The boron contribution to the unoccupied B–X orbital σ•(B-X) is bigger (89.51% B vs. 68.09% B) for BF than for BH, and the carbon contribution to the occupied C-H orbital σ(C-H) is bigger (53.30% C vs. 51.84% C) for CH_2 than for C(F)H. The %C character for σ(C-F) is only 21.23%. Also, the largest energy gap between the occupied orbitals of CH_2 and the unoccupied lone pair orbital n*(B) of BF, 0.8991 hartree, is only slightly larger than the smallest energy gap between the corresponding orbitals of C(F)H and BH, 0.8788 hartree. Thus, the combination of CH_2 with BF (**1**) should lead to a stronger Lewis acid-base interaction than the combination of C(F)H with BH (**2**).

Perhaps an even better qualitative understanding of the large difference in energy between **1** and **2** is obtained by considering the reaction sequence given in equations 2 – 4. Isomerization of H_2CBF **1** to H(F)CBH **2** requires breaking a B-F and a C-H bond and forming a B-H and a C-F bond. We have estimated the enthalpy changes associated with these bond-breaking and bond-making processes in **1** and **2** from the enthalpies of formation of BF, BH, CH and CF taken from the NIST Chemistry WebBook[46].

$$BF \rightarrow BH \qquad \Delta_{rx}H = 559 \text{ kJ/mol} \qquad (2)$$

$$CH \rightarrow CF \qquad \Delta_{rx}H = -339 \text{ kJ/mol} \qquad (3)$$

$$BF + CH \rightarrow BH + CF \qquad \Delta_{rx}H = 220 \text{ kJ/mol} \qquad (4)$$

This analysis suggests that the large endothermicity of the conversion **1** → **2** arises primarily from the greater strength of the B-F bond compared to that of the B-H bond: the **1** → **2** conversion is endothermic by 250 kJ/mol comparable to the above 220 kJ/mol for the endothermicity of reaction 4. Indeed, both values are comparable to the 207 kJ/mol found for reaction 5, again using the WebBook thermochemical data[46].

$$1/3\ [BF_3 + CH_4 \rightarrow BH_3 + CHF_3] \qquad (5)$$

Table 3.4 Reaction Thermochemistry on the Singlet PES: BH Affinities, Hydrogen Bond Strengths, Barrier Heights and Proton Affinities.

Reaction	$\Delta_{rx}E$	$\Delta_{rx}(E + ZPE)$	$\Delta_{rx}H_{298}$[b]	$\Delta_{rx}G_{298}$[b]
H_2CBF **1** → CH_2 + BF	478.9	456.0	462.0	420.0
	(478.9)	(455.9)	(461.9)	(419.9)
	488.5	**465.7**	**471.6**	**429.6**
H(F)CBH **2** → HCF + BH	497.2	471.7	478.1	436.8
	(497.2)	(471.6)	(478.0)	(436.7)
	508.7	**483.2**	**489.6**	**448.3**
HCH…BF **4** → CH_2 + BF	4.2	1.8	0.0	-13.8
	(4.2)	(1.8)	(0.0)	(-13.8)
	3.6	**1.2**	**-0.4**	**-14.4**
HCH…FB **5** → CH_2 + BF	1.9	0.2	-2.0	-13.6
	(1.9)	(0.2)	(-2.0)	(-13.6)
	1.6	**-0.1**	**-2.2**	**-13.8**
HCBFH **6** → HCB + HF	115.1 (115.1)	98.6 (100.9)	103.4 (105.8)	65.6 (68.0)
	118.8	**102.3**	**107.2**	**69.4**
H(C)BFH **7** → HBC + HF	43.4	35.7	38.9	8.8
	(43.4)	(35.7)	(38.9)	(8.8)
	44.6	**36.9**	**40.0**	**10.0**
H_2…C(F)B **8** → FCB + H_2	2.0	-2.0	-2.3	-16.3
	(2.0)	(-1.9)	(-2.2)	(-16.2)
	1.2	**-2.7**	**-3.0**	**-17.0**
H_2…FCB **9** → FCB + H_2	1.3	-1.9	-2.8	-13.5
	(1.3)	(-1.9)	(-2.8)	(-13.5)

	0.8	**-2.4**	**-3.3**	**-13.8**
HCF…BH **10** → HCF + BH	6.7	2.5	2.3	-20.7
	(6.8)	(2.6)	(2.3)	(-20.7)
	6.5	**2.2**	**2.0**	**-21.0**
H_2CBF **1** → **TS1-2**	307.2	300.4		
	(308.3)	(301.6)		
	309.4	**302.7**		
H(F)CBH **2** → **TS1-2**	57.6	53.2		
	(58.5)	(54.1)		
	57.8	**53.3**		
H_2CBF **1** → **TS1-3**	446.6	442.7		
	(450.1)	(446.1)		
	452.0	**448.1**		
$BC(H)_2F$ **3** → **TS1-3**	99.1	93.4		
	(102.5)	(96.9)		
	96.1	**90.4**		
H_2CBF **1** → **TS1-6**	501.0	490.0		
	(502.2)	(492.0)		
	503.6	**493.4**		
HCBFH **6** → **TS1-6**	2.3	-3.2		
	(2.4)	(-3.1)		
	2.5	**-2.9**		
H(F)CBH **2** → **TS2-3**	189.5	181.8		
	(189.4)	(181.7)		
	192.3	**182.8**		
$BC(H)_2F$ **3** → **TS2-3**	91.6	79.8		
	(91.6)	(79.9)		
	88.1	**74.5**		
H^+ + HCBFH **6** → $[H_2CBFH]^+$ **4′**	-959.4	-930.7	-936.2	-937.8

	-958.2	**-929.6**	**-935.1**	**-936.7**
$H^+ + H_2CBF$ **1** → $[H_3CBF]^+$ **1′**	-902.0	-867.3	-873.7	-873.4
	-900.1	**-865.4**	**-871.8**	**-871.5**
$H^+ + H(F)CBH$ **2** → $[H(F)CBH_2]^+$ **2′**	-773.0	-746.5	-752.0	-753.7
	-769.5	**-743.0**	**-748.4**	**-750.3**
$H^+ + H(F)CBH$ **2** → $[HF(H)CBH]^+$ **5′**	-616.1	-589.6	-594.2	-597.5
	-613.5	**-587.1**	**-591.7**	**-595.0**
$H^+ + BC(H)_2F$ **3** → $[BC(H)_2FH]^+$ **8′**	-598.5	-575.2	-578.7	-584.4
	-594.9	**-571.6**	**-575.1**	**-580.8**
$H^+ + H_2CBF$ **1** → $[H_2CBFH]^+$ **4′**	-460.6	-436.7	-440.7	-447.6
	-457.2	**-433.3**	**-437.3**	**-444.2**

[a]CCSD(T)/MP2, BD(T)/MP2 (in parentheses) and CCSD(T)/CBS (in boldface) thermochemical values in kJ/mol. [b]Proton affinity ($-\Delta_{rx}H_{298}$) and gas phase basicity ($\Delta_{rx}G_{298}$): C-protonation, reactions 18 and 19; B-protonation, reaction 20; F-protonation, reactions 21-23.

3.4.1.2 Binding Affinities

The BH affinities of borane(1) complexes HB…X have been assessed previously in our group. In particular, we have evaluated enthalpies of complexation for $HBCN^-$, HBCO and $HBCF^+$[47] With calculated BH affinities of 236 and 279 kJ/mol (using a smaller basis set than was used in this work), $HBCN^-$ and $HBCF^+$ were viewed as "chemically" rather than "physically" bound and as new chemical species. Recognizing H(F)CBH **2** as a borane(1) complex for which X is C-bonding C(F)H, the enthalpy of complexation of 478 kJ/mol is indicative of tight B-C binding and another new chemical compound. As a point of reference, the computed B–C

binding enthalpy for H_2CBF **1**, a compound observed by Lanzisera and Andrews[4] in their study of the B + CH_3F reaction, is the nearly equal 462 kJ/mol (Table 3.4).

In contrast, HCF...BH **10**, with its BH affinity of 2.3 kJ/mol, is a weak, "physically"-bound complex between BH and F-bonding FCH. Consistent with the weak interaction between the fragments in **10**, the natural charges from the NBO analysis show a mere 0.004e donated from C(F)H to BH. The NBO analysis also gives a total energy of just 22.5 kJ/mol for the hyperconjugative interactions involving only valence-shell orbitals. The primary contributions to the hyperconjugation energy are from the fluorine lone pairs delocalizing into the unfilled lone pair orbital on boron, with a total $\Delta E^{(2)}(n(F)\rightarrow n^*(B))$ = 14.7 kJ/mol. The second largest contribution of 3.3 kJ/mol is associated with the $n(B)\rightarrow\sigma^*(C\text{-}H)$ hyperconjugation.

The most weakly bound complexes are HCH…BF **4**, HCH…FB **5**, H_2…C(F)B **8** and H_2…FCB **9** (Table 4). Each of these isomers can be classified as a hydrogen-bonded X-H…Y complex. In their model of hydrogen bonding, Alabugin et al.[48] propose that two competing factors determine whether a hydrogen bond is conventional or unconventional. The first factor is the strength of the hyperconjugative interaction between the lone pair of the electron donor Y and the unfilled antibonding H-X orbital, $n(Y)\rightarrow\sigma^*(H\text{-}X)$, upon complexation. This charge transfer elongates the H-X bond and when it is the dominant effect, a conventional hydrogen bond is formed. The second factor is based on Bent's rule[49] and is the increase in s-character in the X hybrid orbital of the H-X bond upon complexation. This rehybridization shortens the H-X bond and when it is the dominant effect, an

unconventional hydrogen bond is formed. Weinhold and coworkers[48] suggest that unconventional hydrogen bonding is likely to occur only when $\Delta E^{(2)}(n(Y)\rightarrow\sigma^*(H\text{-}X))$ is less than about 13-20 kJ/mol and the structure of the proton-donating molecule allows sufficient polarization and concomitant rehybridization of the H-X bond.

As Alabugin et al.[48] point out, the H-H bond is probably the best example of an H-X bond for which rehybridization cannot occur. For this reason, all H-H...Y complexes are expected to have a longer H-H bond than H_2, despite $\Delta E^{(2)}$ values below the threshold energy range. The HH…OH_2, HH…$O(CH_3)_2$ and HH…Cl^- complexes examined by Weinhold and coworkers all show the expected structural change as does complex **8** (and to a lesser extent **9**). The H-H bond length is 0.755 Å for the H_2 molecule and 0.756 Å for **8**. This bond elongation is comparable in magnitude to that found for the H-H…OH_2 complex[48].

Interestingly, HCH…BF is not a minimum, although ClH…BF is bound more strongly than ClH…FB by some 10 kJ/mol[50]. The intermolecular interaction in HCH…FB **5** is an example of very weak unconventional hydrogen bonding. Nevertheless, as expected for this type of hydrogen bonding, a small C-H bond shortening is observed when the complex is formed. In this case, there is essentially no $n(F)\rightarrow\sigma^*(H\text{-}C)$ charge transfer, and the 0.0003 Å decrease in bond length arises from the small increase in % s-character of the carbon hybrid orbital in the H-C bond (from 21.65% in CH_2 to 21.79% in **5**). Again, this bond shortening and increase in % s-character are similar in magnitude to the values found by Weinhold and coworkers for complexes of alcohols with Ne or CF_4, which were among the more weakly bound complexes they studied[48].

Isomer H(C)BFH **7** can also be considered a complex between the fragments HBC and FH. Although the B-F bond in **7** is about 0.3 Å longer than the B-F bond in HCBFH **6**, the other isomer with a bridged fluorine atom (Table 1), the intermolecular interaction in **7** is significantly stronger than that in **5** or **8** – **10** (Table 4). Consistent with the moderately strong B-F binding in **7**, bond lengths differ by as much as 0.02 Å in HBC, HF and **7**. The HBC angle also bends by 13° (Table 3.1). Moreover, the natural charges show a redistribution of electron density within the fragments as well as a transfer of 0.141e from HF to B(C)H.

3.4.1.3 Proton Affinities

Only six neutral [B, C, F, H_2] and cationic [B, C, F, H_3]$^+$ pairs correlate with respect to protonation at carbon, boron or fluorine (Table 3.4), partially because no isomers with B-F-C linkages were identified for [B, C, F, H_2] (Table 3.1). The six pairs are combinations of four of the [B, C, F, H_2] isomers and five of the [B, C, F, H_3]$^+$ isomers. Isomer H_2CBF **1** has C-protonated and F-protonated cationic analogues, [H_3CBF]$^+$ **1′** and [H_2CBFH]$^+$ **4′** respectively. (The primes are used here to distinguish between the neutral and cationic species.) [H_2CBFH]$^+$ **4′** is also connected to HCBFH **6**, protonated at carbon. [$F(H)CBH_2$]$^+$ **2′** and [HF(H)CBH]$^+$ **5′** are the B-protonated and F-protonated counterparts of F(H)CBH **2**, respectively. Finally, protonation of $FC(H)_2B$ **3**, again at fluorine, correlates with [$HFC(H)_2B$]$^+$ **8′** . When **3** is protonated at boron the structure rearranges without activation barrier to [H_3CBF]$^+$ **1′**. The

surprisingly high number of neutral and cationic analogues corresponding to protonation at fluorine is consistent with the surprisingly high number of fluorine-bridged structures found at minima for $[B, C, F, H_3]^+$.

The proton affinity (PA) is defined as the negative of the change in standard enthalpy for the reaction of the base B in equation 6 (Table 3.4). The gas phase basicity (GB) is defined as the change in standard free energy for this reaction.

$$B\ (g) + H^+\ (g) \rightarrow BH^+\ (g) \qquad (6)$$

The preferred site of protonation follows the order C > B > F, in agreement with the trend found by Rozas et al.[51] in their study of the proton affinities of monohydride and monofluoride derivatives of B, Al, N, and P. When the proton is added to the carbon of **1**, the PA (and GB) is nearly twice as large as when it is added to the fluorine. However, addition at fluorine is appreciably more favorable for isomers **2** and **3** than for isomer **1** (Table 3.4). Using data from the NIST Chemistry WebBook[46] to place the calculated proton affinity values in perspective, even the smallest of the three fluorine PAs lies between the values of 332 kJ/mol for F_2 and 484.0 kJ/mol for HF. The PAs associated with addition of the proton to carbon are similar in magnitude to those for anthracene (877.3 kJ/mol) and propene (751.6 kJ/mol) but are much larger than that for ethylene (680.0 kJ/mol). At 615.0 kJ/mol, the PA of diborane is significantly smaller than that of B-protonated **2**, which is comparable to the PA of the radical B_5H_8 (763.4 kJ/mol).

Maksić and Vianello[52] have partitioned the PA into the three terms given in equation 7 to provide a basis by which the origin of the intrinsic basicity of neutral bases can be elucidated.

$$PA = BAE + EA(H^+) - (IP)_1^{ad} \quad (7)$$

In equation 7, BAE is the magnitude of the homolytic bond association energy of the B-H^+ bond, $EA(H^+)$ is the magnitude of the electron affinity of H^+ (i. e. ionization energy of H), and $(IP)_1^{ad}$ is the energy required to remove the mostly weakly bound electron from B. Maksić and Vianello[52] applied this approach to the PAs of NH_3, CH_3NH_2, $(CH_3)_2NH$ and $(CH_3)_3N$ and correlated the increase in PA along the series with the decrease in % s-character of the lone pair on nitrogen. One consequence of this decrease in % s-character is that the lone pair electrons are less tightly bound as methyl groups are added; however, a second consequence is that BAE is also reduced. As the base changes from NH_3 to $(CH_3)_3N$, the reduction in $(IP)_1^{ad}$ dominates the reduction in BAE and the PA increases [52]. This approach can also be utilized to rationalize the relative proton affinities of H_2CBF **1**, H(F)CBH **2** and $BC(H)_2F$ **3** when they are protonated at fluorine (Table 3.4). According to the NBO analysis, the % s-character of the relevant fluorine lone pair is 59.9% for **1**, 73.3% for **2**, and 76.3% for **3**. Apparently for this set of molecules, for which the fluorine lone pair is not the HOMO, the fluorine basicity varies directly with BAE.

3.4.1.4 Transition Structures

Figure 3.3 is a partial potential energy diagram for [B, C, F, H_2] showing the interconversion pathways **1→2**, **1→3**, **1→6** and **2→3**. Also included in the figure are the activation barriers in the forward E_a and reverse E_a' directions, which were

calculated as the difference in the zero-point energy corrected total energies (E+ZPE) of the transition structure and the relevant minimum. Since the largest discrepancy in the CCSD(T)/MP2 and BD(T)/MP2 barrier heights is only 3.5 kJ/mol (for E_a' (**3** → **1**)), only the CCSD(T)/MP2 data are reported in the figure. With a negative activation energy $E_a' = -3.2$ kJ/mol, the calculations indicate that HCBFH **6** will convert to H_2CBF **1** without barrier. Therefore, **6** is unlikely to be observed experimentally even at the temperatures at which Andrews and coworkers perform the laser ablation experiments, typically 6 – 7 K with annealing up to 35 K[4,7-9,42]. In contrast, the remaining E_a' values are sufficiently large that isomers H(F)CBH **2** and $BC(H)_2F$ **3** may be experimentally observable at room temperature.

If **2** were formed, the pathways for rearrangement depicted in Figure 3.3 suggest that its primary rearrangement product would be **1**. The 13 kJ/mol difference in barrier heights for the two isomerization processes depicted for **3** suggests that it would predominately rearrange via the pathway through **TS2-3** at lower temperatures while at higher temperatures, direct conversion to **1** would become competitive. Since the ca. 100 kJ/mol exothermicity of reaction **3→2** (Table 3) is sufficient to overcome the activation barrier for reaction **2→1**, the ultimate fate of isomer **3** may be isomer **1** regardless of synthetic pathway.

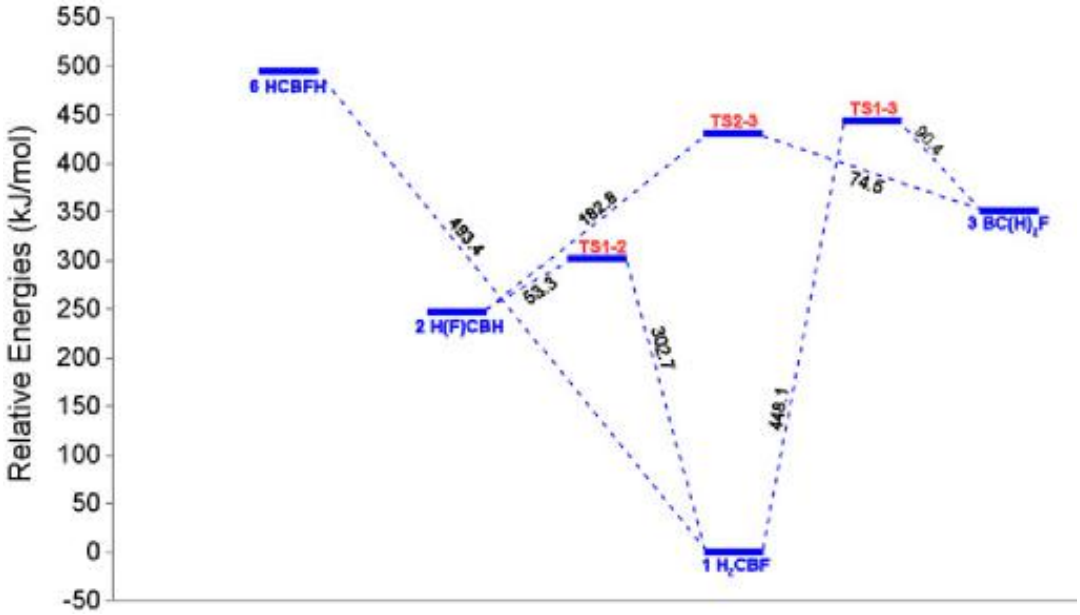

Figure 3.3 Reaction profile for [B, C, F, H_2]. The relative thermochemical data are the CCSD(T)//CBS E + ZPE values.

3.5 Reaction of Boron with Methyl Fluoride

On the basis of the observed vibrational frequencies and photolysis/annealing behavior of various isotopic mixtures of boron and methyl fluoride, Lanzisera and Andrews[4] concluded that only two major products are formed in the boron-methyl fluoride reaction. The matrix infrared spectra were combined with BP86/6-311G(d) density functional calculations to characterize the observed products as H_2CBF **1** and HCBF. Mechanistic information gleaned from previous studies by Andrews and coworkers[4,7-9,42] was utilized to delimit the possible product choices. Their data suggests that reactions of this type proceed primarily via boron insertion into a bond

between two heavy atoms, followed by loss of one or more hydrogens. Frequently, the hydrogen elimination occurs from the more electronegative atom. Minor products are formed by X-H bond insertions, but these insertions appear to be less favorable when X is carbon[4,7-9,42].

In addition to H_2CBF **1** and HCBF, Lanzisera and Andrews[4,7-9,42] considered three other possible products for the reaction of boron with methyl fluoride, H(F)CBH **2**, H_2BCF and HBCF. Our results suggest that $BC(H)_2F$ **3** and HCBFH **6** should also be considered. Isomer **6**, just as **1** and HCBF, could be generated via boron addition to the C-F bond, whereas isomer **3**, just as **2**, H_2BCF and HBCF, could be generated via boron addition to a C-H bond. Formation of both HCBFH **6** and H_2BCF would also require a shift of one of the remaining hydrogens. (Even more rearrangement is necessary to produce isomers **7** - **10**, and the intermolecular interactions in **8** - **10** are so weak that they not likely to be observable (Table 3.4).

The MP2 and QCISD calculated vibrational frequencies and their associated absorption intensities are listed in Table 3.5 for isomers **1**, **2**, **3** and **6**. The vibrational frequencies obtained from these calculations for **1** and **2** are generally in good agreement with those from the BP86/6-311G(d) calculations and from experiment. Similarly to H(F)CBH **2**, H_2BCF, and HBCF[4], $BC(H)_2F$ **3** and HCBFH **6** can be excluded as products because they do not have a strong B=C absorption in the assigned region, have unique frequencies with sufficient intensity for which no peak appeared in the spectra, and/or do not have a C-B-F connectivity. That the **6** → **1** conversion appears to proceed without barrier (Figure 3.3) and H_2BCF is not a minimum on the PES of [B, C, F, H_2] (see above) also makes them unlikely products.

The results of our study reinforce not only Lanzisera and Andrews' product assignments but also their contention that C-H bond insertion is an energetically less favorable pathway[4,7,8]. It is conceivable that C-H insertion occurs in the boron-methyl fluoride reaction but the products formed along this pathway rearrange to **1**. However, the calculated barrier heights for the **2** → **1**, **3** → **1** and **3** → **2** isomerization reactions argue against that possibility (Figure 3.3).

Table 3.5 MP2 and QCISD Calculated Frequencies (cm^{-1}) and Intensities (km/mol)

Structure	MP2 Frequencies[a]	QCISD Frequencies[a]	Observed Frequencies[b]
CH_2BF 1, C_{2v}	b_2: (43.6), 307.0 (5.4), 765.1 3301.0 (3.75) b_1: 387.1 (17.6), 592.6 (63.2) a_1: (2.1), (18.2) 886.6 (29.5), 1324.7 1753.4 (396.1), 3201.7	b_2: (40.4), 315.8 (6.7), 782.2 3269.5 (1.0) b_1: (61.6) 371.3 (12.2), 622.1 a_1: (1.3), (10.6) 883.1 (33.2), 1341.3 1751.0 (381.0), 3177.0	589.5, 755.0, 917.4, 1762.2, 3050.2[c]
H(F)CBH 2, C_s	a′: (47.2), (23.7), (4.3), 285.0 (1.7), 803.7 1009.3 (64.1), 1205.5 1530.9 (18.9), 2868.3 3215.7 (10.7) a″: (37.8) 536.9 (1.8), 684.8	a′: (44.6), (21.8), (4.6), 293.0 (2.1), 799.1 1011.0 (66.1), 1211.8 1528.0 (18.9), 2829.2 3199.8 (8.2) a″: (34.7) 505.1 (2.8), 686.3	1822.3, 3261.7[d]
$BC(H)_2F$ 3, C_s	a′: (87.3), (29.0), (21.4) 239.1 (28.2), 849.8 1030.9 (52.7), 1315.6 1420.8 (19.4), 3054.1 a″: (0.1), 585.0 (28.9), 1197.5 3124.3 (3.9)	a′: (85.2), (21.4), (22.2) 256.5 (23.6), 840.3 1029.3 (60.1), 1318.0 1426.5 (15.2), 3026.1 a″: (0.0015), 604.1 (24.2), 1201.1 3087.1 (8.6)	
HCBFH 6, C_s	a′: (23.0), (218.3), (8.7), 218.3 (106.9), 539.8 614.9 (77.1), 757.0 1646.9 (19.1), 3378.2 3710.1 (238.1) a″: (5.8) 245.9 (83.9), 619.9	a′: (51.3), (253.5), (3.2), 240.8 (101.2), 504.6 631.0 (48.9), 729.6 1544.3 (32.7), 3348.4 3821.4 (185.1) a″: (33.0) 248.1 (86.5), 558.3	

[a]IR intensities in parentheses. [b]Reference [4]. [c]Frequencies assigned to CH_2BF. [d]Other observed frequencies.

3.6 REFERENCES

[1] Tavcar, G.; Tramsek, M.; Bunic, T.; Benkic, P.; Žemva, B. *J. Fluorine Chem*. **2004**, *125*, 1579.

[2] Tramsek, M.; Benkic, P.; Turicnik, A.; Tavcar, G.; Zemva, B. *J. Fluorine Chem.* **2002**, *114*, 143.

[3] Deakyne, C. A.; Li, L.; Liebman, J. F. *Int. J. Mass Spectrom.* **2003** *227*, 555.

[4] Lanzisera, D. V.; Andrews, L. *J. Phys. Chem. A* **2000**, *104*, 9295.

[5] Minyaev, R. M.; Gribanova, T. N. *Russ. J. Gen. Chem.* **2004**, *74*, 1529.

[6] Hassanzadeh, P.; Andrews, L. *J. Phys. Chem.* **1993**, *97*, 4910.

[7] Lanzisera, D. V.; Andrews, L. *J. Phys. Chem. A* **1997**, *101*, 824.

[8] Lanzisera, D. V.; Andrews, L. *J. Phys. Chem. A* **1997**, *101*, 1482.

[9] Lanzisera, D. V.; Andrews, L.; Taylor, P. R. *J. Phys. Chem. A* **1997**, *101*, 7134.

[10] Zhou, M.; Tsumori, N.; Xu, Q.; Kushto, G. P.; Andrews, L. *J. Am. Chem. Soc.* **2003**, *125*, 11371.

[11] Gaussian 98, Revision A.7, Frisch, M. J.; Trucks, G. W.; Schlegel, H. B.; Scuseria, G. E.; Robb, M. A.; Cheeseman, J. R.; Zakrzewski, V. G.; Montgomery, J. A.; Stratmann, R. E.; Burant, J. C.; Dapprich, S.; Millam, J. M.; Daniels, A. D.; Kudin, K. N.; Strain, M. C.; Farkas, O.; Tomasi, J.; Barone, V.; Cossi, M.; Cammi, R.; Mennucci, B.; Pomelli, C.; Adamo, C.; Clifford, S.; Ochterski, J.; Petersson, G.

A.; Ayala, P. Y.; Cui, Q.; Morokuma, K.; Malick, D. K.; Rabuck, A. D.; Raghavachari, K.; Foresman, J. B.; Cioslowsk, J.; Ortiz, J. V.; Stefanov, B. B.; Liu, G.; Liashenko, A.; Piskorz, P.; Komaromi, I.; Gomperts, R.; Martin, R. L.; Fox, D. J.; Keith, T.; Laham, Al M. A.; Peng, C. Y.; Nanayakkara, A.; Gonzalez, C.; Challacombe, M.; Gill, P. M. W.; Johnson, B. G.; Chen, W.; Wong, M. W.; Andres, J. L.; Gordon, Head M.; Replogle, E. S.; Pople, J. A. Gaussian, Inc., Pittsburgh, PA, 1998.

[12] Gaussian 03, Revision C.02, Frisch, M. J.; Trucks, G. W.; Schlegel, H. B.; Scuseria, G. E.; Robb, M. A.; Cheeseman, J. R.; Montgomery, Jr., J. A.; Vreven, T.; Kudin, K. N.; Burant, J. C.; Millam, J. M.; Iyengar, S. S.; Tomasi, J.; Barone, V.; Mennucci, B.; Cossi, M.; Scalmani, G.; Rega, N.; Petersson, G. A.; Nakatsuji, H.; Hada, M.; Ehara, M.; Toyota, K.; Fukuda, R.; Hasegawa, J.; Ishida, M.; Nakajima, T.; Honda, Y.; Kitao, O.; Nakai, H.; Klene, M.; Li, X.; Knox, J. E.; Hratchian, H. P.; Cross, J. B.; Bakken, V.; Adamo, C.; Jaramillo, J.; Gomperts, R.; Stratmann, R. E.; Yazyev, O.; Austin, A. J.; Cammi, R.; Pomelli, C.; Ochterski, J. W.; Ayala, P. Y.; Morokuma, K.; Voth, G. A.; Salvador, P.; Dannenberg, J. J.; Zakrzewski, V. G.; Dapprich, S.; Daniels, A. D.; Strain, M. C.; Farkas, O.; Malick, D. K.; Rabuck, A. D.; Raghavachari, K.; Foresman, J. B.; Ortiz, J. V.; Cui, Q.; Baboul, A. G.; Clifford, S.; Cioslowski, J.; Stefanov, B. B.; Liu, G.; Liashenko, A.; Piskorz, P.; Komaromi, I.; Martin, R. L.; Fox, D. J.; Keith, T.; Al-Laham, M. A.; Peng, C. Y.; Nanayakkara, A.; Challacombe, M.; Gill, P. M. W.; Johnson, B.; Chen, W.; Wong, M. W.;

Gonzalez, C.; and Pople, J. A.; Gaussian, Inc., Wallingford CT, 2004. [13] C. Moller, M.S. Plesset, *Phys. Rev.* **1934**, *46*, 618.

[14] Pople, J. A.; Binkley, J. S.; Seeger, R. *Int. J. Quantum Chem., Symp.* 1976, *10*, 1.

[15] Pople, J. A.; Head-Gordon, M.; Raghavachari, K. *J. Chem. Phys.* **1987**, *87*, 5968.

[16] Dunning, Jr., T. H. *J. Chem. Phys.* **1989**, *90*, 1007.

[17] Woon, D. E.; Dunning, Jr., T. H. *J. Chem. Phys.* **1993**, *98*, 1358.

[18] Brueckner, K. A. *Phys. Rev.* **1954**, *96*, 508.

[19] Raghavachari, K.; Trucks, G. W.; Pople, J. A.; Head-Gordon, M. *Chem. Phys. Lett.* **1989**, *157*, 479.

[20] Stanton, J. F.; Gauss, J.; Bartlett, R. J. *J. Chem. Phys.* **1992**, *97*, 5554.

[21] Gonzalez, C.; Schlegel, H. B. *J. Chem. Phys.* **1989**, *90*, 2154.

[22] Gonzalez, C.; Schlegel, H. B. *J. Phys. Chem.* **1990**, *94*, 5523.

[23] Gonzalez, C.; Schlegel, H. B. *J. Chem. Phys.* **1991**, *95*, 5853.

[24] Cizek, J. *J. Chem. Phys.* **1966**, *45*, 4256.

[25] Cramer, C. J. Essentials of Computational Chemistry: Theories and Models, Wiley & Sons, Hoboken, NJ, 200.

[26] NBO, Version 3.1, Glendening, E. D.; Reed, A. E.; Carpenter, J. E.; Weinhold, F.

[27] Carpenter, J. E.; Weinhold, F. *J. Am. Chem. Soc.* **1988**, *110*, 368.

[28] Foster, J. P.; Weinhold, F. *J. Am. Chem. Soc.* **1980**, *102*, 7211.

[29] Reed, A. E.; Curtiss, L. A.; Weinhold, F. *Chem. Rev.* **1988**, *88*, 899.

[30] Reed, A. E.; Weinhold, F. *J. Chem. Phys.* **1985**, *83*, 1736.

[31] Reed, A. E.; Weinstock, R. B.; Weinhold, F. *J. Chem. Phys.* **1985**, *83*, 735.

[32] Hobza, P.; Havlas, Z. *Chem. Rev.* **2000**, *100,* 4253.

[33] Boldeskul, I. E.; Tsymbal, I. F.; Ryltsev, E. V.; Latajka, Z.; Barnes, A. J. *J. Mol. Struct.* **1997**, *436*-437, 167.

[34] Buděšinsky, M.; Fiedler, P.; Arnold, Z. Synthesis 1989, 858.

[35] Delanoye, S. N.; Herrebout, W. A.; van der Veken, B. J. *J. Am. Chem. Soc.* **2002**, *124*, 7490.

[36] Delanoye, S. N.; Herrebout, W. A.; van der Veken, B. J. *J. Phys. Chem. A* **2005**, *109*, 9836.

[37] Hobza, P.; Havlas, Z. *Chem. Phys. Lett.* **1999**, *303*, 447.

[38] Hobza, P.; Zahradnik, R.; Muller-Dethlefs, K. *Collect. Czech. Chem. Commun*. **2006**, *71*, 443.

[39] Li, X.; Liu, L.; Schlegel, H. B. *J. Am. Chem. Soc.* **2002**, *124*, 9639.

[40] Hargittai, M.; Hargittai, I. The Molecular Geometries of Coordination Compounds in the Vapor Phase, 1977.

[41] Gillespie, R. J.; Popelier, P. L. A. Chemical Bonding and Molecular Geometry: From Lewis to Electron Densities, Oxford University Press, New York, 2001.

[42] Hassanzadeh, P.; Andrews, L. *J. Am. Chem. Soc*. **1992**, *114*, 9239.

[43] Hammond, G. S. *J. Am. Chem. Soc.* **1955**, *77*, 334.

[44] Leffler, J. E. *Science* **1953**, *117*, 340.

[45] Lee, T. J.; Taylor, P. R. *Int. J. Quantum Chem., Quantum Chem. Symp.* **1989**, *23*, 199.

[46] NIST Chemistry Webbook, NIST Standard Reference Data Base Number 69, Eds. Mallard, W. G.; Linstrom, P. J. February 2000, National Institute of Standards and Technology, Gaithersburg, MD 20899, (http://webbook.nist.gov)

[47] Pappova, A.; Deakyne, C. A.; Skancke, A.; Cernusak, I.; Liebman, J. F. *Mol. Phys.* **1996**, *89*, 247.

[48] Alabugin, I. V.; Manoharan, M.; Peabody, S.; Weinhold, F. *J. Am. Chem. Soc.* **2003**, *125*, 5973.

[49] Bent, H. A. *Chem. Rev.* **1961**, *61*, 275.

[50] McDowell, S. A. C.; Buckingham, A. D. *J. Am. Chem. Soc.* **2005**, *127*, 15515.

[51] Rozas, I.; Alkorta, I.; Elguero, J. *J. Phys. Chem. A* **1999**, *103*, 8861.

[52] Maksić, Z. B.; Vianello, R. *J. Phys. Chem. A* **2002**, *106*, 419.

4 The Structure and Energetics of Triplet [B, C, F, H_2]

In the current chapter, we discuss our high-level quantum chemical results for the structure and energetics of triplet (and hence open-shell) isomers corresponding to the stoichiometry of one boron, carbon, and fluorine apiece, and two hydrogens. While partially bond-ruptured excited ketene- and diazomethane-like $H_2C^{\bullet}$–$B^{\bullet}$-F and the carbene H(F)B-C-H plausibly emerge as the most stable isomers, a variety of novel structural features emerge for the assembled energy minima of at least 16 species. All of these species are compared as well as transition states that connect them. Comparison is made with corresponding forms of the singlet species with this stoichiometry, shown earlier by us to have a rich diversity of structures as well as a large range of energies and relative stabilities.

4.1 Introduction

The isomeric compounds with the formula [B, C, F, H_2] are formally among the simplest species containing each of the elements together: boron, carbon, fluorine and hydrogen. They are the simplest such species for which the question of spin state naturally emerges[1]. The formally doubly bonded H_2C=B-F is logically a closed-shell singlet, analogous to the isoelectronic diazomethane and ketene. The corresponding

triplet, roughly drawn as the biradical $H_2C^{\bullet}–B^{\bullet}$-F, is expected to be a weakly bound, excited state corresponding to the excited states of diazomethane and ketene en route to triplet CH_2 as they photolytically dissociate[2]. The structurally related carbene H_2B-C-F with the boron and carbon transposed is plausibly a ground state triplet as we recognize this species to be a substituted derivative of the parent carbene, CH_2. Indeed this isomer was quite dominant in earlier literature discussions of [B, C, F, H_2] [3,4], even though our more exact calculations failed to confirm it to be a minimum on the singlet potential energy surface[1]. Any of our earlier hydrogen bridged or hydrogen bonded complexes containing CH_2, CHF or BH, might also be expected to have triplet counterparts as all of these fragments have energetically low lying states with unpaired electrons [5-7]. Summarizing our query, what are the structure and energetics of open-shell [B, C, F, H_2]?

To our knowledge, the only earlier computational study of triplet species with the formula [B, C, F, H_2] is that of Lanzisera and Andrews [3], in which they evaluated the triplet-singlet energy difference for H_2CBF. The calculations were performed to complement their matrix isolation study of reactions between laser-ablated boron atoms and CH_3X, X = F, Cl, Br. More computational work has been carried out on some of the boron-containing fragments relevant to the [B, C, F, H_2] species. Much of the recent work has focused on the thermochemical properties of these fragment species, in particular their atomization energies, enthalpies of formation, bond dissociation enthalpies BDHs, and excitation energies [8-16]. Most recently, Grant and Dixon [9] have reported these thermochemical data for $H_{(3-n)}BX_n$ compounds for which X is F, Cl, Br, I, NH_2, OH and SH (where $1 \leq n \leq 3$), using the composite ab

initio molecular orbital theory approach Feller, Peterson, Dixon and their coworkers are developing, which allows them to calculate thermochemical properties to near chemical accuracy (±6.5 kJ/mol). (See for example Ref. [10] and references cited therein.) Earlier calculations on these and related cyclic and acyclic borane molecules and radicals were performed by Raabe et al.[11], Poon and Mayer[12], and Rablen and Hartwig[13]. Barreto et al.[14] have provided polynomial fits to the thermochemical data they computed for a series of chemical species, important in the growth of boron nitride thin films, containing B, H, N and F atoms. Bond dissociation enthalpies of a wider range of molecules, those involving all possible A-X single bonds between first- and second-row atoms, have been evaluated by Mó, et al.[15]. Ponomarev et al.[8] have examined the thermodynamic stabilities of bi- and triradicals derived from halogenated molecules of main group elements.

Most of the above articles include a discussion of trends in sequential bond dissociation enthalpies and/or trends in bond dissociation enthalpies along the periodic table. Comparison of B-X bond dissociation enthalpies, X = H, C, F, Cl, Br, I, in analogous compounds has shown that (1) BDHs decrease down the group from F to I[9,11], (2) B–H and B–C bond strengths are similar in magnitude but much smaller than B–F bond strengths [9,12–15], (3) the strengths of B–H and B–C bonds tend to be less dependent on the other boron substituents than do boron-halogen bonds [9,13,14], and (4) replacing a halogen substituent with hydrogen generally increases the BDHs of boron–halogen bonds [9,11,14]. However, because sequential adiabatic BDHs often have large fluctuations resulting from reorganization energy in the product fragments, the authors of some of these articles suggest that intrinsic bond strengths should be

compared by evaluating diabatic BDHs [9,12,17] or the electron density at the bond critical point[15].

4.2 Computational details

All molecular geometries were fully optimized at the MP2/aug-cc-pVDZ level of calculation using the Gaussian 03 program package[18]. Tight convergence criteria were used for the optimizations. Harmonic vibrational frequencies were calculated to ensure stationary points were either minima or transition structures and to evaluate the thermal correction terms. Transition structures were searched for using the QST2 method [19,20] and intrinsic reaction coordinate, IRC, calculations [21-23] were performed on the transition structures located to confirm which minima each connected. Higher-level single-point CCSD(T) energies were calculated with the basis sets aug-cc-pVXZ, X = D, T and Q, to estimate total energies at the complete basis set (CBS) limit. For the open-shell systems, the single-point energies were obtained using the fully unrestricted formalism (UHF, UCCSD(T)). The equation used to extrapolate to the CBS energy is that of Peterson et al.[24] (Eq. (1)) in which X = 2 (DZ), 3 (TZ), or 4 (QZ).

$$E(X) = E_{\mathrm{CBS}} + A\,e^{-(\mathrm{X}-1)} + B\,e^{-(\mathrm{X}-1)^2} \qquad (1)$$

T_1 diagnostic values were computed at the CCSD(T)/aug-cc-pVDZ level to assess the possibility of non-trivial multireference character in the wave functions[25].

All of the T_1 diagnostics are 0.03 or below, indicating that these wave functions are dominated by a single configuration.

Following the protocol developed by Feller, Peterson, Dixon and their coworkers, the total atomization energy ΣD_0 of a compound is given by equation (2). (See for example Refs. [9], [10] and [26].)

$$\Sigma D_0 = \Delta E_{\text{elec}}(\text{CBS}) - \Delta E_{\text{ZPE}} + \Delta E_{\text{CV}} + \Delta E_{\text{DKH-SR}} + \Delta E_{\text{SO}} \qquad (2)$$

The last three terms in equation (2) contribute small corrections to the total atomization energy. Component ΔE_{CV} accounts for core-valence correlation energy effects and was obtained as the difference between the CCSD(T)(CV)//cc-pwCVTZ and CCSD(T)(FC)//cc-pwCVTZ energies[27]. Douglas-Kroll-Hess[28,29] scalar relativistic corrections $\Delta E_{\text{DKH-SR}}$ were evaluated with the DKH implementation of Gaussian 03 at the CCSD(T)(FC)//cc-pVTZ-DK level of theory[30]. The term ΔE_{SO} gives the contribution of the atomic spin-orbit coupling to the atomization energy. The spin-orbit corrections, from the tabulated values of Moore[31], are –0.93 kJ/mol for B, –0.36 kJ/mol for C and –1.59 kJ/mol for F. To calculate ΔE_{ZPE} in equation (2), the C–H stretches were scaled by the factor of 0.9701 suggested by Matus et al.[26] in their theoretical study of the thermochemical properties of CHFO and CFO.

Molecular enthalpies of formation at 0 K were computed from the total atomization energies and the experimental enthalpies of formation at 0 K[32] for the atoms H (216.0 kJ/mol), C (711.2 kJ/mol) and F (77.27 kJ/mol). The value of $\Delta_f H^\circ$ = 565.3 kJ/mol for B was taken from Ref. [33]. Enthalpies of formation at 298 K were assessed following the procedure established by Curtiss et al[34].

NBO[35,36] and AIM[37] analyses were carried out to obtain information on bonding. The AIM analysis was used to determine the presence of bond critical points and the magnitude of the bond critical point density. The bond critical point density is the electron density $\rho(\mathbf{r})$ at the unique point at which the bond path between two atoms intersects the interatomic surface[37]. This electron density ρ_b is often used as a measure of the strength of the bond between the atoms[15,38,39]. The NBO analysis of the Hartree-Fock orbitals was used to examine the influence of hyperconjugative effects on the stabilities of the hydrogen-bonded and van der Waals complexes identified in this work. Orbital interaction energies $\Delta E^{(2)}$(donor $\rightarrow$ acceptor) were estimated with the second-order NBO perturbation approach[36]. For many of these complexes, the largest interaction energy is associated with a lone pair or unpaired electron on atom Y delocalizing into an unfilled H–X natural bond orbital, a n(Y) $\rightarrow$ σ^*(H–X) hyperconjugation. For the remaining complexes, the dominant contribution to $\Delta E^{(2)}$ is from a σ(Y–Z) $\rightarrow$ σ^*(H–X) hyperconjugation, involving delocalization of electron density from a filled Y–Z orbital into an unfilled H–X orbital

4.3 Results and analysis

4.3.1 Minima and transition structures identified

4.3.1.1 Minima

Sixteen minima have been located for open-shell [B, C, F, H_2]. As in all computational studies of this nature there is always the possibility that minima have

not been identified and that some of those found will collapse. In fact, we have located two new minima on the singlet potential energy surface PES of [B, C, F, H_2] as a result of the triplet investigation. We also have evidence that one triplet may collapse to a related minimum when re-optimized at a higher level of theory (see below).

The triplet isomeric structures depicted in Figure 4.1 are arranged in order of decreasing stability. The two new singlet isomeric structures have also been included in the figure. All bonds shown in the figure were confirmed by AIM analysis[37]. Geometrical parameters for each of the 18 minima and related fragment species are collected in Table 4.1.

A wide range of acyclic connectivities was found for the open-shell [B, C, F, H_2] stoichiometry. We have chosen semi-systematic designations for our minima, realizing that proper names are often cumbersome and not designed for most of our species. As with the singlets[1], no cyclic triplet compounds are at minima. Unlike the singlets, no fluorine-bridged triplet compounds are at minima. Many of the isomers that were located display conventional covalent bonding; most of the remaining, more loosely bound isomers display conventional or unconventional hydrogen bonding. Three of the covalently bound structures are the partially bond-ruptured excited ketene- and diazomethane-like **1** $H_2C^{\bullet}–B^{\bullet}–F$, analogous to **S1** $H_2C=B–F$ on the singlet PES, and the related partially bond-ruptured **5** *t*-$H(F)C^{\bullet}–B^{\bullet}–H$ and **6** *c*-$H(F)C^{\bullet}–B^{\bullet}–H$, analogous to **S2** H(F)C=B–H. (Note: in this article species denoted without a letter prefix are triplet minima. Singlet minima[1] will be denoted with the prefix "S" to distinguish them from the triplet species.) Isomer **11** H(F)CBH is an oddly-shaped

molecule with the same connectivity as **5** and **6** but a linear HCB angle (Table 4.1 and Figure 4.1). The odd shape led us to re-optimize the geometry of **11** at the CCSD/aug-cc-pvdz level of theory, and at this calculational level **11** collapses to **6**. That the C–B–X angle, X = F, H, is <180° in **1**, **5** and **6** is indicative of the unpaired electron occupying an sp^2-orbital rather than a p-orbital on boron and gives rise to the possibility of three-coordinated boron species. Exchange of the boron and carbon atoms in **5**, **6**, and **1** yields the carbenes **2** *c*-HCB(F)H, **3** *t*-HCB(F)H, and **4** $FCBH_2$, respectively. The latter three structures have no singlet counterparts. The only four-coordinated carbon atom is found in **10** $BC(H)_2F$, which is related to **S3** $BC(H)_2F$**.** Overall, in contrast to the singlets[1], with the exception of a 4-coordinate boron atom, all possible arrangements of the remaining atoms on boron and carbon are observed for open-shell [B, C, F, H_2].

Turning now to the hydrogen-bonded species, **7** and **8** consist of a CH_2 group loosely bound through an unconventional C-H…Y hydrogen bond. Boron is the electron-donating atom Y in **7** H_2C…BF and fluorine is the electron-donating atom in **8** H_2C…FB. The series of molecules **12** – **15** contain conventional hydrogen bonds with HF as the proton donor. In isomers **12** FH…C(B)H and **15** FH… BCH the fragment HCB is the proton acceptor, through the C for **12** and B for **15**. Complex **12** FH…C(B)H is unique among the hydrogen-bonded complexes, with its connection between HF and the medial fragment atom and consequent T-shaped structure. When the triatomic HBC is the proton acceptor (**13** and **14**), only FH…C hydrogen bonds are observed. Isomer **14** FH…CBH, C_s has the same connectivity as **13** FH…CBH, $C_{\infty v}$, but with a bent H…CB bond angle (Table 4.1 and Figure 4.1).

The new isomers on the singlet PES, **S11** FH…C(B)H and **S12** FH…CBH, have FH…C linkages with HCB and HBC, respectively, and correlate with **12** and **13**, respectively. The only other singlet-triplet hydrogen-bonded pairs are **S4**, **7** and **S5**, **8**[1]. It must be noted that AIM analysis[37] finds no bond path linked to boron in **S11**, despite a shorter C–B distance in this molecule than in **S12** and most of the triplet molecules (Table 4.1). When the geometry of **S11** was re-optimized at the CCSD/aug-cc-pvdz level of theory, a C_1 structure more similar to that of its triplet counterpart **12** was obtained (e.g., C–H_1 = 1.089 Å, <BCH_1 = 128.6°). At this calculational level, a bond path does exist between the B and C.

The last two triplet structures identified are van der Waals complexes. Structure **9** HH…FBC has a hydrogen molecule interacting with the fluorine end of the triatomic FBC and is analogous to the singlet **S9** HH…FBC[1]. As a boron-centered planar complex, **16** H_2BF…C is a surprising minimum with the fluorine loosely bound to the carbon 2.554 Å away (Table 4.1 and Figure 4.1).

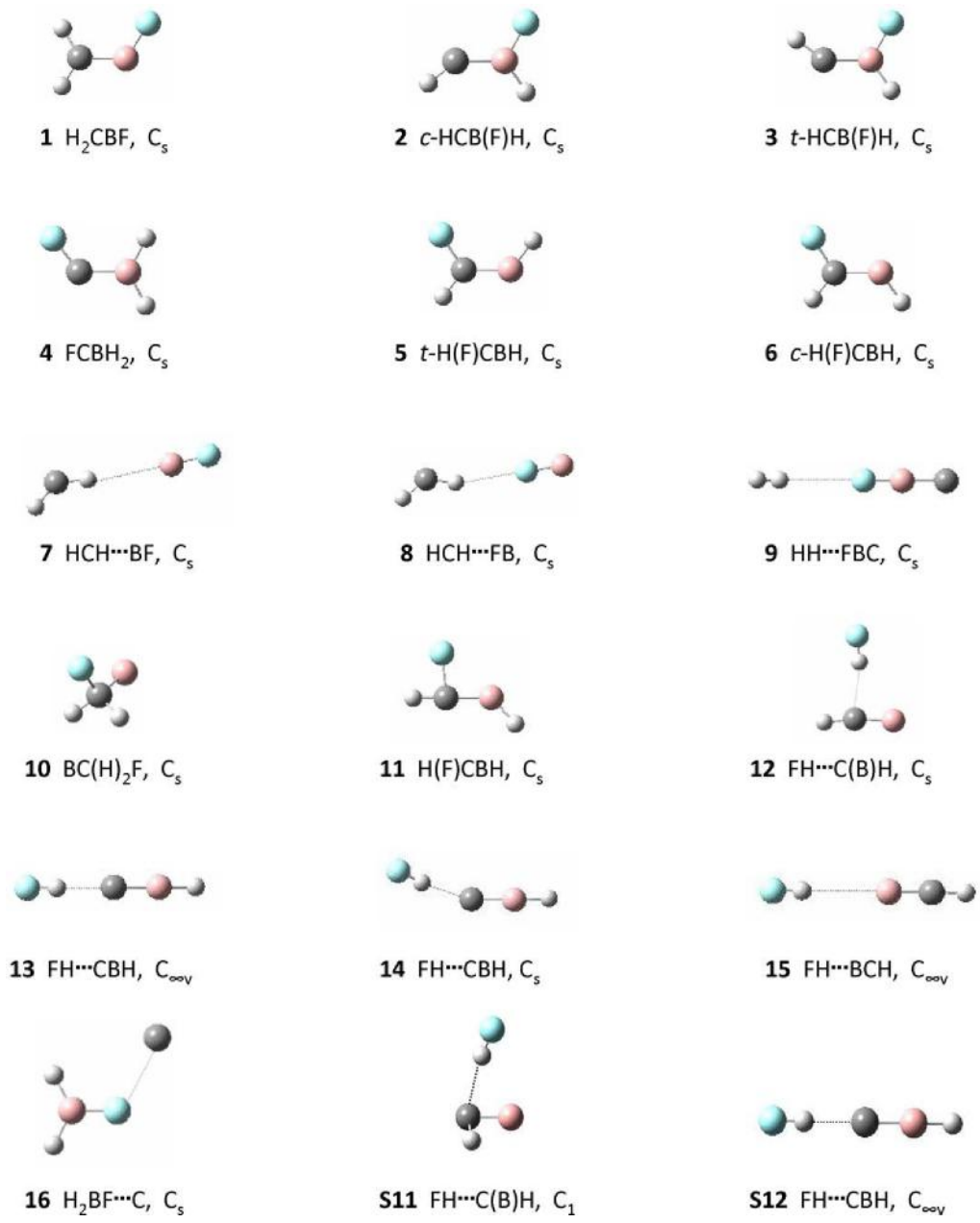

Figure 4.1 Structures of the 16 isomers located on the triplet potential energy surface and two additional singlets. C: grey, H: white, B: pink, F: cyan. (For grayscale, the degrees of coloration are C > B > F > H.) (For interpretation of the references to color in this figure legend, the reader is referred to the web version of the article.)

Table 4.1 Geometrical parameters[a]

Isomer	Bond Lengths	Bond Angles	Dihedral Angles
1 H_2CBF, C_s	CB: 1.542	HCB: 121.8	HCBF: 0.0
	BF: 1.356	H_1CB: 122.1	
	CH: 1.096	CBF: 121.9	
	CH_1: 1.091		
2 *c*-HCB(F)H, C_s	CB: 1.534	HCB: 141.0	HCBF: 180.0
	BF: 1.362	CBH: 123.3	
	CH: 1.090	CBF: 119.5	
	BH: 1.204		
3 *t*-HCB(F)H, C_s	CB: 1.535	HCB: 143.1	HCBF: 0.0
	BF: 1.368	CBH: 123.5	
	CH: 1.090	CBF: 119.2	
	BH: 1.200		
4 $FCBH_2$, C_s	CB: 1.526	CBH: 118.2	FCBH: 0.0
	CF: 1.326	CBH_1: 118.0	
	BH: 1.202	FCB: 128.2	
	BH_1: 1.196		
5 *t*-H(F)CBH, C_s	CB: 1.511	FCB: 121.9	FCBH: 0.0
	CF: 1.361	HCB: 128.2	
	CH: 1.094	CBH: 128.6	
	BH: 1.196		
6 *c*-H(F)CBH, C_s	CB: 1.511	FCB: 121.2	FCBH: 180.0
	CF: 1.352	HCB: 128.9	

	CH: 1.097	CBH: 125.3	
	BH: 1.197		
7 $H_1CH…BF$, C_s	BF: 1.302	H_1CH: 133.2	CH…BF: 0.0
	CH: 1.089	CH…B: 174.8	$H_1CH…B$: 180.0
	CH_1: 1.089	H…BF: 175.8	
	H…B: 2.900		
8 $H_1CH…FB$, C_s	BF: 1.305	H_1CH: 132.7	CH…FB: 180.0
	CH: 1.088	CH…F: 163.7	$H_1CH…F$: 180.0
	CH_1: 1.088	H…FB: 179.7	
	H…F: 2.602		
9 HH…FBC, C_s	CB: 1.485	CBF: 180.0	BF…HH: -2.2
	BF: 1.305	BF…H: 179.9	CBF…H: 3.1
	HH: 0.755	F…HH: 179.8	
	F…H: 2.833		
10 $BC(H)_2F$, C_s	CB: 1.550	FCB: 115.5	HCBF: ±121.0
	CF: 1.431	HCF: 106.9	HCBH: 118.1
	CH: 1.105	HCB: 109.8	
11 H(F)CBH, C_s	CB: 1.512	FCB: 95.9	HCBH: -89.9
	CF: 1.503	HCB: 180.0	FCBH: 180.0
	CH: 1.093	CBH: 132.4	FH…CB: 180.0
	BH: 1.197		
12 $FH…C(B)H_1$, C_s	CB: 1.374	H_1CB: 171.9	
	CH_1: 1.082	H…CB: 88.1	

	H…C: 2.062	FH…C: 170.4	
	HF: 0.941		
13 FH…CBH, $C_{\infty v}$	CB: 1.457		
	BH: 1.183		
	H…C: 1.832		
	HF: 0.952		
14 FH…CBH, C_s	CB: 1.458	CBH: 176.3	H…CBH: 0.0
	BH: 1.183	H…CB: 158.8	FH…CB: 0.0
	H…C: 1.848	FH…C: 171.4	
	HF: 0.951		
15 FH…BCH, $C_{\infty v}$	CB: 1.359		
	CH: 1.080		
	H…B: 2.758		
	HF: 0.926		
16 H_2BF…C, C_s	BF: 1.362	FBH: 117.2	C…FBH: 0.0
	BH: 1.200	FBH_1: 116.8	
	BH_1: 1.200	BF…C: 118.1	
	F…C: 2.543		
S11 FH…C(B)H_1, C_1	C…B: 1.412	B...CH_1: 77.3	FH…C...B: 14.7
	CH_1: 1.176	B…C…H: 74.5	FH…CH_1: 87.7
	C…H: 2.099	FH…C: 172.1	
	HF: 0.939	H…CH_1: 102.0	
S12 FH…CBH, $C_{\infty v}$	CB: 1.478		

	BH: 1.182		
	H…C: 1.853		
	HF: 0.949		
TS 1-2, C_1	CB: 1.491	CBF: 127.1	FBCH: 169.4
	BF: 1.361	HCB: 140.0	FBC...H: 123.1
	CH: 1.091	C...H...B: 63.9	
	C...H: 1.488		
	B...H: 1.315		
TS 1-3, C_1	CB: 1.478	CBF: 132.7	FBCH: -16.9
	BF: 1.361	HCB: 144.1	FBC...H: -123.4
	CH: 1.099	C...H...B: 62.1	
	C...H: 1.525		
	B...H: 1.318		
TS 2-3, C_1	CB: 1.523	HCB: 180.0	FBCH: -89.5
	BF: 1.366	CBF: 119.7	
	CH: 1.082	CBH: 123.5	
	BH: 1.201		
TS 4-5, C_1	CB: 1.489	CBH: 127.4	FCBH: -7.1
	CF: 1.331	FCB: 130.5	FCB…H: 105.8
	BH: 1.197	C...H...B: 63.1	
	C...H: 1.512		
	B...H: 1.314		
TS 4-6, C_1	CB: 1.504	CBH: 123.8	FCBH: 178.1
	CF: 1.330	FCB: 125.2	FCB...H: 72.8

	BH: 1.191	C...H...B: 65.3	
	C...H: 1.460		
	B...H: 1.319		
TS 5-6, C_s	CB: 1.479	CBH: 177.4	FCBH: 180.0
	CF: 1.372	FCB: 122.1	
	CH: 1.095	HCB: 129.9	
	BH: 1.178		
TS 1-5, C_1	C…B: 1.766	HC…H: 124.4	HC…BF: 96.8
	CH: 1.115	H…BF: 96.1	FB…C…H: -122.3
	BF: 1.506	C…H…B: 80.9	
	C…F: 1.719		
	C…H: 1.430		
	B…H: 1.285		
TS 3-5, C_s	CB: 1.404	HCB: 171.6	F…CBH: 180.0
	CH: 1.080	CBH: 179.7	HCBH: 0.0
	BH: 1.178	F…CB: 81.3	
	C…F: 1.854	C…F…B: 40.2	
	B…F: 2.150		
TS 1-10, C_s	CB: 1.445	BCH: 120.7	HCB…F: ±95.9
	CH: 1.093	HCH: 117.6	HCH…F: 106.6
	C…F: 1.849	F...CB: 80.5	BCH…F: 84.7
	B…F: 2.151	HC...F: 99.8	BCHH: -168.6
TS 6-10, C_1	CB: 1.462	FCB: 124.0	HCB…H: 58.4
	CF: 1.380	FCH: 107.7	FCH…H: 130.7

	CH: 1.099	BCH: 127.9	BCF…H: 65.7
	C…H: 1.508	FC…H: 127.3	BCFH: 173.5
	B…H: 1.312	BC…H: 52.4	
^{3}BF	BF: 1.353		
^{3}BH	BH: 1.198		
^{2}CH	CH: 1.130		
^{2}CF	CF: 1.300		
$^2BH_2$	BH: 1.173	HBH: 104.3	
$^3CH_2$	CH: 1.088	HCH: 132.6	
^{3}HCF	CF: 1.339	HCF: 121.0	
	CH: 1.095		
^{3}CBH	CB: 1.468	CBH: 180.0	
	BH: 1.186		
^{3}BCH	CB: 1.363	BCH: 180.0	
	CH: 1.081		
^{3}CBF	CB: 1.485	CBF: 180.0	
	BF: 1.305		
^{2}HBF	BH: 1.209	HBF: 120.5	
	BF: 1.343		
^3H_2BF, C_s	BH: 1.303	FBH: 115.6	FBHH: ±105.5
	BF: 1.367	HBH: 58.2	

[a] Bond lengths in Å, bond angles and dihedral angles in degrees.

Table 4.2 Relative thermochemical data for minima identified[a,b]

Isomer	ΔE	$\Delta(E+ZPE)$	$\Delta_{298}H$	Δ_{298}G
1 H_2CBF	0.0	0.0	0.0	0.0
2 *c*-HCB(F)H	10.7	5.9	5.8	5.9
3 *t*-HCB(F)H	13.6	9.0	8.8	8.7
4 $FCBH_2$	195.9	189.3	189.1	189.5
5 *t*-H(F)CBH	196.8	194.5	194.0	194.6
6 *c*-H(F)CBH	197.5	194.9	194.4	195.3
7 HCH…BF	268.6	250.3	257.7	236.5
8 HCH…BF	271.3	251.6	260.1	234.5
9 HH…FBC	298.8	271.1	278.9	271.3
10 $BC(H)_2F$	301.0	303.1	302.4	303.3
11 H(F)CBH	332.3	323.4	324.0	322.9
12 FH…C(B)H	342.4	334.6	337.9	328.7
13 FH…CBH, $C_{\infty v}$	354.4	344.1	347.2	342.8
14 FH…CBH, C_s	356.4	345.4	347.8	341.4
15 FH…BCH	361.7	351.6	359.1	339.1
16 H_2BF…C	385.0	370.7	374.7	361.9
S11 FH …C(B)H[c]	599.0	588.2	591.1	580.2
S12 FH…CBH	613.5	603.1	606.3	599.0

[a] CCSD(T)/CBS data in kJ/mol.
[b] Energies for **1** in hartrees are E=-163.7543384, $E+ZPE$=-163.7256481, H_{298}=-163.7210084, and G_{298}=-163.7511744.
[c] **S11** and **S12** energies are relative to the ground-state singlet. Energies [1] for **S1** in hartrees are E=-163.8217944, $E+ZPE$=-163.7932734, H_{298}=-163.7884414, and G_{298}=-163.8167594.

4.3.1.2 Transition Structures

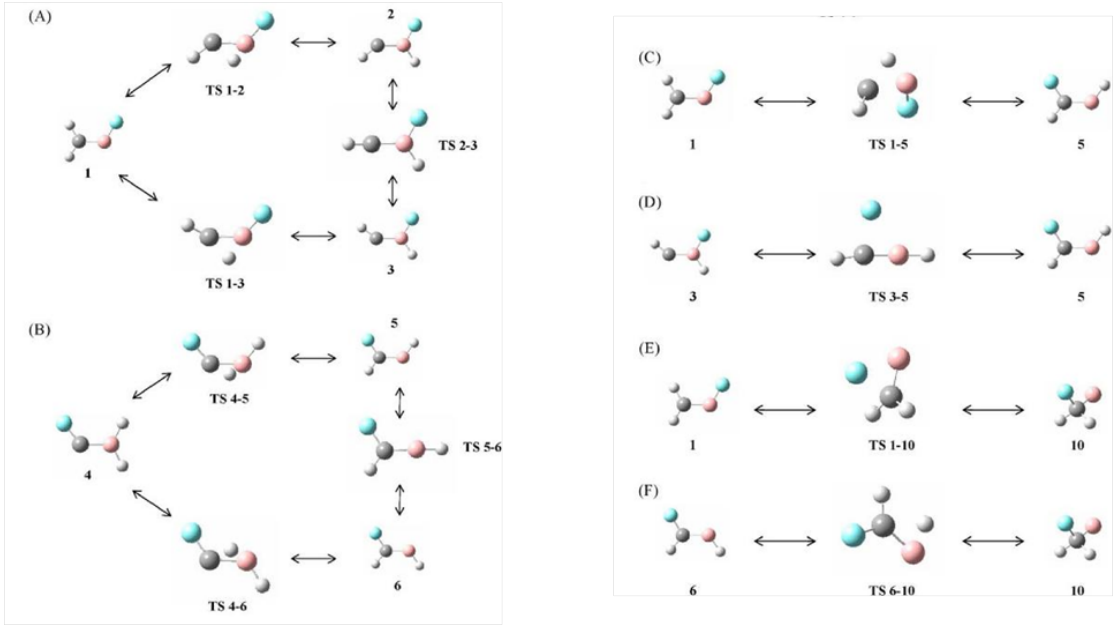

Figure 4.2 Transition states and the minima they connect. C: grey, H: white, B: pink, F: cyan. (For grayscale, the degrees of coloration are C > B > F > H.) (For interpretation of the references to color in this figure legend, the reader is referred to the web version of the article.)

In our search for transition structures connecting the minima, we focused on those isomers for which rearrangement rather than fragmentation may be more likely. The most relevant isomerization pathways are illustrated in Figure 4.2; each pathway is endothermic as written. Bond lengths, bond angles and dihedral angles for the transition structures can be found in Table 4.1. The label associated with each transition structure designates the minima it connects. Conversion between the cis and

trans isomers of HCB(F)H or H(F)CBH proceeds through **TS 2-3** or **TS 5-6** (Figure 4.2(A) and Figure 4.2(B)), which have the expected linear HCB angle (**TS 2-3**) and nearly linear HBC angle (**TS 5-6**, Table 4.1). Other transition structures that concur with chemical intuition include **TS 1-3** and **TS 4-5** (Figure 4.2(A) and Figure 4.2(B). Both of these rearrangements involve the transfer of a hydrogen atom between the carbon and boron. In each case as the hydrogen shifts along the C–B bond, it remains on the same side of the bond on which it started. It does, however, move out of the molecular plane. The **1-2** and **4-6** rearrangements require the hydrogens, which start out on the same atom, to end up in the cis configuration. The transition structures show the out-of-plane movement of the hydrogen as it crosses the C–B bond. The geometries of all four of these transition structures are similar in that the B…H distance is ~1.3 Å, the C…H distance is ~1.5 Å and the B…H…C angle is ~65°. In addition, the angle the "immobile" hydrogen makes with B and C has opened up to within ~1° of its value in the product (Table 4.1).

The straightforward B→C shuttling of the fluorine or hydrogen atom observed in **TS 1-10** and **TS 6-10** (Figure 4.2(E) and Figure 4.2(F) leads to rehybridization of the carbon atomic orbitals. The atom that is shifting has moved out of the molecular plane, but the pyramidalization of the H_2CB geometry has not yet occurred. Similar structural features were found in the transition structures connecting the analogous singlet minima, **S1-S3** and **S2-S3**[1].

One of the more unexpected characteristics of **TS 1-5** is that the hydrogen is inserted between the C and B stretching the C–B bond (Figure 4.2(C)). Also, in order to effect a transition in which the exchanging H and F atoms end up on the same side

of the C–B bond, the HC and BF fragments twist perpendicularly (<HC…BF = 96.8°, Table 4.1). Overall, the **1-5** isomerization occurs in a stepwise manner; the B–H bond is within 7% of its equilibrium distance in **5** and the B–F bond is stretched by only 11%. In **TS 3-5** the fluorine is displaced by 37% from the C–F bond distance in **5** and the hydrogens, initially trans, have flattened out to within 10° of linearity to facilitate their rotation about the B–C bond when the fluorine transfer is complete.

Other than the cis-trans interconversions, each of the reactions depicted in Fig. 2 possesses a transition structure shifted toward a "later", more product-like position, on the reaction coordinate. Nevertheless, not all of these reactions obey the Leffler-Hammond postulate[40,41] because some of the most product-like transition structures are associated with the reactions that are essentially thermoneutral (see below).

4.4 Energetics

4.4.1 Minima

4.4.1.1 Triplet-triplet and singlet-triplet energy gaps.

The energies, enthalpies and free energies of the triplet minima relative to the corresponding values for **1** H_2CBF are given in Table 4.2. The data for the two new singlet minima relative to that for **S1** H_2CBF are also included in the table. The relative enthalpies of the set of triplet [B, C, F, H_2] isomers are compared with those of the set of singlet [B, C, F, H_2] isomers in Figure 4.3 (this work and Ref. [1]). The

singlet isomers have not been renumbered with respect to relative energy, so the grouping in Figure 4.3 that lies at ca. 600 kJ/mol represents **S11** FH…C(B)H, **S7** H(C)BFH and **S12** FH…CBH, respectively.

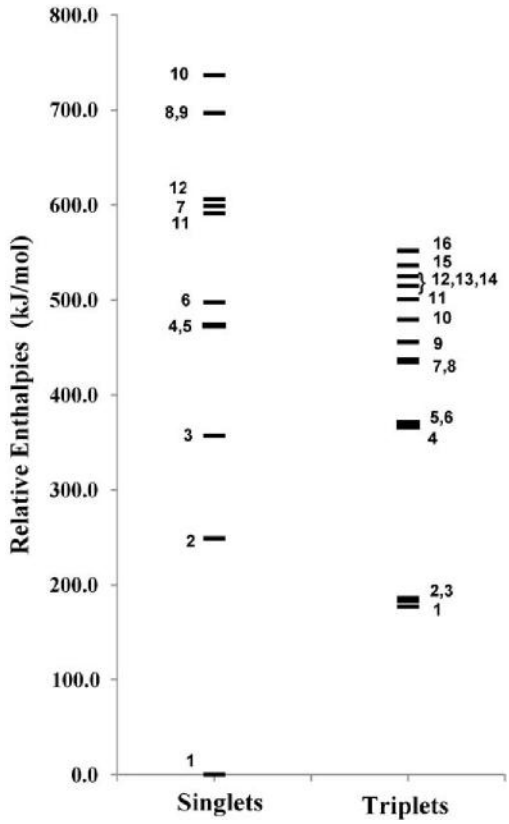

Figure 4.3.Comparison of the relative enthalpies of isomers on the singlet [1] and triplet potential energy surfaces. Dotted lines connect analogous isomers of different multiplicities.

The entropy term (298 K) makes only a minor contribution to the relative stabilities of many of these species but when it does have a non-negligible effect, it

stabilizes the species with respect to **1** H_2CBF (Table 4.2). Because the relative enthalpies of some of these minima are clustered so closely together, the trends in ΔH and ΔG are similar but not identical. Isomers **9** CBF…HH and **10** $BC(H)_2F$ account for the only deviation in relative enthalpies between the MP2 and CCSD(T) methods. At the MP2/aug-cc-pVDZ level of calculation, the hydrogen-bonded isomer **9** is about 13 kJ/mol less stable than **10**, the only isomer with a 4-coordinate carbon. However, this difference is reversed by ca. 25 kJ/mol at the CCSD(T) level.

Among the conventionally bound triplets, the CBF connectivity is more favorable than the FCB connectivity. As it was for the analogous singlets[1], this preference can be rationalized primarily on the basis of the greater strength of the B–F bond compared to that of the B–H bond[9,12–15,42]. The stabilities of **5** *t*-H(F)CBH (**6** *c*-H(F)CBH) relative to **1** H_2CBF and of **S2** H(F)CBH relative to **S1** H_2CBF are not greatly different in magnitude (195 vs. 250 kJ/mol, this work and Ref. [1]). A similar difference in stability is found between **4** $FCBH_2$ and **2** *c*-HCB(F)H (**3** *t*-HCB(F)H), ca. 180 kJ/mol (Table 4.2). Given the CBF or FCB connectivity, however, rearrangement of the hydrogens on the C and B atoms has little effect on stability; for each set of related isomers the enthalpies and free energies are all within 10 kJ/mol of each other. This result is consistent with the similar magnitudes of the CH (340-345 kJ/mol) and BH (341 kJ/mol) bond dissociation enthalpies derived from the relevant gas-phase enthalpies of formation in the NIST Chemistry WebBook[42]. Although evaluated at a lower level of theory, Schleyer and coworkers[43,44] obtained essentially equal energies for triplet H_2CBH and $HCBH_2$, suggesting that substituting F for H also has little effect on the relative stabilities of these species.

The most striking difference structurally in the two sets of cis and trans isomers is the magnitude of the HCB angle. This angle in **2** and **3** (and $HCBH_2$[43]) is at least 12 – 15° closer to linear than is any angle in **5** and **6** (and H_2CBH[44]) (Table 4.1), which is one manifestation of the greater concentration of p-character in the in-plane C orbital directed toward the unpaired electron than in the corresponding B orbital. The difference in hybridization around the central C and B atoms is consistent with Bent's rule[45], since carbon and hydrogen are more electronegative elements than is boron. The greater repulsion between the fluorine atom and unpaired electron in the oddly-shaped isomer **11** H(F)CBH than in isomer **6** makes it about 130 kJ/mol less stable than **6**. The increased repulsion in **11** arises from its more acute <FCB, less acute <HBC, longer C–F bond (Table 4.1), and associated greater p-character in the C orbital directed toward the fluorine and B orbital directed toward the unpaired electron.

Triplet **10** $BC(H)_2F$ is closer in energy to triplet **1** H_2CBF than **S3** $BC(H)_2F$ is to **S1** H_2CBF[1], but **10** is less favorable than its singlet counterpart (Table 4.2 and Figure 4.2). Replacing the fluorine atom with hydrogen decreases the observed energy gaps, for both the triplet and singlet species. The singlet-singlet and triplet-triplet separations are both less than 100 kJ/mol for BCH_3 vs. H_2CBH[44].

Interestingly, the cluster of complexes with unconventional hydrogen bonds, **7** – **9**, has lower total energies than the cluster of complexes with conventional hydrogen bonds, **12** – **15** ((Table 4.2). In contrast, the energies of the conventionally hydrogen-bonded singlet complexes, **S11** FH…C(B)H and **S12** FH…CBH, lie between those of the two sets of unconventionally hydrogen-bonded singlet

complexes[1] **S4** HCH…BF, **S5** HCH…FB and **S8** H_2…C(F)B, **S9** H_2…FCB (Figure 4.3). Within each group of triplet complexes the stabilities differ by no more than 20 kJ/mol, whereas the separation between the groups is 60 kJ/mol. At the CCSD(T)/CBS level of calculation, the enthalpy difference $\Delta H[HBC(^3\Sigma^-) - HCB(^3\Pi)]$ = 27.1 kJ/mol, which is identical to the G3(MP2) value computed by Zeng et al.[16]. That **12** FH…C(B)H is only 10 kJ/mol more stable than **13** FH…CBH can be partially attributed to the 8° bending of the linear HCB fragment on complexation (Table 4.1). The van der Waals complex **16** H_2BF…C lies only 15 kJ/mol above the second cluster of hydrogen-bonded isomers (Figure 4.2).

The enthalpies and free energies of the triplet minima are much more compressed than those of the singlet minima. Although the three lowest-lying [B, C, F, H_2] singlets are considerably more stable than the corresponding triplets, which was also observed for the [B, C, H_3] species[43,44], the trend is reversed for the more "physically" bound triplets and their corresponding singlets. This reversal produces a shift in the stability order for the two sets of isomers. Overall, the most stable [B, C, F, H_2] species is **S1** H_2CBF. Its enthalpy is 177 kJ/mol below that of triplet **1** and the enthalpies of triplets **1** – **3**, H_2CBF, *c*-HCB(F)H and *t*-HCB(F)H, are about 75 kJ/mol below that of **S2** H(F)CBH. At the MP2/D95* level of theory, Lanzisera and Andrews[3] found a similar difference of 163 kJ/mol in the energies of singlet and triplet CH_2BF.

Singlet-triplet splittings for the fragments relevant to the binding affinities discussed below are given in Table 4.3. Experimental and computed S-T splittings have been reported previously for several of these species, and the CCSD(T)/CBS

values are included here for comparison and to provide the thermodynamic data required to compute diabatic bond dissociation enthalpies for the [B, C, F, H_2] isomers. A positive value for the S-T splitting signifies that the triplet lies higher in energy than the singlet.

Table 4.3 Singlet-triplet splittings[a,b]

Species	Δ(*E*+*ZPE*)	Species	Δ(*E*+*ZPE*)
BH	129.5	HBC	-77.7
BF	348.7[c]	HCB	-70.0
CH_2	-37.0	CBF	-85.2
HCF	62.8	H_2BF	410.4

[a] CCSD(T)/CBS values in kJ/mol.

[b] Negative values indicate that the triplet species is more stable.

[c] Ref. [9].

For CH_2 and HCF the CCSD(T)/CBS results are in excellent agreement with the results from both experiment (to within 1 kJ/mol, Refs. [46,47]) and the W1′ procedure (to within 1.5 kJ/mol, Ref. [48]). The discrepancy between the CCSD(T)/CBS and experimental (124.3 kJ/mol, Ref. [49]) singlet-triplet gaps for BH is somewhat larger at 5.2 kJ/mol, but the discrepancy is smaller between our value

and the FCI/aug-cc-pVDZ value of 126.7 kJ/mol[50]. The tabulated singlet-triplet splitting for BF was reported earlier by Dixon and Grant[9].

4.4.1.2 Binding affinities

Photolytic decomposition of the excited states of ketene and diazomethane has been used as a source of $^3CH_2$[2]. In triplet H_2CCO, the C–C adiabatic bond dissociation energy forming $^3CH_2$ and ^1CO is calculated to be 88.3 kJ/mol at the QCISD(T)/cc-pVQZ//B3LYP/cc-pVQZ level of theory[51], consistent with the expected weak binding in this system. On the other hand, the adiabatic B–C BDHs and bond critical point electron densities ρ_b in isomers **1** – **6** and **10** (and **11**) demonstrate that the binding in these systems is significantly tighter (Table 4.4), as has been observed for other corresponding first adiabatic C–C and B–C BDHs[13,15]. The strength of the B–C bonds in **1** – **6** and **10** is not unusual; the adiabatic BDHs in these molecules are comparable in magnitude to those in a number of organoborane closed- and open-shell species examined previously[1,12,13,15,52]. For example, our calculated adiabatic B–C BDHs are 443.4 and 489.6 kJ/mol in the neutral species **S1** H_2CBF and **S2** H(F)CBH, respectively[1] and are 373 and 447 kJ/mol (with a smaller basis set) in the triplet ionic species $HBCN^-$and $HBCF^+$, respectively[52]. Other reported examples of adiabatic B–C BDHs in closed-shell organoboranes include the G3 value[12,15] of 434.9 kJ/mol in H_2BCH_3 and the G2 values[13] of 465.3 kJ/mol in F_2BCH_3 and 384.5 kJ/mol in BCH_3. The corresponding G2 adiabatic B–C BDH in $^3BCH_3$ is 202.1 kJ/mol[13], implying that

fluorination has stabilized the triplet with respect to the singlet since the decrease in bond strength on excitation is 122 kJ/mol for **S3** $BC(H)_2F$ and **10**[1]. Further comparison can be made with our calculated BDHs in ^{3}HCB (501.7) and ^{3}HBC (467.6 kJ/mol), which are at the high end of the range of values in Table 4.4. The dissociation energy D_e in ^{3}HBC is 479.4 kJ/mol, in excellent agreement with the MRCI+Q/[$(cc\text{-}pVQZ)_H$/$(cc\text{-}pV5Z\text{-}h)_{B,C}$] theoretical value of 477 kJ/mol reported by Tzeli and Mavridis[53]. Overall, as we have suggested previously[1,52], with such tight boron-carbon bonds these species are "chemically" bound and should be considered new and different species.

Although the B-C bond in **1** H_2CBF is apparently 2-3 times stronger than the C–C bond in ketene, it is dramatically weaker than the B–C bonds in the related isomers **2**-**6** and even **11** (Table 4.4). As has been pointed out for similar systems, the lower adiabatic B–C BDH in **1** results from the unusual stability of the closed-shell singlet BF product[9,12,13]. Use of a diabatic process[9,17], which accounts for the reorganization enthalpy of the product fragments, will perhaps yield a more appropriate comparison of the B–C bond strengths. The diabatic BDH gives a better estimate of the intrinsic or instantaneous strength of a bond, as does the bond critical point electron density ρ_b[15]. Focusing on **1** H_2CBF and **5** *t*-H(F)CBH, for which there are corresponding singlets, as defined by Dixon and coworkers[9,17] the diabatic process involves formation of ^{3}BX where one unpaired electron comes from the radical reactant and one from the bond breakage. From the singlet-triplet splittings in Table 4.3, the diabatic B–C BDHs in **1** and **5** are 615 and 560 kJ/mol, respectively. The analogous dissociation channels in **S1** H_2CBF and **S2** H(F)CBH are 792 and 682

kJ/mol, respectively (this work and Ref. [1]). The differences in the diabatic B–C BDHs in the singlets vs. the triplets are more congruous with the expected stronger intrinsic bonding in the singlets and with the larger ρ_b(B–C) values calculated for the singlets (Table 4.4). The diabatic B–C BDHs in **1** and **5** are also consistent with the diabatic B–C BDH in triplet HBC of 597 kJ/mol.

Table 4.4 Reaction thermochemistry: Adiabatic bond dissociations

Reaction	$\Delta_{rxn}E$	$\Delta_{rxn}(E+ZPE)$	$\Delta_{rxn}H$	$\Delta_{rxn}G$	ρ_b [b]
1 $CH_2BF \rightarrow {}^3CH_2 + {}^1BF$	272.9	251.1	257.6	218.6	0.182 [0.225]
2 *c*-HCB(F)H → ^{2}HC+^{2}FBH	493.2	469.2	475.8	434.0	0.179
3 *t*-HCB(F)H → ^{2}HC+^{2}FBH	490.3	466.1	472.8	431.1	0.179
4 $FCBH_2 \rightarrow {}^2CF + {}^2BH_2$	369.4	346.6	353.3	310.6	0.170 [0.222]
5 *t*-H(F)CBH → ^{3}FCH + ^{1}BH	448.7	423.3	430.3	388.6	0.191
6 *c*-H(F)CBH → ^{3}FCH + ^{1}BH	448.1	422.9	429.9	388.0	0.184
7 HCH…FB → $^3CH_2 + {}^1$BH	4.0	0.8	-0.1	-17.9	0.00572
8 HCH…BF → $^3CH_2 + {}^1$BH	1.3	-0.4	-2.5	-15.9	0.00448
9 HH…FBC → ^{3}CBF + $^1H_2$	0.5	-1.9	-2.2	-25.6	0.00264

10 $BC(H)_2F \rightarrow {}^2CH_2F + {}^2B$	215.0	203.6	208.7	173.8	0.181 [0.183]
11 $H(F)CBH \rightarrow {}^3FCH + {}^1BH$	313.2	294.4	300.3	260.3	0.175
12 $FH\ldots C(B)H \rightarrow {}^3HCB + {}^1HF$	21.4	16.5	19.3	-7.5	0.0250
13 $FH\ldots CBH,\ C_\infty \rightarrow {}^3HBC + {}^1HF$	43.2	33.9	37.0	4.9	0.0400
14 $FH\ldots CBH,\ C_s \rightarrow {}^3HBC + {}^1HF$	41.2	32.7	36.4	6.4	0.0382
15 $FH\ldots BCH \rightarrow {}^3HCB + {}^1HF$	2.2	-0.5	-2.0	-17.9	0.00543
16 $H_2BF\ldots C \rightarrow {}^1H_2BF + {}^3C$	7.2	5.6	5.8	-14.7	0.0142
S11 $HF\ldots C(B)H \rightarrow {}^1HCB + {}^1HF$	20.9	10.5	13.9	-18.4	[0.0260] (0.0192)[c]
S12 $FH\ldots CBH \rightarrow {}^1HBC + {}^1HF$	38.8	29.8	32.7	1.3	[0.0359]

[a] CCSD(T)/CBS//MP2/aug-cc-pVDZ data in kJ/mol. [b] Bond critical point electron density, in a.u., for the bond broken during fragmentation. Values for analogous singlets are in brackets. [c] Data for **S11** re-optimized at the CCSD(T)/CBS//CCSD(T)/aug-cc-pVDZ level.

As both conventional **12** – **15** and unconventional **7** – **9** hydrogen-bonded complexes were located in this study among the more weakly bound triplet isomers, different types of geometrical rearrangements may be exhibited on complex formation. When an X–H…Y complex containing a conventional hydrogen bond is formed, the X–H bond lengthens typically as a result of electron donation from Y to an antibonding X–H orbital[54]. In an unconventional hydrogen-bonded complex, X is usually a much less electronegative atom, attracting less charge transfer. In this case,

the X–H bond may shorten slightly on complex formation[55], which can be explained[54] by the increase in s-character in the X hybrid orbital of the X–H bond dominating the effect of the charge transfer. For purposes of comparison, at the MP2/aug-cc-pVDZ level of theory the bond lengths in H_2, HF and $^3CH_2$ are 0.755 Å, 0.926 Å and 1.088 Å, respectively.

The strongest FH…Y interactions in isomers **12** – **15** occur when the electron-donating atom in Y is carbon (Table 4.4). In fact, at 2.2 kJ/mol the $\Delta_{rxn}E$ value for **15** FH…BCH is an order of magnitude smaller than those for **12** – **14**. Among the latter three isomers, the hydrogen bond in **13** FH…CBH, $C_{\infty v}$, with its link through the terminal carbon of HBC is about twice as strong as that in **12** FH…C(B)H, with its link through the medial carbon in HCB. Bending of the linear H…CB angle in **13** to form **14** FH…CBH, C_s weakens the hydrogen bond by only ca.1 kJ/mol. Analysis of the geometrical properties of these four complexes shows that the expected increase in F–H bond length Δr(XH) is observed and that this structural change is directly related to $\Delta_{rxn}E$. The values for Δr(XH) are 0.026 Å (**13** FH…CBH, $C_{\infty v}$,) ≈ 0.025 Å (**14** FH…CBH, C_s) > 0.015 Å (**12** FH…C(B)H) > 0.000 Å (**15** FH…BCH). For the three isomers with carbon as the electron-donating atom, $\Delta_{rxn}E$ is inversely related to the H…C distance.

Comparing **7** HCH…BF and **8** HCH…FB, from the second set of hydrogen-bonded species, it is slightly more favorable for CH_2 to bind through the boron rather than the fluorine. The difference of ~2.5 kJ/mol in the hydrogen-bond strengths of these two complexes is essentially equal to the difference that was observed for the singlet counterparts **S4** HCH…BF and **S5** HCH…FB[1]. For **7** HCH…BF, **8** HCH…FB

and **9** HH…BCF, there is essentially no change in the XH bond length on complex formation. Specifically, the values for Δr(XH) are 0.001 Å (**7**) or 0.000 Å (**8** and **9**), indicative of the weak binding and, perhaps, more effective competition between the hyperconjugative and rehybridization effects on formation of these systems (and **15** FH…BCH). The $\Delta_{rxn}E$ values for complexes **7** – **9** and **15** do, however, correlate with the total energy of the hyperconjugative interactions $\Delta E^{(2)}$(donor → acceptor) and with the bond critical point electron densities in the H…Y bonds ρ_b(H…Y).

For all seven of these hydrogen-bonded complexes $\Delta_{rxn}E$ decreases when $\Delta E^{(2)}$ and ρ_b(H…Y) decrease (Table 4.4), and the correlation holds across the two sets of isomers despite the variation in both proton-donating and electron-donating atoms. Only the primary contributions to the NBO total hyperconjugation energies will be discussed below. For **13** and **14** the energy ($\Delta E^{(2)}$) contributed by the n(C) → σ*(H–F) hyperconjugation is 203.3 and 181.5 kJ/mol, respectively, whereas for **12** the energy contributed by the σ(C–B) → σ*(H–F) hyperconjugation is 85.2 kJ/mol. Although the magnitudes of these $\Delta E^{(2)}$ values are significantly larger than $\Delta_{rxn}E$ for each of these species (Table 4.4), because the charge transfer energy is offset by the steric repulsion between the fragment[36], the $\Delta E^{(2)}$ values do account for the relative strengths of the hydrogen bonds in these species. The considerably weaker $\Delta E^{(2)}$ = 14.7 kJ/mol is associated with the n(B) → σ*(H–C) hyperconjugation in **7** HCH…BF. There is an even smaller charge transfer in **15** FH…BCH from the boron unpaired electron delocalizing into the H–F antibonding orbital, with $\Delta E^{(2)}$ = 5.2 kJ/mol. Weaker still are the n(F) → σ*(H–C) and n(F) → σ*(H–H) charge transfers in **8** HCH…FB ($\Delta E^{(2)}$ = 3.4 kJ/mol) and **9** HH…FBC ($\Delta E^{(2)}$ = 1.1 kJ/mol), respectively. Consistent with

the smaller electron transfer and thus smaller covalent character of the hydrogen bonds in **7** – **9** and **15**, the ρ_b(H…Y) values for these complexes are also an order of magnitude smaller than those for **12** – **14** (Table 4.4).

As noted earlier, there are four hydrogen-bonded complexes that were located on both the singlet and triplet potential energy surfaces, **7** and **S4** HCH…BF; **8** and **S5** HCH…FB; **12** and **S11** FH…C(B)H; and **13** and **S12** FH…CBH (this work and Ref. [1]). With the exception of **13** and **S12** FH…CBH, the hydrogen bond strengths are essentially identical for the corresponding triplet and singlet complexes. Excitation has enhanced the electron-donating ability of the CBH moiety in **13**, making the hydrogen bond in this complex about 4 kJ/mol stronger than in **S12**. Chan et al. saw a similar enhancement in carbonyl oxygen basicity in their comparison of singlet vs. triplet *p*-methoxyacetophenone-H_2O complexes[56].

Finally, isomer **16** can be considered a complex between the fragments H_2BF and C. In this case, the F…C bond has been stretched by ca. 1.1 Å compared to its values in the more tightly bound complexes. The flatness and other structural features of the H_2BF fragment indicate that **16** is a complex between ^1H_2BF and ^3C and the associated BDH of 6 kJ/mol reflects the weak interaction resulting from the elongated C…F bond. The NBO analysis[36] gives a total energy of 20 kJ/mol for the hyperconjugative interactions involving only valence-shell orbitals, and the ρ_b(H…Y) value (Table 4.4) is an order of magnitude smaller than that found for the other C–F bonds (0.23-0.25).

4.4.1.3 Atomization energies and enthalpies of formation.

Total atomization energies ΣD_0 were computed for the most stable triplet, H_2CBF **1**, and singlet, H_2CBF **S1**, minima using equation (2). The scalar relativistic corrections $\Delta E_{DKH\text{-}SR}$ are small, negative and essentially identical for the singlet (–1.82 kJ/mol) and triplet (–1.73 kJ/mol) species. The spin-orbit correction is ΔE_{SO} = –2.88 kJ/mol for both species. The core-valence corrections ΔE_{CV} are larger, with values of 10.0 kJ/mol for H_2CBF **S1** and 8.0 kJ/mol for H_2CBF **1**. With the scaled C-H stretches, the ΔE_{ZPE} contribution is 73.7 kJ/mol for singlet **S1** and 74.2 kJ/mol for triplet **1**. Combined with the ΔE_{elec}(CBS) values of 1999.6 kJ/mol and 1822.5 kJ/mol for the singlet and triplet, respectively, these correction terms lead to total atomization energies of 1931 kJ/mol and 1752 kJ/mol for the singlet and triplet, respectively (equation 2). The enthalpies of formation at 0 K derived from these ΣD_0 values are $\Delta_f H^\circ$ (^1H_2CBF **S1**) = –145 kJ/mol and $\Delta_f H^\circ$ (^3H_2CBF **1**) = 34 kJ/mol, which yield enthalpies of formation at 298 K of $\Delta_f H^\circ_{298}$ (^1H_2CBF **S1**) = –148 kJ/mol and $\Delta_f H^\circ_{298}$ (^3H_2CBF **1**) = 31 kJ/mol. Overall, the differences in the total atomization energies and enthalpies of formation for singlet H_2CBF **S1** and triplet H_2CBF **1** deviate from the differences in the calculated *E* + *ZPE* values by only 2 kJ/mol (Table 4.2). We expect the correction terms for the remaining singlet and triplet isomers to be similar in magnitude, indicating that the enthalpies of formation for the remaining isomers can be estimated to ±10 kJ/mol from the relative *E* + *ZPE* values given in Table 4.2 and Ref. [1].

4.4.1.4 Transition structures

The ten identified interconversion pathways between the triplet [B, C, F, H_2] species are depicted in the potential energy diagram in Figure 4.4. The barrier heights in the forward and reverse directions, Δ(E+ZPE), for the pathways are given in Table 5. The transition structure **TS 2-3** lies ≤3.5 kJ/mol above the reactant **2** *c*-HCBFH and product **3** *t*-HCBFH, implying that there would be essentially free interchange between these isomers and that they would be inseparable or possibly indistinguishable at 298 K. In contrast, the 24 kJ/mol barrier connecting **5** *t*-H(F)CBH and **6** *c*-H(F)CBH suggests that these isomers may be distinguishable and possibly separable at 298 K. Despite the similarity in the stability of **1** H_2CBF compared to **2** and **3** and **4** $FCBH_2$ compared to **5** and **6**, with barrier heights of over 150 kJ/mol these rearrangements are even less likely to be observed at room temperature.

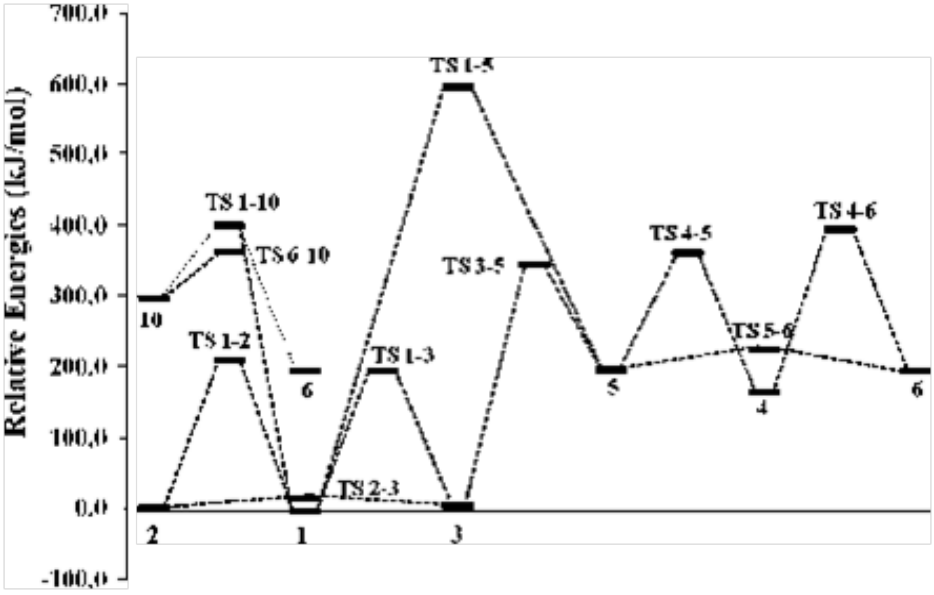

Figure 4.4. Reaction profile for the ten identified interconversion pathways. Relative energy data are CCSD(T)/CBS E+ZPE values.

Other than the cis-trans isomerizations the most kinetically viable conversions are **10** → **6** and **10** → **1**, but these conversions still have barriers of more than 55 kJ/mol. The H atom displacement (from the four-coordinate carbon atom to the boron) in the first process encounters a barrier about half as high as that of the F atom displacement in the latter process (Figure 4.2). Sizable energy barriers also impede the two other processes involving a fluorine atom transfer (**1**↔**5** and **3**↔**5**), which is not surprising given that bridged fluorine species are uncommon and F radical transfers are less efficient than those of other halogens[57,58]. With respect to the barrier heights, the most noticeable difference in the closed-shell vs. open-shell [B, C, F, H_2] potential energy surfaces is the significantly lower barrier connecting **S1** and **S2** (53 kJ/mol) than that connecting the analogous **1** and **5** (this work and Ref. [1]).

These results help to explain why it was more difficult to locate transition structures associated with fluorine migrations, and in particular, why we could not locate **TS 1-4**, which would involve exchange of the fluorine and both hydrogens. The remaining interconversions among isomers **2**-**6** and **10** require either a F atom migration or migration of two atoms, and we expect that these processes will pass through transition structures that lie at least as high as those reported in Table 4.4.

Our results therefore suggest that there are no low-energy barrier pathways separating the other isomers from 1 or from each other, again with exception of the cis-trans isomerizations. As was noted for the singlet PES[1], the barriers are sufficiently high that these species may be experimentally observable at room temperature. In fact, some of these species may be less prone to isomerize than to undergo other reactions.

4.5 References

[1] Deakyne, C. A.; Corum, A. K.; Thomas, H. M.; Liebman, J. F. *J. Fluorine Chem.* **2006**, *127*, 1355.

[2] Duncan, F. J.; Cvetanovic, R. J. *J. Am. Chem. Soc.* **1962**, *84*, 3593.

[3] Lanzisera, D. V.; Andrews, L. *J. Phys. Chem. A* **2000**, *104*, 9295.

[4] Minyaev, R. M.; Gribanova, T. N. *Russ. J. Gen. Chem*. **2004**, *74*, 1529.

[5] Jensen, P.; Bunker, P. R. *J. Chem. Phys.* **1988**, *89*, 1327.

[6] Gilles, M. K.; Ervin, K. M.; Ho, J.; Lineberger, W. C. *J. Phys. Chem*. **1992**, *96*, 1130.

[7] Brazier, C. R. *J. Mol. Spectrosc*. **1996**, *177*, 90.

[8] Ponomarev, D.; Takhistov, V.; Slayden, S.; Liebman, J. *J. Mol. Struct*. **2008**, *876*, 15.

[9] Grant, D. J.; Dixon, D. A. *J. Phys. Chem. A* **2009**, *113*, 777.

[10] Feller, D.; Peterson, K. A.; Dixon, D. A. *J. Chem. Phys*. **2008**, *129*, 204105/1.

[11] Raabe, I.; Himmel, D.; Krossing, I. *J. Phys. Chem. A* **2007**, *111*, 13209.

[12] Poon, C.; Mayer, P. M. *Can. J. Chem*. **2002**, *80*, 25.

[13] Rablen, P. R.; Hartwig, J. F. *J. Am. Chem. Soc*. **1996**, *118*, 4648.

[14] Barreto, P. R. P.; Vilela, A. F. A.; Gargano, R. *Int. J. Quantum Chem.* **2005**, *103*, 659.

[15] Mó, O.; Yáñez, M.; Eckart-Maksić, M.; Maksić, Z. B.; Alkorta, I.; Elguero, J. *J. Phys. Chem. A* **2005**, *109*, 4359.

[16] Zeng, Y.; Su, K.; Deng, J.; Wang, T.; Zeng, Q.; Cheng, L.; Zhang, L. THEOCHEM **2008**, *861*, 103.

[17] Grant, D. J.; Matus, M. H.; Switzer, J.; Dixon, D. A.; Francisco, J. S.; Christe, K. O. *J. Phys. Chem*. A **2008**, *112*, 3145.

[18] Gaussian 03, Revision C.02, Frisch, M. J.; Trucks, G. W.; Schlegel, H. B.; Scuseria, G. E.; Robb, M. A.; Cheeseman, J. R.; Montgomery, Jr., J. A.; Vreven, T.; Kudin, K. N.; Burant, J. C.; Millam, J. M.; Iyengar, S. S.; Tomasi, J.; Barone, V.; Mennucci, B.; Cossi, M.; Scalmani, G.; Rega, N.; Petersson, G. A.; Nakatsuji, H.; Hada, M.; Ehara, M.; Toyota, K.; Fukuda, R.; Hasegawa, J.; Ishida, M.; Nakajima, T.; Honda, Y.; Kitao, O.; Nakai, H.; Klene, M.; Li, X.; Knox, J. E.; Hratchian, H. P.; Cross, J. B.; Bakken, V.; Adamo, C.; Jaramillo, J.; Gomperts, R.; Stratmann, R. E.; Yazyev, O.; Austin, A. J.; Cammi, R.; Pomelli, C.; Ochterski, J. W.; Ayala, P. Y.; Morokuma, K.; Voth, G. A.; Salvador, P.; Dannenberg, J. J.; Zakrzewski, V. G.; Dapprich, S.; Daniels, A. D.; Strain, M. C.; Farkas, O.; Malick, D. K.; Rabuck, A. D.; Raghavachari, K.; Foresman, J. B.; Ortiz, J. V.; Cui, Q.; Baboul, A. G.; Clifford, S.; Cioslowski, J.; Stefanov, B. B.; Liu, G.; Liashenko, A.; Piskorz, P.; Komaromi, I.; Martin, R. L.; Fox, D. J.; Keith, T.; Al-Laham, M. A.; Peng, C. Y.; Nanayakkara, A.; Challacombe, M.; Gill, P. M. W.; Johnson, B.; Chen, W.; Wong, M. W.; Gonzalez, C.; and Pople, J. A.; Gaussian, Inc., Wallingford CT, 2004.

[19] Peng, C.; Schlegel, H. B. *Isr. J. Chem*. **1993**, *33*, 449.

[20] Peng, C.; Ayala, P. Y.; Schlegel, H. B.; Frisch, M. J. *J. Comp. Chem*. **1996**, *17*, 49.

[21] Gonzalez, C.; Schlegel, H. B. *J. Chem. Phys*. **1989**, *90*, 2154.

[22] Gonzalez, C.; Schlegel, H. B. *J. Phys. Chem*. **1990**, *94*, 5523.

[23] Gonzalez, C.; Schlegel, H. B. *J. Chem. Phys.* **1991**, *95*, 5853.

[24] Peterson, K. A.; Woon, D. E.; Dunning Jr., T. H. *J. Chem. Phys.* **1994**, *100*, 7410.

[25] Lee, T. J.; Taylor, P. R. *Int. J. Quant. Chem. Quant. Chem. Symp*. **1989**, *23*, 199.

[26] Matus, M. H.; Nguyen, M. T.; Dixon, D. A.; Christe, K. O. *J. Phys. Chem. A* **2008**, *112*, 4973.

[27] Peterson, K. A.; Dunning Jr., T. H. *J. Chem. Phys*. **2002**, *117*, 10548.

[28] Douglas, M.; Kroll, N. M. *Ann. Phys*. **1974**, *82*, 89.

[29] Jansen, G.; Hess, B. A. Phys. Rev. A 39 1989, 6016.

[30] EMSL basis set library, http://www.emsl.pnl.gov/forms/basisform.html.

[31] Moore, C.E. Atomic Energy Levels as Derived from the Analysis of Optical Spectra, Volume 1, H to V; U.S, National Bureau of Standards Circular 467; U.S. Department of Commerce, National Technical Information Service, COM-72-50282, Washington DC, 1949.

[32] Chase Jr., M. W. NIST-JANAF Tables, 4th Ed., J. Phys. Chem. Ref. Data 9 1998, 1-1951.

[33] Karton, A.; Martin, J. M. *J. Phys. Chem. A* **2007**, *111*, 5936.

[34] Curtiss, L. A.; Raghavachari, K.; Redfern, P. C.; Pople, J. A. *J. Chem. Phys*. **1997**, *106*, 1063.

[35] Glendening, E. D.; Reed, A. E.; Carpenter, J. E.; Weinhold, F. NBO, Version 3.1., 1993.

[36] Reed, A. E.; Curtiss, L. A.; Weinhold, F. *Chem. Rev*. **1988**, *88*, 899.

[37] Bader, R. F. W. Atoms in Molecules. A Quantum Theory; Clarendon Press, Oxford, U.K., 1990.

[38] Kraka, E.; Cremer, D. in: Maksić (Ed.), Z. B. Theoretical Models of Chemical Bonding. Part 2: The Concepts of the Chemical Bond, Springer Heidelberg, 1990.

[39] Alcamí, M.; Mó, O.; Yáñez, M.; Abboud, J. L. M.; Elguero, J. *Chem. Phys. Lett.* **1990**, *172*, 471.

[40] Hammond, G. S. *J. Am. Chem. Soc.* **1955**, *77*, 334.

[41] Leffler, J. E. *Science* **1953**, *117*, 340.

[42] Afeefy, H. Y.; Liebman, J. F.; Stein, S. E. in: Linstrom, P. J.; Mallard (Eds.), W.G. NIST Chemistry WebBook, NIST Standard Reference Database Number 69, National Institute of Standards and Technology, Gaithersburg MD, 20899, http://webbook.nist.gov (retrieved May, 2009).

[43] Luke, B. T.; Pople, J. A.; Krogh-Jespersen, M. B.; Apeloig, Y.; Karni, M.; Chandrasekhar, J.; Schleyer, P. v. R. *J. Am. Chem. Soc.* **1986**, *108*, 270.

[44] Schleyer, P. v. R.; Luke, B. T.; Pople, J. A. *Organomet*. **1987**, *6*, 1997.

[45] Bent, H. A. *Chem. Rev*. **1961**, *61*, 275.

[46] Jensen, P.; Bunker, P. R. *J. Chem. Phys*. **1988**, *89*, 1327.

[47] Gilles, M.K.; Ervin, K. M.; Ho, J.; Lineberger, W. C. *J. Phys. Chem*. **1992**, *96*, 1130.

[48] Scott, A. P.; Platz, M. S.; Radom, L. *J. Am. Chem. Soc*. **2001**, *123*, 6069.

[49] Brazier, C. R. *J. Mol. Spectrosc*. **1996**, *177*, 90.

[50] Larsen, H.; Hald, K.; Olsen, J.; Jørgensen, P. *J. Chem. Phys*. **2001**, *115*, 3015.

[51] Feltham, E.J.; Qadiri, R. H.; Cottrill, E. E. H.; Cook, P. A.; Cole, J. P.; Balint-Kurti, G. G.; Ashfold, M. N. R. *J. Chem. Phys*. **2003**, *119*, 6017.

[52] Pappová, A.; Deakyne, C. A.; Skancke, A.; Cernusák, I.; Liebman, J. F. *Mol. Phys*. **1996**, *89*, 247.

[53] Tzeli, D.; Mavridis, A. *J. Phys. Chem. A* **2001**, *105*, 1175.

[54] Alabugin, I.V.; Manoharan, M.; Peabody, S.; Weinhold, F. *J. Am. Chem. Soc*. **2003**, *125*, 5973.

[55] Hobza, P.; Havlas, Z. *Chem. Rev*. **2000**, *100*, 4253.

[56] Chan, W. S.; Ma, C.; Kwok, W. M.; Phillips, D. L. *J. Phys. Chem. A* **2005**, *109*, 3454.

[57] Liebman, J. F.; Jarvis, B. B. *J. Fluorine Chem*. **1975**, *5*, 41.

[58] Liebman, J. F. *J. Fluorine Chem*. **1975**, *5*, 55.

VITA

Haunani Thomas was born on November 19th, 1979, in Ann Arbor, Michigan. She attended Drury University in Springfield, MO. She graduated in 2003 with a Bachelors of Science in Biology. In 2005, Haunani joined Prof. Carol Deakyne in the physical chemistry division of the Chemistry Department at the University of Missouri-Columbia as a doctoral candidate. Under Prof. Deakyne's supervision she completed her doctoral research with emphasis on electronic structure calculations. She completed her thesis entitled, "Computational Studies of Three Chemical Systems" and graduated in December, 2011. After completing graduate school she will work as a postdoctoral researcher at the J. Heyrovsky Institute of Physical Chemistry within the Academy of Sciences of the Czech Republic in Prague, Czech Republic.